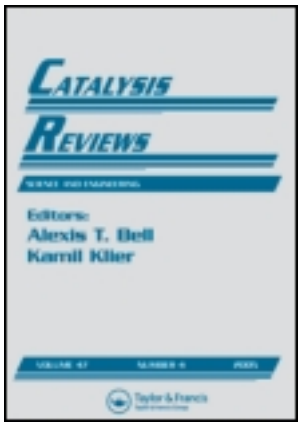

Catalysis Reviews
Publication details, including instructions for authors and subscription information:
http://www.tandfonline.com/loi/lctr20

A Critical Assessment of Li/MgO-Based Catalysts for the Oxidative Coupling of Methane

Sebastian Arndt [a], Guillaume Laugel [a], Sergey Levchenko [b], Raimund Horn [c], Manfred Baerns [c], Matthias Scheffler [b], Robert Schlögl [c] & Reinhard Schomäcker [a]

[a] Technical University Berlin, Department of Chemistry, Berlin, Germany

[b] Fritz Haber Institute of the Max Planck Society, Theory Department, Berlin, Germany

[c] Fritz Haber Institute of the Max Planck Society, Department of Inorganic Chemistry, Berlin, Germany

Available online: 27 Oct 2011

To cite this article: Sebastian Arndt, Guillaume Laugel, Sergey Levchenko, Raimund Horn, Manfred Baerns, Matthias Scheffler, Robert Schlögl & Reinhard Schomäcker (2011): A Critical Assessment of Li/MgO-Based Catalysts for the Oxidative Coupling of Methane, Catalysis Reviews, 53:4, 424-514

To link to this article: http://dx.doi.org/10.1080/01614940.2011.613330

Catalysis Reviews: Science and Engineering, 53:424–514, 2011

ISSN: 0161-4940 print / 1520-5703 online
DOI: 10.1080/01614940.2011.613330

A Critical Assessment of Li/MgO-Based Catalysts for the Oxidative Coupling of Methane

Sebastian Arndt[1], Guillaume Laugel[1], Sergey Levchenko[2], Raimund Horn[3], Manfred Baerns[3], Matthias Scheffler[2], Robert Schlögl[3], and Reinhard Schomäcker[1]

[1]Technical University Berlin, Department of Chemistry, Berlin, Germany
[2]Fritz Haber Institute of the Max Planck Society, Theory Department, Berlin, Germany
[3]Fritz Haber Institute of the Max Planck Society, Department of Inorganic Chemistry, Berlin, Germany

Li/MgO is one of the most frequently investigated catalysts for the oxidative coupling of methane. Besides catalytic testing, it is also a suitable system to perform surface science experiments and quantum chemical calculations, which is not possible for many other active catalysts. However, the real structure of Li/MgO, the nature of the active center and the structure - activity relationship remain unclear, despite all the research that has been done. The aim of this review is to summarize the available knowledge on Li/MgO to structure and accelerate and improve the ongoing work on this catalytic system.

Keywords Li/MgO, Oxidative coupling of methane, Oxidative dehydrogenation of ethane, OCM, ODH

1. INTRODUCTION

The resources of natural gas rival those of crude oil. The composition of natural gas depends on its origin, but the main component is always methane. Therefore, there is a large economical interest in making methane available as a carbon source for the chemical industry.

Received February 23, 2011; accepted July 26, 2011.
Address correspondence to Reinhard Schomäcker, Technical University Berlin, Department of Chemistry, Strasse des 17. Juni 124, Berlin 10623, Germany.

A direct way for the conversion of methane into value added products is the oxidative coupling (OCM) to ethane or ethylene. The overall pathway is shown in Reaction 1. This reaction has attracted a lot of attention since the fundamental work of Keller and Bhasin and Hinsen and Baerns (1, 2). However, until now no economically viable process has been put into practice despite all efforts (3–6).

$$CH_4 + {}^1/_2O_2 \rightarrow {}^1/_2C_2H_4 + H_2O \tag{1}$$

$$\Delta_r H^{\emptyset}(800\ ^\circ C) = -139\ kJ/mol$$

$$\Delta_r G^{\emptyset}(800\ ^\circ C) = -153\ kJ/mol$$

The coupling of methane without an oxidant is a highly endothermic reaction and due to thermodynamic constraint the conversion is limited. By introducing an oxidizing agent, the process becomes exothermic and the thermodynamic restrictions can be overcome. However, from a thermodynamic point of view, the partial oxidation (Reaction 2) and the total oxidation (Reaction 3) are thermodynamically much more favored than the oxidative coupling of methane.

$$CH_4 + {}^3/_2O_2 \rightarrow CO + 2H_2O \tag{2}$$

$$\Delta_r H^{\ominus}(800\ ^\circ C) = -519\ kJ/mol$$

$$\Delta_r G^{\ominus}(800\ ^\circ C) = -611\ kJ/mol$$

$$CH_4 + 2O_2 \rightarrow CO_2 + 2H_2O \tag{3}$$

$$\Delta_r H^{\ominus}(800\ ^\circ C) = -801\ kJ/mol$$

$$\Delta_r G^{\ominus}(800\ ^\circ C) = -801\ kJ/mol$$

To obtain reasonable yields of C_2 hydrocarbons (C_2H_6 and C_2H_4), the reaction must be controlled kinetically. For this, suitable catalysts are necessary. However, the known catalysts are not very active at low temperatures; thus, the reaction requires temperatures between 700–900 °C, which leads to low yields (due to consecutive CO_x formation) and severe catalyst deactivation (due to decomposition or sintering, caused by the high reaction temperatures).

In the past, the research strategy was often characterized by random testing of catalysts with a focus on maximization of the C_2 yield. This strategy has

not led to a final breakthrough with respect to high selectivity and yield of C_2 hydrocarbons. Thus, studying only one catalytic system to understand the reasons for these limitations in detail is necessary. The outcome of this research may be the basis for further efforts in optimizing catalyst formulations and maximizing catalyst performance. At a later stage, high throughput testing of numerous different catalysts may be of advantage. A combinatorial approach could also be a suitable strategy to establish a structure activity relationship, as recently reported (7).

In the search for better catalysts, hundreds of materials have been tested. Li-doped MgO showed higher performance than most other materials. Lunsford et al. were among the first to publish extensive details about this catalytic system (8–10). Li-doped MgO was and still is the object of intensive studies for several research groups. Studies on MgO doped with other alkali metals did not lead to better catalysts (11–16).

In spite of all the research that has been done, many aspects remain unclear. As it will be outlined in this review, the active center, the maximum solubility of Li in the MgO lattice, the position and nature of Li in the MgO, the stability of the catalyst, and many other questions are still not answered, despite the substantial amount of literature published on this topic. Therefore, identifying the points that need further investigation is not easy. The aim of this article is to summarize the existing knowledge on Li/MgO and point out problems and unclarities that need further investigation.

Moreover, it is possible to perform quantum chemical studies and surface science experiments on Li-doped MgO, which is a rather difficult task for many other catalysts. Such studies will identify the role and importance of different surface species within the catalytic reaction pathway. This information will be used for the design of catalysts with better performance. A very important question is the presence of species that contribute to unselective reactions, that should be avoided.

This publication focuses on Li/MgO and where necessary on MgO. Further additives on Li/MgO are only discussed in Section 6. Engineering aspects are not within the scope of this publication, although a variety of reports exist dealing with the engineering aspects of Li/MgO (17–27).

2. PREPARATION OF LI/MGO CATALYSTS

The preparation of the Li/MgO catalyst is crucial for its performance and many different methods have been used as described below.

2.1. Wet Impregnation

In the first publications from the Lunsford group (8–10), a suspension of Li_2CO_3 in deionized H_2O was added to MgO. The slurry was stirred and

heated until a thick paste remained, which was dried overnight at 140 °C. The obtained material was calcined for one to several hours at temperatures between 450 and 465 °C under flow of O_2.

Korf et al. synthesized Li/MgO via wet impregnation of MgO with an aqueous solution of LiOH (28). The procedure was done under a stream of CO_2 for some samples. Afterwards, the samples were dried at 140 °C, calcined in air at various temperatures, and then crushed and sieved.

Matsuura et al. prepared Li/MgO via adding Li_2O to a suspension of ultra fine crystalline MgO in C_2H_5OH, followed by drying at 78 °C and calcination at 740 °C for 4 h. The use of ultra fine crystalline MgO resulted in a catalyst with an exceptionally high activity for the OCM (29).

Choudhary and co-workers reported a highly stable Li/MgO, which showed no deactivation for 15 h on stream (temperature: 750 °C; feed gas composition: CH_4:O_2 = 4:1; flow rate: 85 ml/min) (30). This Li/MgO was prepared by impregnation of $Mg(CH_3COO)_2$ with aqueous $Li(CH_3COO)$ and subsequent calcination. The stability was attributed to the high content of CO_2, which reduced the loss of Li and improved the resistance against sintering of the catalyst.

The Li precursor was reported to play an important role in the nature of the surface species and the development of the specific surface of the Li/MgO catalyst (31–33). Also the precursors for MgO (which was either obtained by thermal decomposition of hydroxy carbonates or the precipitation of nitrates) had an influence on the Li/MgO, indicating a "memory" effect of the catalyst with regard to the MgO precursor.

Choudhary et al. studied the influence of the precursors for Li_2O and MgO for the surface and catalytic properties of Li/MgO in more detail (34). They prepared the catalysts by thorough mixing of the precursor powders in deionized H_2O. The precursors for Li were nitrate, ethanoate, and carbonate. For MgO, the precursors were nitrate, ethanoate, carbonate, oxide, and hydroxides (MgO from $Mg(OH)_2$ was prepared using different Mg salts and precipitation agents). The amount of added water was just sufficient to form a thick paste. Subsequent drying at 120 °C for 4 h and calcination at 750 °C for 6 h followed. The CH_4 conversion, the C_2 yield (C_2H_6 + C_2H_4), and the C_{2+} yield (C_2H_6 + C_2H_4 + higher hydrocarbons), comprising the formation of C_2H_6 and C_2H_4 for C_2 and the formation of all hydrocarbons in the case of C_{2+}, were reported for different temperatures, feed gas compositions, and gas flows. In Figure 1 the reported data as described in Tables 4 and 6 of reference (34) are plotted. The precursors for Li_2O and MgO had a strong effect on the surface area, the basicity, the CO_2 content, and the catalytic performance, but a strong variation of the catalytic results was not observed. However, a direct relationship between these factors could not be observed. In agreement with other groups, it was found that catalysts with a high CO_2 content showed a better performance in the OCM.

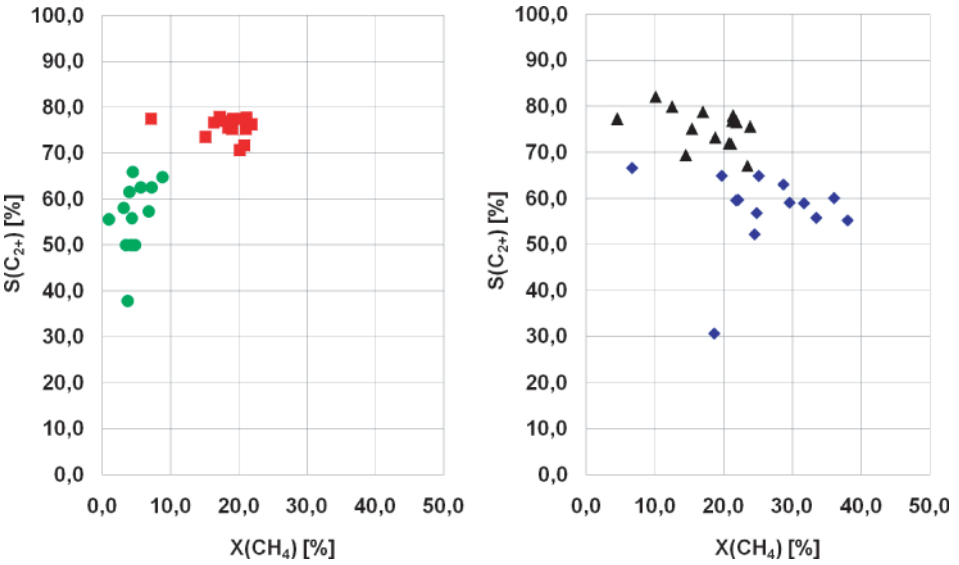

Figure 1: Left Part: The applied reaction conditions were 100 mg catalyst, CH_4/O_2 ratio 8.0, and a gas flow of 8.6 ml/min. The green circles were obtained at 650 °C, the red squares at 750 °C. The selectivity was calculated from the formula $S_{C_{2+}} = Y_{C_{2+}}/X_{CH_4}$. The plotted data are derived from Table 4 of (34). Variations cannot be observed. Right Part: The applied reaction conditions were 100 mg catalyst, temperature of 750 °C, and a gas flow of 17.1 ml/min. The blue diamonds were obtained at a CH_4 to O_2 ratio of 3.0 and the black triangles at a CH_4 to O_2 ratio of 8.0. The selectivity was calculated from the formula $S_{C_{2+}} = Y_{C_{2+}}/X_{CH_4}$. The plotted data are taken from Table 6 of (34). Strong variations of the results can also not be observed (color figure available online).

Kuo and co-workers tried to increase the specific surface area of the Li/MgO via adding charcoal during the preparation (using a wet impregnation procedure of MgO with Li_2CO_3) and subsequent burning off during the calcination (35). Indeed, the result was that the addition of charcoal did increase the surface area and it also modified the morphology of the Li/MgO; however, no major improvement in terms of the yield was achieved.

2.2. Molecular Mixing

López et al. prepared Li-doped MgO via a sol-gel method. They studied the effect of the pH value on the surface hydroxylation and characterized the prepared MgO (36). It was found that Li/MgO catalysts prepared via the sol-gel method had comparable activities to Li/MgO catalysts prepared by wet impregnation of commercial MgO, but significantly higher C_2 selectivities (37, 38).

Trionfetti and co-workers showed that via sol-gel synthesis a high surface-area, nano-scale Li/MgO could be prepared, with low Li loadings (39, 40). This procedure limited the formation of separate Li phases, therefore, suppressing sintering and loss of surface area during thermal treatment. Furthermore, the

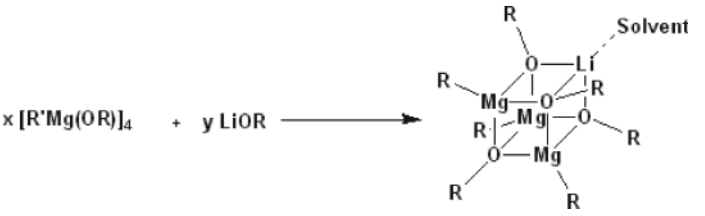

Figure 2: The preparation of heterobimetallic magnesium lithium alkoxide clusters, which are then thermally decomposed to Li/MgO. Changed Figure adapted from (43, 44).

application of high temperatures to incorporate Li into the MgO lattice could be avoided. It was reported that it had a strongly improved activity for the oxidative dehydrogenation (ODH) of C_3H_8 compared to Li/MgO prepared via wet impregnation.

A co-precipitation procedure was described by Roussy and co-workers (41). To an aqueous solution of $Mg(NO_3)_2$ and LiOH, oxalic acid was added until a pH of 2.2 was reached. The precipitate was obtained and dried at 120 °C and calcined at 750 °C under argon for 24 h. The catalytic performance was compared for the cases of classical and micro-wave heating, showing a high improvement of the selectivity in the case of micro-wave heating.

Chevalier et al. applied a surface organo-metallic approach for the preparation of Li/MgO (42). The Li is introduced to the MgO surface via Li-neopentyl, as shown in Reaction 4.

$$\text{Li-Neopentyl} + \text{Mg}_{\text{Surface}} - \text{OH} \rightarrow \text{Mg}_{\text{Surface}} - \text{O} - \text{Li} + \text{Neopentyl} - \text{H}. \quad (4)$$

In contrast to Lunsford, the applied preparation procedure led to a precursor catalyst, which did not contain anions such as carbonate species. The prepared catalyst was more active but less selective towards the formation of C_2 products than the Lunsford catalyst.

The group of Dreiss applied a single source precursors approach. They prepared magnesium alkoxide clusters, which were thermally decomposed. The substitution of a Mg atom for a Li atom in one corner of the cubane, led to the formation of Li/MgO (43, 44). A reaction scheme of the cubane synthesis is shown in Figure 2. The prepared material was characterized in detail; however, its catalytic performance is presently under investigation.

2.3. Other Methods

Berger et al. applied chemical vapor deposition (CVD) for the preparation of Li-doped MgO nanoparticles (45).

The addition of SiO_2 to Li/MgO via hydrothermal treatment led to basic magnesium hydrosilicates. If the added amount of silica was not too large

(Si/MgO ratio of 0.0 to 1.2), the catalyst became more active and selective towards C_2H_4, however, the overall C_{2+} selectivity remained unchanged. The addition of SiO_2 reduced the evaporation of Li and increased the specific surface area, which resulted in a more stable catalyst (46).

Sarkas and co-workers prepared unsupported nanocrystalline Li/MgO using an inert gas condensation-based smoke source and applied it in the oxidative coupling of methane (47). One sample showed total oxidation activity already at 300 °C, a temperature where conventional catalysts are still not active.

Choudhary et al. synthesized Li/MgO supported on commonly used supports, such as Al_2O_3, ZrO_2, HfO_2, SiC, and SiO_2 containing materials (48). Conversion and selectivity were approximately reduced by a factor of 3, compared to unsupported Li/MgO. This observation was attributed to the reduction of the surface basicity, which could be an effect of a strong interaction of the supported material with the support. With Al_2O_3, SiO_2, and ZrO_2, the formation of mixed oxides containing Li or MgO was found, indicating that these materials are not suitable as inert carriers.

The gel-combustion technique, which was reported for Pt nanoparticles (49), was recently applied for the synthesis of Li-doped MgO (50). A series of different Li loadings was prepared by thermal ignition of the metal nitrates in a mixture of glycerol and ethanol, with subsequent calcination in argon or air at 800 °C for 2 h. Detailed catalytic data was not reported, since the study was focused on the structure and morphology.

2.4. Summary

A variety of preparation procedures, including wet impregnation, sol-gel, and organometallic approaches, have been reported so far. The wet impregnation is by far the most applied procedure, used in more than 80% of the publications. Compared to this, other important procedures like co-precipitation, solid state reactions, mixed milling, or combustion synthesis are comparably underrepresented in the literature. Unfortunately, a direct comparison of the catalytic performance of the differently synthesized materials is very difficult due to vastly varying testing conditions.

In studies on the active center, many publications follow the suggestions of Driscoll et al. that the active center is $[Li^+O^-]$ (10) (see also Section 5.4). However, the main preparative route in these publications has been wet impregnation. In this approach, it is necessary to calcine at high temperatures to enable the Li to diffuse into the MgO. But this also accelerates side reactions, like evaporation of Li or carbonate formation and decomposition. Moreover, some publications applied rather low calcination temperatures. It remains unclear if these temperatures are sufficient for the diffusion of Li into the MgO.

Other preparative routes, although they are more intricated and more sophisticated, should be more suitable for the preparation Li/MgO solid solutions and, therefore, of $[Li^+O^-]$. Moreover, the molecular mixing should result in a catalyst that is less pronounced to a phase separation of Li- and Mg-containing phases. However, these preparation procedures have hardly been applied.

For wet impregnation, it was shown that the properties of the obtained catalyst (surface basicity, surface area, CO_2 content, etc.) depend on the used precursors. A strong variation of the catalytic results was not observed and a correlation between the properties and the catalytic performance was not fond.

The realized studies on the preparation of Li/MgO could not reveal the essential factors determining the catalytic performance so far. A comparative study of differently prepared Li/MgO materials, applying the same reaction conditions for the catalytic tests, could therefore be useful.

3. STRUCTURAL CHARACTERIZATION

3.1. Basicity and Acidity

The effect of the basicity and acidity on the OCM has already been the subject of discussion, including not only Li/MgO (51, 52) but also other OCM catalysts. However, as the following review shows, no consensus has been reached how basicitiy and acidity influence OCM performance, since there are different kinds of basic sites with different strength and there is no unambiguous correlation between the C_2 selectivity and the basicity.

3.1.1. Pure MgO

Davydov and co-workers studied basic sites of various oxides used as catalysts in the oxidative coupling of methane via infrared spectroscopy (IR) of adsorbed molecules such as CO_2 (53, 54). It was demonstrated that the basic sites can be titrated with CO_2. The correlation between the spectral behavior of the carbonates and the strength allowed a discrimination between the different sites. The presence and concentration of the strongest basic sites were reported to determine the catalytic activity.

Kuś et al. observed that both the presence or absence of impurities, such as Ca or Na, and the gas atmosphere during calcination also influenced surface basicity (55, 56).

Bailly and co-workers studied the nature of possible active sites of MgO by investigating the relationship between the thermodynamic Brønsted basicity and reactivity of basic sites (CH_3OH deprotonation and conversion of 2-methyl-3-butyn-2-ol (MBOH)) (57). The relative distribution of low coordinated O^{2-} was varied via different preparative routes and measured via

photoluminescence. Moreover, the hydroxylation of clean MgO surfaces and its influence on the Brønsted basicity were studied. Hydroxylated surfaces were found to be more reactive, although they had a lower deprotonation ability than clean surfaces. The specific reactivity of OH groups, compared to low coordinated O^{2-}, was found to be determined by the variable stability of the resulting alcoholate intermediates. As OH groups are poor Brønsted bases, the number of alcoholate species is lower on clean surfaces, however, these intermediates were less stabilized and therefore more reactive.

Chizallet et al. used ^{1}H Mas NMR (MAS—magic angle spinning; NMR—nuclear magnetic resonance) to distinguish between different OH groups that can exist on a defective MgO surface (58, 59). They found a clear correlation between the area of NMR signals below -0.7 ppm chemical shift and the conversion of 2-methylbut-3-yn-2-ol (MBOH) to acetone and acetylene as test reaction. As these NMR signals ≤ -0.7 ppm could be identified as hydroxyl groups coordinated to surface Mg^{2+} ions, these O_{LC}-H sites (LC—low coordination), with L = 1, 2, were reported as active sites. DFT (Density Functional Theory) calculations showed that nucleophilicity of the O_{LC} groups rather than basicity of the surface oxygen ions determines reactivity towards MBOH conversion. No statement was made whether the same holds for reactivity and/or selectivity in methane oxidative coupling.

3.1.2. Li/MgO

The surface basicity and acidity of MgO promoted with alkali metals (Li, Na, K, Rb, and Cs), prepared via impregnation, was compared with the catalytic performance of these materials (16). The surface properties strongly depended on the promoter and on the calcination temperature. The following order was found for the BET surface area after preparation: Li/MgO $\ll$ Na/MgO $\leq$ Rb/MgO $\leq$ K/MgO $\leq$ Cs/MgO. Acidic sites of different strengths were found, and basic sites were found to be broadly distributed and strongly influenced by the promoter. A correlation between the density of the strongly basic sites and the formation of C_2 products per unit surface area was observed. In another study using other dopants (Li_2O, Na_2O, PbO, La_2O_3, $MgCl_2$, $CaCl_2$), the result was a significant increase in surface basicity, without significant correlation between basicity and C_2 yield (60). This was considered as an indication that further factors play an important role for the catalytic performance.

The acid-base properties and the base-catalyzed elimination reaction of 2-propanol, giving either acetone or propylene, was studied for MgO and alkali-doped MgO by Díez et al. (61). The basic properties depended on the relative concentration of certain surface species (OH groups, for instance). The addition of alkali metals, prepared via impregnation, increased the density of basic sites and also modified the strength. Dopants with a higher electron-donating

strength led to the formation of stronger basic sites. The activity in the test reaction also increased with an increasing base strength.

3.2. Structure and Properties

The known literature about the morphological aspects of OCM catalysts, among them Li/MgO, is summarized in detail in a book chapter of Martin and Mirodatos (62). The loss of Li, the phase organization of Li/MgO, and the influence of the surface area and the structure on the OCM is discussed. In the present review, the aspects are discussed in the following sections.

3.2.1. Pure MgO

Spoto and co-workers reviewed the research on the adsorption of CO on MgO, in the form of single crystals, films, and powders (63). CO was chosen as a test molecule because it can react with both Mg^{2+} and O^{2-}. Results obtained via IR and high-resolution transmission electron microscopy (HR-TEM) were considered in particular. However, the results of other techniques are described as well. It was shown that the gap between surface science experiments and powders, as typically used in catalysis, can be progressively bridged.

Choudhary and co-workers reported that the thermal decomposition of $MgCO_3$ leads to MgO, which was highly active in the OCM (64). They found a strong influence of the preparation conditions on the thermal decomposition and the surface properties (surface area, total basicity, base strength distribution) (65, 66). That the surface properties of MgO, prepared from $Mg(OH)_2$, also depends on the preparation and calcination conditions had been shown before (67).

Ardizzone et al. applied X-ray photoelectron spectroscopy (XPS) to study different precursors for MgO (68, 69). Different defects were characterized and considered to be responsible for the activation step of CH_4 in the OCM. From the experimental data obtained at different temperatures, it had been shown that the chemical state and the basicity of MgO is a result of the competition of O_2, hydrocarbon, and H_2O for the different reactive surface sites.

Mellor and co-workers investigated the impact of the MgO structure on the heterolytic oxygen exchange with the surface (70). Either the particle size or the termination plane was varied. The exchange was independent of the particle size (particles with a (100) termination plane were used). The activity order of different planes was (111) or (110) *mean* surface planes > (100) > (111), indicating that low coordinated $Mg^{2+}O^{2-}$ pairs play a beneficial role.

3.2.2. Li/MgO

Kimble and Kolts showed in thermogravimetric studies with different phases of Li/MgO that Li is present as LiOH, if prepared from $LiNO_3$ or as Li_2CO_3, if prepared from Li_2CO_3 (71). They reported, that the LiOH exposed

to the reaction gas at 700 °C was converted to Li_2CO_3. Treating MgO with the same conditions, it did not gain weight, suggesting that no change took place. If treated at 775 °C in a N_2 atmosphere, Li_2CO_3/MgO showed a partial decomposition of the carbonate. The decomposition was completed at 900 °C. Being exposed to the reaction mixture at 700 °C, it was converted back to Li_2CO_3. If H_2O was added at 700 °C, the quantity of carbonate seemed to decrease. Kimble and Kolts assumed that in return the amount of hydroxides increased. Cycles of carbonate formation and decomposition did not effect the activity as a catalyst. It was assumed that in the presence of a mixture of CO_2 and H_2O an equilibrium will be established, with carbonate as the predominant species (72). A loss of Li during the calcination of the Li/MgO was reported. The loss of Li from the catalyst at high temperatures under reaction conditions was also reported by Kimble and Kolts (73). Moreover, it was reported that the Li content was stabilized at approximately 1% when supported on CaO. That a limit for the maximum concentration of Li could exist, was underlined by these authors.

The chemistry of Li in Li/MgO during the OCM was investigated by Korf et al. (74). Their conlcusions were:

1. Behavior of Li/MgO was found to depend strongly on the preparation procedure.
2. Passing CO_2 through the solution while impregnating MgO led to higher amounts of Li_2CO_3 and segregation of Li to the surface of the catalyst.
3. The optimum loading of Li in the fresh catalyst was reported to be 2–4 wt%.
4. The active site was formed on the surface by a gradual decomposition of Li_2CO_3 in the presence of O_2. The absence of O_2 had an adverse effect on the activity.
5. The active sites were found to be unstable. The deactivation was due to a loss of Li, via evaporating of the volatile LiOH or the formation of Li_2SiO_3, from Li and the quartz glass material of the reactor. H_2O in the feed had, therefore, an adverse effect.
6. In hot spot areas, the loss of Li was reported to occur most rapidly.
7. CO_2 in the feed was found to lead to:
    a. reversible poisoning of the active site,
    b. but also to stabilization of the active site against deactivation.
8. Measures for a stable catalyst points out that:
    a. equilibrium between Li_2CO_3 and LiOH is necessary,

b. periodic reversal of the flow direction improves the stability,

c. application of an Al_2O_3 instead of a quartz glass reactor can improve the stability.

While investigating the reaction of CO_2 during the oxidative coupling of methane, Galuszka found that a substantial amount of Li formed a carbonate, which was stable up to 800 °C (75). The carbonate formation started at 400 °C, as shown via Fourier transform infrared spectroscopy (FT-IR), temperature programmed reaction (TPR), and temperature programmed desorption (TPD). Interestingly, several hours of calcination at 800 °C were necessary to remove the CO_2 from the catalyst. There was no CO_2 on pure MgO above 600 °C, therefore, chemisorbed CO_2 on Li/MgO above 600 °C had to be attributed to the Li. Furthermore, different types of carbonates can be assumed, and they should have different properties and activities. However, the identification of surface species by IR has proven to be difficult (76, 77).

In the publication of Ito et al., the optimum loading of Li was reported to be 7 wt% (9). In a later discussion, it was noted that for achieving a monolayer of Li^+ on MgO ca. 0.2 wt% Li is required, which is a relatively low loading (78). Therefore, Hutchings and co-workers reinvestigated the optimum loading of Li on MgO (79). They found that a sub-monolayer loading, i.e., the above-mentioned 0.2 wt% Li, enhances the activation of CH_4 and the selectivity towards coupling products, indicating that the optimum loading of Li is much lower than reported in previous publications, e.g., 7 wt% reported by Ito et al. (9).

Hargreaves and co-workers investigated the morphology of Li/MgO and its relationship to catalytic performance (80–83). For pure MgO, it was demonstrated that the morphology is an important factor for the catalytic performance in the oxidative coupling of methane. The addition of Li to MgO led to changes due to grain growth. It was concluded that corner and edge sites did not significantly contribute to the catalytic activity. A special "bottom step" site was suggested to be the active center. For Li/MgO, immobile dislocations were detected in the bulk of these grains. It was suggested that pinning of these dislocations by Li led to the formation of $[Li^+O^-]$, a frequently suggested candidate for the role of the active sites, as outlined in Section 5.4.

The results of Hargreaves et al. (80–83) were confirmed via atomistic simulation techniques by Lewis' group (84). They also showed that the presence of Li increased the concentration of oxygen defects (in the form of $[Li^+O^-]$) and promoted their segregation to surface sites. $[Li^+O^-]$ centers were reported to be trapped in low coordinated surface sites, which should lead to a modified activity. They assumed that the activity of pure, undoped MgO was the result of more complex surface defects.

The relationship between surface morphology and reactivity was investigated by testing several differently prepared and well-characterized MgO and Li/MgO catalysts by the group of Lunsford (85). The comparison of the results showed that the surface area and the morphology did not have a significant impact on the OCM. However, small structural effects, which could have a strong catalytic impact, might have remained undetected.

Berger et al. observed the changes of the surface properties of MgO when small amounts of Li were introduced (45). It was found that the addition of only 0.2 at% Li to pure MgO decreased already the thermal stability of the resulting material. After the Li segregated to the surface, it changed the spectroscopic properties significantly (e.g., IR fingerprint of active hydroxyls and hydrides, surface-trapped electrons, and adsorbed oxygen radicals). It was concluded that Li preferentially moves to surface sites associated with low coordinated ions and higher surface reactivity.

Choudhary et al. investigated MgO, Li/MgO, and MgO doped with other additives as catalysts for the oxidative coupling of methane (86). The doping with Li led to a severe sintering of the MgO and, therefore, to lower specific surface areas. The selectivity obtained with the doped material increased significantly. It was found that the C_2 selectivity increased nearly linearly with the decrease of the specific surface area. The involvement of lattice oxygen of the catalysts was investigated in a pulsed micro-reactor (87). It was found that with increasing pulse number, in each pulse only CH_4 was dosed to the reactor, the conversion of CH_4 decreased sharply, and the C_2 selectivity increased. It was concluded that lattice oxygen was involved. The re-oxidation of the catalysts after the pulses, led to a decrease of the C_2 selectivity as compared with fresh catalyst. The reason could be the formation of active chemisorbed species and/or restructuring of the catalyst surface.

Sinev et al. studied the redox properties of differing catalyst, among them Li/MgO (88). Based on the results, a new mechanism for the catalyst re-oxidation was suggested, viz. that under steady state, the re-oxidation can proceed via the oxidative dehydrogenation of surface OH groups.

Taniewski and co-workers oxidized C_2H_4 over Li/MgO without co-feeding of O_2, to obtain information on the oxidation properties of Li/MgO (89). Since large amounts of CO and H_2 were found, it was clearly demonstrated that Li/MgO exhibits a high oxygen mobility. After the reduction of the catalyst, it was possible to restore the activity by its re-oxidation with air. The results on the oxidation of C_2H_4 can also be used to draw conclusions about the fate of C_2H_4 in the post-catalytic zone, being still in the reactor.

Anderson and Norby analyzed the liquid phases in Li/MgO by means of thermoanalytical and electrical conductivity measurements and electron microscopy (90). The results indicated that the solubility of Li in MgO increases with increasing oxygen activity, which is also predicted by defect

theory. At 700 °C and in a CO_2-rich, oxidizing atmosphere, the solubility of Li in MgO was estimated to be in the order of magnitude of 0.1 mol%, respectively 0.02 wt%.

Pure MgO is a poor electronic conductor at low temperatures, however, doping with Li leads to *p*-type semiconductivity (91, 92). Norby and Anderson studied the electrical conductivity of sintered Li/MgO at different temperatures (≤1200 °C) and under different O_2 partial pressures. The effect of H_2O and CO_2 was also investigated. It was found that Li dissolves in MgO, such that an Mg^{2+} is being substituted by Li^+, forming a negative defect and increasing *p*-type conductivity, which was dominating at near atmospheric O_2 partial pressures and high temperatures. Surface and/or grain boundary conductivity became important at intermediate temperatures (≤700 °C), which was also probably mainly due to *p*-type conductivity. It was observed that Li readily evaporated from the surface at high temperatures and that Si containing impurities reacted with Li/MgO forming non-conducting silicate phases. Under ambient pressures of H_2O or H_2, proton defects seemed to play a minor role (93).

When measuring the direct current (DC) conductivity of Li/MgO as a function of H_2O vapor and O_2 partial pressure, Balint and Aika observed that proton species dominated the conductivity at low temperatures (400 °C) (94), *p*-type conductivity dominated at high temperatures (800–900 °C), corresponding to the results of Norby and Anderson, which indicated a mixed conduction mechanism at intermediate temperatures (500–700 °C). A mechanism was proposed in which doping with Li leads to the formation of oxygen vacancies, which play an important role in the generation of O^- sites. These oxygen vacancies were believed to be blocked by hydrogen defects at low temperatures.

Balint and Aika investigated the defect sites formed when MgO was doped with Li or Ti (95). Pure MgO and Li/MgO always exhibited *p*-type conductivity, whereas Ti/MgO showed *n*-type conductivity. Doping with Li favored the formation of oxygen vacancies, while doping with Ti had the inverse effect. That showed that the defect structure of MgO can be controlled via doping. Tardío and co-workers also determined *p*-type semiconductor properties of Li/MgO single crystals (96).

For MgO and Li/MgO, the dependency of DC conductivity on the partial pressures of O_2 and H_2O was investigated at OCM temperature (97, 98). The DC conductivity of Li/MgO increased with increasing O_2 pressures, indicating a *p*-type conductivity of this material. The effect of H_2O was stronger on MgO than on Li/MgO. A model for the defect generation due to H_2O inclusion was proposed. Two different activation energies for DC conductivity were found, one at low temperatures (400–600 °C) the other at high temperatures (700–900 °C). Based on the pressure dependencies, different conductivity mechanisms were proposed. For the low temperature, an OH-vehicle mechanism and at high temperature a *p*-type mechanism due to O^- defects was

proposed. TPD experiments showed the release of H_2 above 600 °C. Therefore, a mechanism with O-H bond rapture for the formation of O^- defects in the high temperature region was proposed.

That the electronic semiconductor properties could be very important features of catalysts for the oxidative coupling of methane, has also been discussed in a review of Zhang and co-workers [5].

In 1971, Abraham and co-workers reported a variation of the carbon arc-fusion technique, which allowed them to grow highly pure MgO and CaO single crystals. This method was successfully applied for doping single crystals of MgO with a variety of different metals, Li for instance (99). Electron paramagnetic resonance spectroscopy (EPR) experiments with a variety of different alkali earth metals with alkaline doping indicated the formation of $[Li^+O^-]$ centers. Schirmer provided evidence using EPR, that the Li substitutes an Mg in the MgO lattice (100). Electron nuclear double resonance (ENDOR) experiments supported this finding (101, 102). The formation of $[Li^+O^-]$ centers is favored by heavy electron irradiation and high temperature quenching, which were stable at room temperature. However, γ-radiation resulted in the formation of these centers, but they were not stable at room temperature. EPR and ENDOR experiments revealed that the defects produced via different ways had the same local configuration (101, 103). The irradiation with neutrons did not lead to stable $[Li^+O^-]$ centers (104). At high temperatures, a Li_2O precipitate led to the formation of a so called "microgalaxy," i.e., a localized $[Li^+O^-]$-rich environment in the neighborhood of the precipitate. Diffusion in the MgO crystal and replacement of Mg^{2+} or formation of vacancies followed (105). The formation of stable $[Li^+O^-]$ centers strongly depended on the surrounding atmosphere, the presence of O_2 was inevitable for the thermal generation of the defects. The $[Li^+O^-]$ centers formed at higher temperatures were stable, however, the cooling procedure effected the stability. When a slow cooling took place, the Li, which had diffused into the MgO crystal, diffused back into the more stable Li-precipitates (106). Since impurities, such as Fe and Cr, could not be avoided, the formation of $[Li^+O^-]$ centers was partly accompanied by a valence change of these metals (107). Interestingly, the $[Li^+O^-]$ centers were also found in CaO (108). From the investigation of current-voltage characteristics, it was concluded, that at oxidizing temperatures the crystals of Li/MgO had a significant effect on the $[Li^+O^-]$ concentration and the electrical conductivity, thermal aging did not seem to have a significant effect on these features (109). For further information, the review of Chen and Abraham on trapped hole centers in alkali earth oxides is recommended (110).

The solubility of hydrogen or deuterium was reported to be much higher in Li/MgO than in pure MgO (104, 111). The mimimum temperature for a diffusion of deuterium in pure MgO was reported to be 1477 °C, for Li/MgO the mimimum temperature was reported to be 527 °C, the higher diffusivity

was attributed to the presence of Li_2O precipitates (111, 112). Furthermore, it was observed that D_2O adsorbs dissociatively on Li/MgO.

Matsuura et al. prepared Li/MgO using ultra fine crystaline MgO. A good correlation between the intensity of the photoluminescence signal (at λ = 450 nm) and the activity was found, also indicating that lower coordinated surface sites, which were formed through the incorporation of Li into the (111) plane of MgO, are playing a significant role (29, 113).

Padró et al. studied Li/MgO with different Li loadings with x-ray diffraction (XRD), XPS, and scanning electron microscopy (SEM) in order to characterize the surface and the catalytic behavior (114). It was found that the catalytic behavior and the surface composition depend strongly on the Li loading. Furthermore, it was concluded that di-oxygen species, e.g., O_2^- could be present at the surface and that a complex equilibrium between the surface oxygen species and the O^- centers exists.

Aritani and co-workers characterized Li/MgO by means of XRD, XPS, Mg K-edge X-ray absorption near edge structure (XANES) and SEM techniques (115, 116). It was found that for low Li loadings (2.5 wt%), Li ions tended to stay in the near surface region. Furthermore, the surface Li tended to form separate phases, without a strong effect on the surface MgO structure. For higher Li loadings (7.5 wt%), the Li was also found in the bulk. An effect of Li incorporation in the bulk was the reduction of the MgO crystallinity. The Li-atoms—being located in the near surface region and in the bulk—had an effect on the activity in the OCM. It was assumed that the near surface defects had a strong positive influence on the CH_4 conversion, while the bulk defects positively influenced the C_2 selectivity.

The surface morphology of Li/MgO was investigated via low temperature infrared spectroscopy of adsorbed CO by Trionfetti et al. (117). These authors demonstrated that the morphology and the defect structure was of great importance in the oxidative dehydrogenation of C_3H_8. Step sites were unselective sites and the major feature on the surface of pure MgO. When the MgO was doped with Li, it tended to occupy the surface step sites and to replace Mg^{2+} (cf Figure 9). When the loading of Li was increased, the step sites were decorated with Li^+ and oxygen vacancies, leading to a higher reactivity. Li/MgO prepared via sol gel, had higher amounts of incorporated Li and they showed a higher selectivity in the ODH of C_3H_8 and the cracking of propane.

Myrach and co-workers recently tried to elucidate the role of Li in MgO, by investigating two model systems: a MgO film—with and without Li-doping—on Mo(001) and powder samples prepared via calcination of the respective precursors in an O_2-atmosphere (118). Their study mainly focused on the physical properties. It was found, that at low concentrations of Li, it most probably incorporates into the MgO together with oxygen vacancies, changing the optical properties of the system. Above 427 °C, the segregation of Li towards the surface and the formation of irregular Li-enriched areas was observed. Above

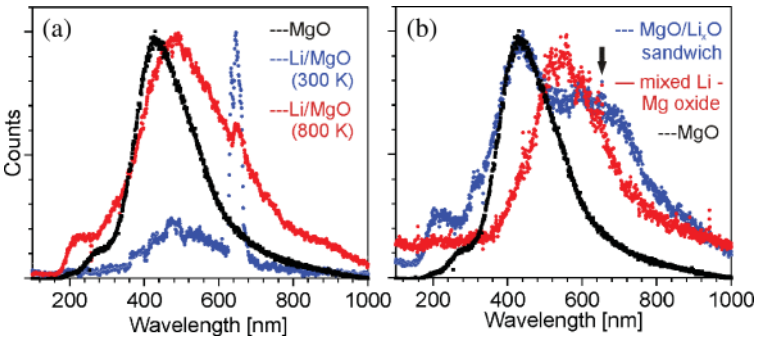

Figure 3: Photon-emission spectra of 12 ML MgO/Mo(001) (black), after deposition of 1 ML Li (blue) and after annealing to 800 K (red). The radiation was stimulated by the injection of 100 eV electrons at 1 nA current; (b) Emission spectra of 12 ML MgO/Mo(001) (black), a layered MgO-Li$_x$O-MgO film annealed to 500 K (blue) and a Li-doped MgO film annealed to 700 K (red). The arrow indicates Li D-transitions. The spectral parameters are identical to those for (a). Figure unchanged from (118). Myrach, P.; Nilius, N.; Levchenko, S.V.; Gonchar, A.; Risse, T.; Dinse, K.P.; Boatner, L.A.; Frandsen, W.; Horn, R.; Freund, H.J.; Schlögl, R.; Scheffler, M. Temperature-Dependent Morphology, Magnetic and Optical Properties of Li-Doped MgO. *ChemCatChem.* **2010**, *2*, 854–862. Copyright Wiley-VCH Verlag GmbH & Co. KGaA. Reproduced with permission (color figure available online).

777 °C, Li desorbed from the MgO surface, leaving behind distinct defects. The Li was not completely removed by heating, very small amounts dissolve in the MgO, as indicated by different optical properties. The change of the optical properties is shown in Figure 3. The principle possibility to detect [Li^+O^-] with EPR was demonstrated on Li/MgO single crystals from Oak Ridge National Laboratories. EPR signals that could be assigned to the [Li^+O^-] center, proposed by Lunsford (10), which is often considered as the active center of this material (as outlined in Section 5.4), were found neither on the Li/MgO films nor in the powder samples. The possible reasons are absence, low concentration, or electron tunneling from the Mo(001) support into the hole centers. However, the results do not exclude the general possibility of the formation of [Li^+O^-].

Recently, the preparation of Li/MgO from gel-combustion was reported (50). Combined studies with transmission electron microscopy (TEM) and SEM were applied to characterize the structure and morphology. A hierarchical pore structure was found for samples with low loadings of Li. Calcination at 800 °C changed the morphology from cubic via truncated octahedral to platelet morphologies, depending on the Li-loading. Indications were found that the Li enhances this transformation. Modifications in the primary morphology of the particles caused severe changes in the secondary structure. Edge-and-step structures and protrusions on flat terraces were found to be the two kinds of high-energy structures found in the micro-structure of the primary particles. It was reported that a relation between the transformation from cubic to complex terminated particles and the catalytic function for the OCM existed.

3.3. Summary

MgO itself is a basic material with various basic, low coordinated and defect sites. Doping with Li leads to a variety of modifications in the MgO structure, partly depending on the added amount of Li. Surface defects are induced, the surface area is reduced, and the spectroscopic properties and the morphology changes upon Li addition.

In Li/MgO single crystals, it was found that Li can replace an Mg in the MgO lattice, forming a $[Li^+O^-]$ defect, which was studied in detail by Abraham et al. However, other suggestions were also made. In the mechanism proposed by Balint and Aika, for instance, the Li is involved in the formation of oxygen vacancies, which play a role in the formation of O^-. A complex equilibrium between the different surface oxygen species exists, which is not yet fully understood.

However, the Li was found to be instable in the Li/MgO catalyst. The publications on the optimal Li-loading report very different amounts. There seems to be an agreement that Li tends to form separate phases or at least Li-enriched regions within the lattice.

The strong dependence of the presence of the different surface species on preparation and operation conditions results in a complex picture of the mechanism of OCM and the difficulty to derive clear structure-reactivity relation.

4. CATALYTIC PERFORMANCE OF LI/MGO-BASED CATALYSTS

4.1. Stability of Li/MgO-Based Catalysts

Ito et al. prepared Li/MgO catalysts with Li loadings of 1 to 26 wt%. All these prepared materials showed a catalytic activity. They found that CH_4 conversion and C_{2+} selectivity increased with increasing reaction temperature up to approximately 700 °C (8, 9). After the catalytic tests, the specific surface area of Li/MgO was considerably lower than the specific surface area of pure MgO. A separate experiment with high and low surface area MgO (34 m^2/g and 8 m^2/g), respectively, showed comparable conversions of 16%, but different selectivities (5% and 29%). A deactivation experiment at 700 °C with 7 wt % Li/MgO was conducted. The catalyst was stable, after approximately 15 to 32 h time on stream. However, the reaction conditions applied for this test were 1 g catalyst, 700 °C, flow rate of 49.8 ml/min, and a feed gas composition of CH_4:O_2:He = 3:1:21.3, being highly diluted. Ito et al. proposed that C_2H_6 forms via the coupling of two $CH_3\cdot$ radicals. It was also found that C_2H_4 was formed via the oxidative dehydrogenation of C_2H_6.

Mirodatos et al. studied the deactivation of MgO and Li/MgO in detail, together with chemical and morphological changes (119). Two kinds of

sintering phenomena were found. At 727 °C (the melting point of Li_2CO_3 is 720 °C), the deactivation coincided with sintering of the solid, a loss of BET surface area (Brunauer, Emmett, Teller) and of Li. Nevertheless, at 634 °C, the deactivation coincided only with a reduction of the BET surface area, a loss of Li was not found. The stability of the surface area depended on the temperature treatment (the surface collapsed above 727 °C) and on the gas phase. In an O_2 atmosphere, the surface was observed to be stable up to 634 °C, it started sintering when it was in contact with the reaction gas mixture. The formation of Li_2CO_3 significantly reduced the stability of the MgO surface area, this was also shown for other dopants and other supports (120, 121). Li_2CO_3 was held responsible for the formation of CO_x (122); the increase of the C_2 selectivity with time on stream was, therefore, explained with the decomposition of Li_2CO_3.

Choudhary and co-workers reported a highly stable Li/MgO, which showed no deactivation for 15 h on stream (temperature: 750 °C, 0.5 g catalyst, feed gas composition: CH_4:O_2 = 4:1, flow: 85.6 ml/min) (30). The catalyst was prepared via impregnation of $Mg(CH_3CO_2)_2$ with aqueous $Li(CH_3CO_2)$ and subsequent calcination. The stability was attributed to the high content of CO_2 (determined via heating the catalyst in a N_2 flow), which reduced the loss of Li and improved the resistance against sintering of the catalyst.

In their study on the nature of the active site of Li/MgO, van Kasteren and co-workers compared the activity and deactivation of Li/MgO and Li_2CO_3 supported on ZrO_2 (123). In terms of activity, for a 7 wt% "home made" Li/MgO, an increase in O_2 conversion and CH_4 conversion is observed, until 16 h time on stream, followed by a steady deactivation. The Li content decreased continuously throughout the experiment. For 0.2 wt% Li/MgO, deactivation and loss of Li were observed from the beginning. However, Li_2CO_3/ZrO_2 suffered from a comparatively fast deactivation to nearly zero activity after approximately 15 h time on stream. The working principle of the catalysts derived from these experiments is discussed in detail in Section 5.1. However, the increase in activity in the first hours times on stream has not been reported by other research groups, but the deactivation of the activity of Li/MgO has been reported.

The catalyst deactivated due to a loss of Li as volatile LiOH or as Li_2SiO_3, due to the fact that the laboratory reactors are made of quartz glass (123). This result was confirmed by Korf and co-workers (28, 74). A consequence is, that the use of experimental equipment made of quartz glass had a negative effect on the stability of Li/MgO. Figure 4 shows the result of a deactivation experiment with and without quartz dilution. It is evident that without quartz, the deactivation process is strongly retarded. After the experiment done by Korf et al. (28), the Li content had fallen to 0.1 wt%, which is significantly lower than previously described by other authors (73, 119). The reason could be the higher reaction temperature.

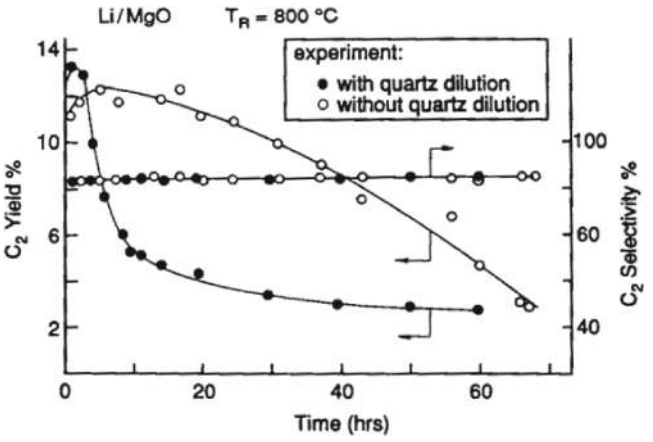

Figure 4: Aging experiments at $T_{Reaction\ Temperature}$ = 800 °C with Li/MgO (ca. 3.1 wt% Li) ($T_{Calcination}$ = 850 °C), with and without quartz dilution. Figure unchanged from (28). Reprinted from, Korf, S.J.; Roos, J.A.; de Bruijn, N.A.; van Ommen J.G.; Ross, J.R.H. Oxidative Coupling of Methane over Lithium Doped Magnesium Oxide Catalysts. *Catal. Today* **1988**, *2* (5), 535–545. Copyright (1988), with permission from Elsevier via the Copyright Clearance Center.

Rapid deactivation of Li/MgO was observed by Korf et al. (124). They also showed that, if Li was still available, the catalyst could be regenerated by treatment with CO_2 under reaction conditions. The deactivation could be avoided if CO_2 was added to the reaction mixture in low concentrations. Furthermore, they concluded that CO_2 temporarily poisoned the active site and simultaneously stabilized it against deactivation; the selectivity was not affected by the CO_2 addition (28, 124). The selectivity did not change much in their long-term experiments, therefore, the conclusion was that the nature of the active site had not changed much, but their number decreased. For Li/Nb/MgO, the prevention of deactivation by adding CO_2 could not be observed (125).

Aigler and Lunsford studied the oxidative coupling of methane over MgO and Li/MgO monoliths (126). Pure MgO was more active but less selective for the formation of C_2 products, than Li/MgO. This high activity of pure MgO was at least partly attributed to Ca^{2+} impurities, which were concentrated at the surface.

The addition of silica to Li/MgO via hydrothermal treatment led to basic magnesium hydrosilicates. If the added amount of silica was not too large, the catalyst became more active and selective towards C_2H_4, however, the overall C_{2+} selectivity remained unchanged. Furthermore, silica addition reduced the evaporation of Li and it increased the specific surface area, resulting in a more stable catalyst (46).

Roos and co-workers tested a series of different catalysts, MgO, Li/MgO (3.8% and 5.3% Li), Cu/MgO, Na/Al_2O_3, Ca/Al_2O_3, Bi/Al_2O_3, Mn/Al_2O_3, Pb/Al_2O_3, $Na/Pb/Al_2O_3$, $Fe/Cr/Al_2O_3$, $Bi_2Sn_2O_7$, and SiC (127). The Li- and

Pb-containing materials seemed to have a superior catalytic performance compared to the other tested materials; and Li/MgO was found to be more stable than the Pb-containing ones.

Galuszka showed that carbonate-free Li/MgO initially showed a good activity, but it decreased after 20 min on stream. The deactivation, the appearance of CO_2, and the disappearance of C_2H_4 coincided. Furthermore, he found that a substantial amount of Li formed carbonate, which was stable until 800 °C (75).

Hutchings et al. compared O_2 and O_3 as an oxygen source for the OCM over Li/MgO (128). In their study, they observed that the catalysts steadily lost their activity because of sintering and recrystallization.

Perrichon and Durupty investigated the thermal stability of Li, Na, and K deposited on MgO, SiO_2, Al_2O_3, and Cr_2O_3 (121). It was found that on SiO_2, Al_2O_3, and Cr_2O_3 the alkali metals are rather stable, however, on MgO a loss of alkali metal was observed at calcination temperatures higher than 500 °C. This effect increased from Li to K at 800 °C, showing that the loss of alkali metals is not limited to Li. A reason for this could be that MgO is not able to form stable compounds, unlike SiO_2, Al_2O_3, and Cr_2O_3, which can form silicates, aluminates, and chromates. Supports impregnated with alkali metals always had a lower surface area; the temperature had no influence on this. This effect was explained with the formation of a conglomerate of alkali metal salt and support. Furthermore, it was assumed that the alkali metal phase, which was present at the interface between the support particles, underwent transformations, especially fusion during sintering. Therefore, it induced partial dissolution of the support and, thus, the growth of larger crystals.

Choudhary et al. observed the effect of doping MgO and Li/MgO with Mn, Cd, and Zn on the catalytic activity in the OCM. The addition of the dopants caused a severe sintering of the MgO, resulting in a decreased specific surface area, but the selectivity also significantly increased. It was found that the C_2 selectivity increased nearly linearly with the decrease of the specific surface area. After 12 h time on stream, the conversion of CH_4 of Li/MgO was approximately 35% (reaction conditions: feed gas composition CH_4:O_2:N_2 = 2.3:1:10.4, temperature 780 °C, flow 60 ml/min, and 0.2 ml catalyst). Doping with Mn, Cd, and Zn led to a generally lower conversion, in the range of 25–30%. However, the Li-promoted catalysts suffered from heavy sintering and deactivation during the catalytic experiments (86).

Al-Zahrani and co-workers studied the effect of CO_2, steam and liquid water treatment, and the process conditions on the oxidative coupling of methane over Li/MgO (129–131). It was shown that CO_2 has not only a poisoning effect on the formation rate of CO, CO_2, and C_2 products. However, the C_2 selectivity remained unaffected. H_2O in the feed enhanced the deactivation rate. This is accelerated with increasing partial pressure of H_2O. Small amounts of CO_2 decreased the deactivation. The addition of liquid H_2O into

the catalyst bed increased the CH_4 conversion. Due to the water treatment, it was reported that the Li content decreased and the specific surface area increased. It was also shown that the catalyst lost Li, by deposition on the reactor walls.

Taniewski and co-workers did research on the effective utilization of the catalyst bed, which deactivated during the reaction (26). It was reported that a hot-spot area was the only working region of the bed and the place of catalyst aging. In a scaled-up laboratory reactor, it was shown that the deactivation could be attributed to a significant loss of Li, which led to the decrease of C_2 selectivity. Changing the feed inlet locations made it possible to involve successive layers of catalyst in the reaction. Furthermore, transformations of the bed, prepared from fresh and deactivated Li/MgO, led to the transport of Li from the fresh catalyst (deactivation) to the deactivated catalyst (regeneration). However, other researchers reported that the highly mobile Li caused severe corrosion and loss of physical integrity in their reactors made from different materials (21, 22).

4.2. Comparison of Catalytic Performance of Several Li/MgO Catalysts

In Table 1, the different reaction conditions and catalytic results taken from different publications are presented. The applied reaction conditions vary significantly, often a large amount of inert dilutent was applied in the feed gas. The strong differences in the reaction conditions hinder a comparison of results, obtained by different research groups (132); no correlation can be observed in the obtained results due to the strong variation.

4.3. Influence of Process Parameters

The required minimum temperature for CH_4 conversion is concordantly reported to be at approximately 600 °C. The CH_4 conversion and the C_2 yield increase with increasing reaction temperature, reaching a maximum at ca. 750 to 800 °C. However, since some authors reported Li/MgO to be an instable catalyst, the catalytic performance of different Li/MgO catalysts after several hours time on stream is questionable. Studies on this subject have not been published yet.

In 1994, Machocki showed that the OCM at temperatures below 700 °C could be applied without the loss of effectiveness, via applying a much longer contact time. He showed that the required contact times were much longer than previously reported in the majority of publications. Therefore, an extended contact time could lead to lower reaction temperatures, i.e., 600 to 650 °C, even for catalysts that are regarded to be suitable for the high temperature range (137).

Table 1: Overview of the reaction conditions and catalytic performance taken from selected publications. Usually the C_2 selectivity is reported, meaning the combined selectivity towards C_2H_6 and C_2H_4. However, in few publications the C_{2+} selectivity, which also takes higher hydrocarbons into account, is reported. The difference between C_2 and C_{2+}, which is usually small, has been neglected and reported as C_2. The space time yield for the C_2 products (STY) was calculated according to the formula STY $= n_p/m_{catalyst}$; if the catalyst was given as a volume, then this has been used.

No.	Catalyst	Mass	CH_4:O_2: Dilutent	Temperature	Flow rate	X_{CH_4} (%)	X_{O_2} (%)	S_{C_2} (%)	C_2H_6/ C_2H_4	STY	Comment	Ref.
1	7 wt%	4.000 g	1.9:1:3.6	720 °C	49.8 ml/min	37.5	n.s.	46.5	0.48	1.69 mol/h × kg_{cat}	—	(8, 9)
2	7 wt%	0.800 g	2.1:1:17.5	700 °C	55.2 ml/min	22.6	n.s.	56.7	—	2.37 mol/h × kg_{cat}	—	(11)
3	4.8 wt.	4.000 g	5.1:1 6.2	700 °C	50.0 ml/min	14.6	n.s.	57.4	—	1.15 mol/h × kg_{cat}	After 10 h	(85)
4	4.5 wt.	4.000 g	5.1:1:6.2	700 °C	50.0 ml/min	13	n.s.	58.9	—	1.05 mol/h × kg_{cat}	After 10 h	(85)
5	5.5 wt.	4.000 g	5.1:1:6.2	700 °C	50.0 ml/min	20.3	n.s.	59.6	—	1.66 mol/h × kg_{cat}	After 10 h	(85)
6	1.3 wt.	2.000 g	2:1:2	760 °C	50.0 ml/min	37	n.s.	40	0.25	3.96 mol/h × kg_{cat}	—	(42)
7	1.3 wt.	2.000 g	2:1:2	780 °C	50.0 ml/min	37	n.s.	40	0.21	3.96 mol/h × kg_{cat}	—	(42)
8	1.3 wt.	2.000 g	2:1:2	800 °C	50.0 ml/min	37	n.s.	40	0.18	3.96 mol/h × kg_{cat}	—	(42)
9	3.1 wt.	0.093 g	9.6:1:3.7	780 °C	25.2 ml/min	13.3	100	73	0.72	47.21 mol/h × kg_{cat}	—	(133)
10	0.63 wt.	2.000 g	5.5:1:5.5	750 °C	—	25.2	100	41.9	1.00	—	—	(81, 83)
11	1 mol.	0.100 g	3:1:0	700 °C	50.0 ml/min	38.5	94.8	49	0.52	189.49 mol/h × kg_{cat}	—	(29)
12	3 mol.	0.100 g	3:1:0	700 °C	50.0 ml/min	38.3	91.4	55	0.51	211.59 mol/h × kg_{cat}	—	(29)
13	5 mol.	0.100 g	3:1:0	700 °C	50.0 ml/min	30.4	68.4	54.1	0.54	165.20 mol/h × kg_{cat}	—	(29)
14	10 mol.	0.100 g	3:1:0	700 °C	50.0 ml/min	16.1	43.4	56.2	0.61	90.89 mol/h × kg_{cat}	—	(29)

15	15 mol.	0.100 g	3:1:0	700 °C	50.0 ml/min	5.8	12.8	54	0.67	31.46 mol/h × kg_{cat}	—	(29)
16	Li/Mg = 0.1	0.100 g	3:1:0	750 °C	17.0 ml/min	28.7	n.s.	63.1	0.91	61.85 mol/h × kg_{cat}	Code A	(34)
17	Li/Mg = 0.1	0.100 g	3:1:0	750 °C	17.0 ml/min	22.1	n.s.	59.7	1.25	45.06 mol/h × kg_{cat}	Code B	(34)
18	Li/Mg = 0.1	0.100 g	3:1:0	750 °C	17.0 ml/min	24.8	n.s.	56.9	1.25	48.19 mol/h × kg_{cat}	Code C	(34)
19	Li/Mg = 0.1	0.100 g	3:1:0	750 °C	17.0 ml/min	19.7	n.s.	65	1.25	43.73 mol/h × kg_{cat}	Code D	(34)
20	Li/Mg = 0.1	0.100 g	3:1:0	750 °C	17.0 ml/min	33.5	n.s.	55.8	0.71	63.84 mol/h × kg_{cat}	Code E	(34)
21	Li/Mg = 0.1	0.100 g	3:1:0	750 °C	17.0 ml/min	18.6	n.s.	30.6	2.00	19.44 mol/h × kg_{cat}	Code F	(34)
22	Li/Mg = 0.1	0.100 g	3:1:0	750 °C	17.0 ml/min	6.6	n.s.	66.6	3.33	15.01 mol/h × kg_{cat}	Code G	(34)
23	Li/Mg = 0.1	0.100 g	3:1:0	750 °C	17.0 ml/min	21.8	n.s.	59.6	1.43	44.37 mol/h × kg_{cat}	Code H	(34)
24	Li/Mg = 0.1	0.100 g	3:1:0	750 °C	17.0 ml/min	31.7	n.s.	59	0.63	63.87 mol/h × kg_{cat}	Code I	(34)
25	Li/Mg = 0.1	0.100 g	3:1:0	750 °C	17.0 ml/min	29.6	n.s.	59.1	0.77	59.74 mol/h × kg_{cat}	Code J	(34)
26	Li/Mg = 0.1	0.100 g	3:1:0	750 °C	17.0 ml/min	36.1	n.s.	60.1	0.59	74.10 mol/h × kg_{cat}	Code K	(34)
27	Li/Mg = 0.1	0.100 g	3:1:0	750 °C	17.0 ml/min	25.1	n.s.	64.9	0.77	55.63 mol/h × kg_{cat}	Code L	(34)
28	Li/Mg = 0.1	0.100 g	3:1:0	750 °C	17.0 ml/min	38	n.s.	55.3	0.42	71.77 mol/h × kg_{cat}	Code M	(34)
29	Li/Mg = 0.1	0.100 g	3:1:0	750 °C	17.0 ml/min	24.5	n.s.	52.2	1.25	43.68 mol/h × kg_{cat}	Code N	(34)
30	Li/Mg = 0.1	0.500 g	4:1:0	750 °C	86.0 ml/min	11.9	n.s.	50	3.33	21.93 mol/h × kg_{cat}	—	(16)
31	Li/Mg = 0.1	0.500 g	4:1:0	750 °C	86.0 ml/min	27.6	n.s.	64	1.18	65.10 mol/h × kg_{cat}	—	(16)
32	0.66 wt.	0.093 g	10:1:0	780 °C	25.2 ml/min	4.4	50	66.4	1.37	19.30 mol/h × kg_{cat}	—	(28)

(*Continued*)

Table 1: (*Continued*).

No.	Catalyst	Mass	CH_4:O_2: Dilutent	Temperature	Flow rate	X_{CH_4} (%)	X_{O_2} (%)	S_{C_2} (%)	C_2H_6/ C_2H_4	STY	Comment	Ref.
33	1.71 wt.	0.093 g	10:1:0	780 °C	25.2 ml/min	10	75	75.1	75.1	49.60 mol/h × kg_{cat}	—	(28)
34	2.47 wt.	0.093 g	10:1:0	780 °C	25.2 ml/min	11.1	85	71.7	1.12	52.57 mol/h × kg_{cat}	—	(28)
35	3.19 wt.	0.093 g	10:1:0	780 °C	25.2 ml/min	11.4	88	72	1.24	54.21 mol/h × kg_{cat}	—	(28)
36	0.02 wt.	2.000 g	3.7:1:17.4	650 °C	50.0 ml/min	4.1	n.s.	7.6	—	0.03 mol/h × kg_{cat}	—	(134)
37	0.05 wt.	2.000 g	3.7:1:17.4	650 °C	50.0 ml/min	6.2	n.s.	9.6	—	0.07 mol/h × kg_{cat}	—	(134)
38	0.10 wt.	2.000 g	3.7:1:17.4	650 °C	50.0 ml/min	7.6	37.0	17.5	—	0.15 mol/h × kg_{cat}	—	(134)
39	0.15 wt.	2.000 g	3.7:1:17.4	650 °C	50.0 ml/min	9.3	44.4	25.7	—	0.27 mol/h × kg_{cat}	—	(134)
40	0.20 wt.	2.000 g	3.7:1:17.4	650 °C	50.0 ml/min	8.2	38.3	35.7	—	0.33 mol/h × kg_{cat}	—	(134)
41	0.25 wt.	2.000 g	3.7:1:17.4	650 °C	50.0 ml/min	9.6	36.8	30.8	—	0.33 mol/h × kg_{cat}	—	(134)
42	1.00 wt.	2.000 g	3.7:1:17.4	650 °C	50.0 ml/min	9.1	44.8	36.4	—	0.37 mol/h × kg_{cat}	—	(134)
43	5.00 wt.	2.000 g	3.7:1:17.4	650 °C	50.0 ml/min	8	30.4	34.5	—	0.31 mol/h × kg_{cat}	—	(134)
44	7.00 wt.	2.000 g	3.7:1:17.4	650 °C	50.0 ml/min	6	27.4	30.6	—	0.21 mol/h × kg_{cat}	—	(134)
45	10.00 wt.	2.000 g	3.7:1:17.4	650 °C	50.0 ml/min	7.6	n.s.	35.6	—	0.30 mol/h × kg_{cat}	—	(134)
46	0.2	4 ml	3:1:0	700 °C	75.5 ml/min	29.8	94.2	58.8	2.40	6.64 mol/h × l_{cat}	—	(79)
47	2.0	4 ml	3:1:0	700 °C	85.7 ml/min	22.1	63.9	62.8	1.54	5.97 mol/h × l_{cat}	—	(79)
48	5.0	4ml	3:1:0	700 °C	88.0 ml/min	11.8	27.8	53	2.27	2.76 mol/h × l_{cat}	—	(79)

49	5	4 ml	3.3:1:0	720 °C	43.2 ml/min	2.7	n.s.	65.4	0.65	0.39 mol/h × I_{cat}	—	(135)
50	5	4 ml	3.3:1:0	550 °C	43.2 ml/min	1.6	n.s.	22.5	3.5	0.08 mol/h × I_{cat}	—	(135)
51	0.6	1.25 ml	2:1:7.1	680 °C	50.0 ml/min	38	n.s.	35	0.59	2.82 mol/h × I_{cat}	After 10 h	(126)
52	1.2	1.25 ml	2:1:7.1	680 °C	50.0 ml/min	30	n.s.	41	0.71	2.61 mol/h × I_{cat}	After 10 h	(126)
53	4 wt.	3.000 ml	2:1:6.3	700 °C	74.0 ml/min	34.4	n.s.	46.7	0.46	2.28 mol/h × I_{cat}	After 30 min	(136)

n.s., not specified

Asami and co-workers observed that the non-catalytic oxidative coupling of CH_4 was considerably enhanced under pressures up to 16 bar and in a temperature range between 650 and 800 °C (138).

Ekstrom et al. investigated the effect of pressure (range of 1–6 bar) on the OCM reaction (139). They found that with increasing pressure the importance of the uncatalyzed reaction also increased significantly. This is in agreement with the results of Lane and Wolf (140). The pressure dependency of the catalyzed and uncatalyzed reactions were different; at high pressures and low flow rates the uncatalyzed reactions were predominant. Moreover, they found that at high flow rates the C_{2+} selectivity decreased with increasing pressure. Pinabiau-Carlier et al. also investigated the effect of the pressure on the OCM, but not with a Li/MgO catalyst (141).

Edwards and co-workers studied the OCM in a fixed-bed and a fluidized-bed reactor (20). They found that increasing the pressure in the fixed-bed reactor led to an increase in CH_4 conversion, but in a reduced C_2 selectivity.

Chen et al. studied the effect of pressure (up to 10 bar) on the oxidative coupling of methane in the absence of a catalyst (142). The conversion of CH_4 and O_2 increased with pressure at constant temperature and residence time. Increasing pressure favored the oxidative route from C_2H_6 to C_2H_4 compared to the pyrolytic route. The methyl and the hydrogen peroxy radicals were reported to be the most abundant radicals, however, this was concluded on the basis of a model (142, 143).

Parida and Rao found that the key factor of the OCM was a low specific surface area, however, there should be an optimal surface area. Furthermore, it was found that the C_2 selectivity increased with an increasing basicity (144).

Iwamatsu et al. studied different alkali-doped MgO for the oxidative coupling of methane (12, 13, 120). They found that a low surface area was a very important factor for a high C_2 yield. Also, other researchers found that a low surface area was rather beneficial than detrimental for a high yield, for instance, Lunsford et al. (85). In an investigation with a series of metal oxides supported on $SrCO_3$, Aika and co-workers found that a decrease in catalyst surface led to an increase in the C_2 formation, concomitantly suppressing the total oxidation (145).

Rynkowski et al. reported on the influence of the calcination temperature on the surface area of SiO_2, Al_2O_3, and MgO, comparing this with the results obtained when these oxides were promoted with Li (146). The addition of Li led to a significant decrease in the BET surface area after calcination, compared to the undoped sample.

Kuo et al. showed that the reduction of surface area, which is induced by the incorporation of Li, could be compensated by addition of activated charcoal at the start of the preparation procedure (35). The charcoal was burned off in the calcination step. The surface area increased and the morphology was modified. The effect of the charcoal addition could be avoiding the formation

of large MgO crystals. The conversion and selectivity of the catalysts (per unit surface area) was found to be nearly independent of the specific surface area. Therefore, Kuo and co-workers concluded that the effect of the BET surface area on the activity, reported in earlier studies, was probably influenced by the residence time and it is not a pure effect of the BET surface area. However, a correlation was found between the CH_4 conversion, the total surface area in the reactor, and an inverse correlation between catalyst density and specific surface area of the catalyst. The variation of the BET surface area in these experiments was only between approximately 0.5 m^2/g and 3.0 m^2/g.

The results of experiments with different catalysts indicate the idea that an optimal surface area, which is not too high, exists for the OCM (62). However, the authors also argued that more detailed work is necessary to substantiate this idea, as it cannot be excluded that the OCM is a structure sensitive reaction. For such a case, a heat treatment of the catalysts would not only lead to a reduced surface area, but also to a different surface morphology.

4.4. Summary

Deactivation of Li/MgO is due to a loss of Li as LiOH, which is formed from Li-compounds with the reaction product H_2O. Deactivation is partly suppressed by CO_2 transforming Li_2O into the more stable Li_2CO_3. There seems to be a general trend that high carbonate-containing materials are more stable and more selective towards C_2 formation than such with small carbonate content. The role of the LiOH vapor in the gas phase has not yet been investigated, although this problem has been mentioned by Martin and Mirodatos (62).

The rate of deactivation, in particular of sintering, depends on the gas composition around the catalyst. High CH_4 conversions, and, therefore, high partial pressures of H_2O, lead to a high deactivation. High amounts of dilutent in the feed gas seem to supress deactivation. Both are detrimental to an industrial application. Supporting Li/MgO on SiO_2, Al_2O_3, and Cr_2O_3 did not lead to any significant improvement with respect to catalyst stability.

Catalyst selectivity towards C_2 of Li/MgO increased by doping Li/MgO with certain dopants like Mn, Cd, and Zn; however, activity was negatively affected. Operating conditions and the dimensions of the reactor also influence selectivity. Usually, temperatures in the range of 700 to 800 °C lead to the best selectivities, while at lower as well as higher temperatures, selectivity deteriorates due to total oxidation. High ratios of partial pressures of CH_4 to O_2 results in better selectivity than in the reversed case. Furthermore, the absolute pressure of O_2 is also a selectivity-determining factor: higher O_2 partial pressures favor total oxidation. Any excessive hotspots within the reactor as well as transport limitations should be avoided since selectivity is negatively affected.

At higher pressures, non-catalytic gas phase oxidation reactions can occur leading also to some C_2 formation, even though small in comparison to CO_x. Even though under typical OCM conditions, mixtures are outside flammability limits at atmospheric pressure, it cannot be excluded that gas phase reactions also play an important role there, as radicals released of the catalyst might initiate gas phase radical chain processes.

5. MECHANISTIC STUDIES

5.1. General Mechanistic Studies

Ito et al. conducted experiments with a series of differently doped Li/MgO catalysts. It was reported that their 7 wt% Li/MgO prepared catalyst reached a steady state after 15 h time on stream and remained a stable performance until the end of the experiment, 32 h time on stream (9). The reaction conditions were 700 °C, 1 g of catalyst, feed gas composition: CH_4:O_2:He = 3:1:21.3, flow: 50 ml/min, which are typical laboratory conditions. It was proposed that the coupling of two $CH_3\cdot$ radicals lead to the formation of C_2H_6 and that C_2H_4 is formed via the oxidative dehydrogenation of C_2H_6. The measured EPR signals were in agreement with the ones Abraham and co-workers assigned to $[Li^+O^-]$ (147), suggesting the presence of this defect. Later, the EPR technique was used to observe the formation of methyl radicals, when CH_4 was passed over pure MgO at 500 °C (10, 148). Depending on the kind of pretreatment, significant differences in the initial activity were observed. Vacuum pretreatment did not lead to an increase in activity, while pretreatment in O_2 did increase the initial activity, observed as an improved formation of methyl radicals. The formation of $[Li^+O^-]$ centers in single crystals of MgO doped with Li at temperatures between 1000 to 1300 °C was reported and extensively studied before by Abraham et al. (101), Chen et al. (103), Lacey et al. (106), Boldu et al. (107), Olson et al. (108), Chen et al. (109), and Abraham et al. (147). It was shown that these centers also formed at temperatures between 500–1000 °C in an O_2 atmosphere, even if the intensity differed (10).

Yates and Zlotin observed that the uncatalyzed thermal reaction, in an empty reactor, contributed significantly to the oxidative coupling of methane (149). The results obtained at 700 and 720 °C are shown in Table 2. It is evident that in the applied reactor system, the blank reaction contributed significantly to the CH_4 conversion, however, the total oxidation was dominant. Moreover, the main contribution of the catalysts was the oxidation of CO to CO_2. Only Li/MgO showed an increase in C_2H_4 selectivity. Ito and Lunsford et al. (8), Ito et al. (9), and Liu et al. (150) had reported in their earlier studies that only 0.2% conversion in the blanc reactor were observed. Yates and Zlotin explained the difference to their observed values with a difference in the reactor geometry (149). Remarkably, the obtained values for the reactor with catalysts did

Table 2: The applied reaction conditions were: flow rate 50.0 ml/min, composition: CH_4:O_4:Dilutent = 1.8:1:3.6 and 4.1 g catalyst. Table adopted from Table 3A in (149).

				Product Composition (mol%)			
Temperature	**Catalyst**	X_{CH_4}	S_{C_2}	**CO**	CO_2	C_{2H_4}	C_{2H_6}
700 °C	None	22.3%	20.9%	73.9	14.4	6.9	4.8
700 °C	MgO	34.6%	17.4%	15.2	75.5	6.0	3.2
700 °C	3% Li/MgO	39.4%	37.6%	2.1	74.8	15.8	7.3
720 °C	None	26.8%	19.6%	73.0	16.0	7.1	3.8
720 °C	MgO	35.0%	18.2%	13.7	76.3	7.1	2.9
720 °C	3% Li/MgO	39.2%	36.5%	2.1	75.7	15.6	6.6

not differ so significantly. The authors concluded that the function of Li/MgO in the OCM is extremely complex and that homogeneous *and* heterogeneous reaction is important.

In the ensuing discussion, Hatano and co-workers argued that the variations in the results could be explained with differences in residence time (151). The residence time in the experiments of Ito and Lunsford et al. (8), Ito et al. (9), and Liu et al. (150) was shown to be less than 5 sec, whereas the set-up of Yates and Zlotin had a residence of above 20 sec (149). Furthermore, it was emphasized that the extent of the homogeneous reactions was also strongly influenced by the free volume, a factor which was also different in the works of Lunsford and Yates. Different CH_4 conversions were reported in case of an empty reactor or a reactor filled with fused-quartz rings and the question was raised, why Yates and Zlotin (149), but also Lane and Wolf (140), did not observe differences for such experiments. Regarding the O_2 conversion, it was argued that under the conditions Yates and Zlotin applied, most of the O_2 had already been consumed before reaching the catalyst bed. Lunsford and coworkers concluded summarizingly, that in their experiments the homogeneous contribution was not significant and that it seemed unlikely that C_2 yield could be achieved purely by homogeneous reactions (151).

Yates and Zlotin (152) replied that they published a $Li_2B_4O_7$, which did not have any combustion activity and, therefore, did not produce significantly more CO_2 than the empty reactor (153). It was critized that Lunsford and coworkers did not cite this work. They also argued that the O_2 conversion in their work and that of Lunsford did not differ as significantly as argued by Lunsford, since the same reaction conditions were applied. This debate shows that several research groups can obtain different results, alone due to differences in the reactor set-up. Further detailed experiments under controlled and comparable conditions will be necessary to unreveal structure activity correlations.

It is reported that the contribution of the gas phase depends on the exact operating conditions (partial pressures of all compounds, temperature,

residence time, and free reactor volume) (154). Yates and Zlotin and other researchers did observe significant contributions of gas phase reactions for the OCM. Therefore, it can be concluded that Lunsford et al. underestimated the importance of gas phase reactions, maybe due to their small scale experimental set-up and the applied reaction conditions.

Hutchings and co-workers studied the partial oxidation of CH_4 at 5.85 kPa at higher temperatures, ca. 700–800 °C with and without the presence of a catalyst (155). The product yields were similar in the presence and absence of the catalyst, which indicated that a suitable catalyst is of secondary importance at this temperature, in agreement with the results of Yates and Zlotin (149).

Hutchings et al. compared the selectivities of Li/MgO and MgO in order to study the role of Li. Since Li/MgO showed higher selectivities for C_2H_6, they assumed that the role of Li could be the inhibition of the oxidative dehydrogenation activity of the MgO (156).

Korf and co-workers showed that the active sites were formed as a result of the loss of carbonate species and that they were unstable under the reaction conditions of the OCM, namely reducing conditions. Catalysts with a high concentration of carbonate species produced more C_2 products than catalysts with a lower concentration of these species. Because calcination at lower temperatures led to a higher residual CO_2 content of the catalysts, it also led to a higher catalytic activity. Furthermore, the formation of the active sites was suggested to be a direct result of the loss of carbonate species, which were unstable under the reaction conditions of the OCM, namely reducing conditions (28).

Roos and co-workers investigated the reaction pathway of the OCM over Li/MgO (157). A recycle system was applied that behaves like a gradientless reactor with respect to the gas phase concentrations; a description can be found in (158). It was found that at 720 °C the reaction followed a sequential reaction scheme, as shown in Reaction 5. Furthermore, they found that the presence of alkali carbonates and an excess of CH_4 decelerated the total oxidation of C_2H_6 and C_2H_4.

$$CH_4 \rightarrow C_2H_6 \rightarrow C_2H_4 \rightarrow CO_x \tag{5}$$

Van Kasteren and co-workers investigated the nature of the active compound of Li/MgO via comparison of the activity and the deactivation of Li/MgO catalysts and Li_2CO_3 supported on ZrO_2 (123). The O_2 conversion of their 7 wt% Li/MgO increased during the first 16 h, nearly to full conversion, followed by a steady deactivation. It was also shown that the Li content decreased during the whole time on stream. For 0.2 wt% Li/MgO, deactivation and loss of Li were observed from the beginning. However, the initial values of conversion were the same for both catalysts. It was concluded that only a small amount of the Li was responsible for the activity. Li_2CO_3 alone supported on the inert carrier ZrO_2 revealed that Li_2CO_3 was also an active OCM catalyst,

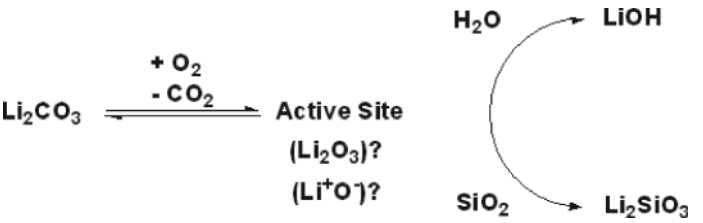

Figure 5: The working hypothesis of the Li/MgO catalysts, as proposed by van der Wiele et al. In the presence of O_2, Li_2CO_3 decomposes to form the active site, which reacts with CH_4. The deactivation proceeds through evaporation, reaction with H_2O to LiOH, or the formation of Li_2SiO_3, reaction with SiO_2 from the quartz of the reactor material, which is being almost inert. Unchanged figure adapted from (123). Reprinted from van Kasteren, J.M.N.; Geerts, J.W.M.H.; van der Wiele, K. Working Principle of Li Doped Mgo Applied for the Oxidative Coupling of Methane. *Stud. Surf. Sci. Catal.* **1990**, *55*, 343–349. Copyright with permission from Elsevier via the Copyright Clearance Center.

with a performance identical to Li/MgO, except for lower activity due to the lower specific surface area. The activity lasted as long as Li_2CO_3 was present. It was shown that Li_2ZrO_3, which was also an active catalyst, was not the active phase here, as it was not present. From this information, a working hypothesis of Li/MgO was developed, as shown in Figure 5. These results are in agreement with results published by Mirodatos and co-workers (119, 122).

Lunsford and co-workers studied the Reaction 6 over (LiCl+NaCl)/MgO (159). With a matrix isolation system, methyl radicals were observed.

$$CH_4 + C_2H_4 \rightarrow C_3H_6 \tag{6}$$

However, vinyl radicals could not be detected. With isotopic experiments it was shown that the methyl group, which was added to the alkene, was derived from the CH_4.

Chen et al. studied the OCM with a co-feed of C_2H_6 in the presence and absence of Li/Sn/MgO as catalyst (19). They found an increase in the feed conversion in the absence of catalyst. It was concluded that this was due to an increase in the concentration of radicals. Co-feeding in the presence of the catalysts resulted in a small increase in O_2 conversion and a decrease in the CH_4 conversion. The later one probably occurred due to a competition with C_2H_6 for the active site. The rate determining step was determined to be the regeneration of the active center. However, a beneficial effect of co-feeding C_2H_6 in the presence of the catalyst was not found. Based on this result, it was concluded that for the upgrade of natural gas the C_2H_6 should be separated beforehand.

Many of the above-described results were obtained by steady state experiments. However, transient experiments can also significantly contribute to a mechanistic understanding of a reaction. Many of the results in the following paragraphs and sections were obtained by transient experiments. In an

excellent review article from Schuurman and Mirodatos, the use of transient kinetic experiments for methane activation, including the OCM, has been summarized and discussed (160).

5.2. Reactant Activation

5.2.1. Oxygen Activation

Nibbelke et al. showed that O_2 interacts strongly with the catalyst. It reversibly adsorbed dissociatively and an exchange between the surface and the bulk oxygen took place (161). Doping with Li, even more with Sn, increased the oxygen diffusion coefficient, therefore, increasing the exchangeable amount of oxygen on the catalyst. CO_2 interacted with the catalyst, in the absence of the reactants, only in the presence of Li.

Peil and co-workers used steady-state isotopic transient kinetic analysis (SSITKA) to investigate surface phenomena in the OCM over MgO and Li/MgO at temperatures up to 645 °C (162–164). They found that the MgO and the Li/MgO catalysts could be divided into three regions:

1. physical surface where the oxygen exchange between gas phase and solid phase takes place,
2. several layers of subsurface oxygen atoms that are readily available for exchanges, and
3. the bulk oxide.

The subsurface oxygen and the bulk oxygen were significant additional oxygen sources. The investigation of the pathway of CO_2 suggested a multi-step oxidation pathway. Active sites that were involved in the coupling process were found to have a lower activity than active sites involved in the selective processes (162–164).

Dahl et al. conducted characterization studies of Li/MgO in a pulse reactor, exposing the catalyst to pulses of air, CH_4, and air-CH_4 mixtures (165). The results indicated that the catalyst was active even with small amounts of Li_2CO_3, and O_2 may reversibly adsorb on the surface. Additionally, Li/MgO could act as an "oxygen reservoir."

Contradictory results to Peil and Nibbelke have been published by Choudhary et al. (166). With pulse of CH_4, C_2H_6, and C_2H_4 in the presence and absence of gas phase O_2 over Li-, La-, and Sm-promoted MgO, it was shown that the lattice oxygen of these catalysts did not have a significant role in the OCM and the presence of free O_2 is necessary for the OCM. The lattice oxygen is involved in the conversion of C_2H_6 and C_2H_4, however, the importance for the oxidation of C_2H_4 seemed to be more significant than for the oxidation of

C_2H_6. Similar results were found for Li/MgO with additives (87) and for the oxidation of C_2H_4 over Li/MgO (89).

Keulks and co-workers studied the oxygen species with temperature programmed reactions in the oxidative coupling of methane over various catalysts, among them: Li/MgO (167). Their results suggested that simple adsorbed oxygen species were not active for coupling, but for total oxidation. For simple oxide catalysts, such as Li/MgO, gas phase O_2 was necessary for the generation of the oxygen species active for the coupling reaction. Nevertheless, for multicomponent catalysts, the lattice oxygen regenerates the active oxygen species. The results of Bhumkar and Lobban also suggested that gas phase O_2 was involved in the regeneration of the active sites and in the CO_2 formation (168).

5.2.2. Alternative Oxygen Sources

Nakamura and co-workers studied the decomposition of N_2O on Li/MgO investigating the adsorbed oxygen species being formed (169). It was demonstrated that a substantial amount of adsorbed oxygen species were formed. Moreover, the formed amount increased by doping MgO with Li. Experiments with molecular oxygen resulted in a much lower formation of adsorbed oxygen species. TPD experiments revealed two types of adsorbed oxygen species on Li/MgO, the α-species desorbing between 400–420 °C and the β-species at 480–495 °C. In contrast, for pure MgO only a weak α-oxygen species was found. It was suggested that the α-oxygen species was present on higher index faces of MgO, whereas the β-oxygen species was present at oxygen vacancies in the neighborhood of places where Li substituted Mg. The hydrolysis of the oxygen species, by soaking the samples in a solution of H_2SO_4, resulted in considerable amounts of H_2O_2, suggesting that they were mainly present as surface peroxides.

The use of different oxygen sources for the oxidative coupling of methane has been reviewed by Hutchings et al. (170, 171). Only publications that refer to Li/MgO as a catalyst will be discussed in detail here.

Hutchings and co-workers investigated the role of surface O^- in the selective oxidation of CH_4 using N_2O as oxygen source (135, 172). They showed that $O^-_{(s)}$ has two roles:

1. at low temperatures: hydrogen abstraction
2. at high temperatures: non-selective oxidation

Using O_2 as an oxygen source, the CH_4 conversion was an order of magnitude higher than with N_2O. However, at comparable conversions, N_2O led to higher selectivities than O_2.

In contrast to this, while studying the decomposition of N_2O and the activation of CH_4 with O_2 and N_2O over Li/MgO and MgO doped with alkaline earth

oxides, Cunningham and McNamara found that O_2 was the more effective oxygen source; generally resulting in higher conversion and higher selectivities (173).

Later, Hutchings et al. studied the OCM over Li/MgO in the presence of NO (174). They found that in the presence of NO, Li/MgO showed at least two different oxidizing species or oxidizing sites, which were significant. In the OCM over MgO and Li/MgO in the presence of different nitric oxides, different trends were observed for these two catalysts, therefore, indicating different reaction mechanisms for MgO and Li/MgO (175).

In 1988, the same group did a comparative study of O_2, O_3, and N_2O as oxygen source for the OCM over Li/MgO, MgO, and γ-Al_2O_3 (128, 176). Below 400 °C, O_3 was more active and selective than O_2. The products under these conditions were only H_2, CO_2, and CO. H_2O could not be detected. The addition of H_2O did not affect the product selectivity. O_2 and O_3 showed a similar performance at higher temperatures, while at low temperatures (200–300 °C) O_3 showed higher performance. Nitrous oxides appeared to enhance the partial oxidation at low temperatures (550 °C), while at higher temperatures (720 °C), it increased the formation of total oxidation products. However, deactivation of the catalyst was observed.

The kinetic isotope effect during the oxidative coupling of methane over Li/MgO was studied by Shi and co-workers (177). When using O_2 as the oxygen source, it was found that a single rate limiting step did not exist. For N_2O, the rate limiting step was the incorporation of the oxygen into the crystal lattice of the Li/MgO.

Yamamoto et al. studied the OCM over Li/MgO with N_2O as the oxygen source (178). The rate of oxygen incorporation into the catalyst was slower with N_2O than with O_2. However, at the same CH_4 conversion levels, N_2O led to higher selectivities than O_2, probably due to a decrease of surface reactions, which led to CO_x. Applying N_2O as oxidant, pure MgO exhibits a much higher CH_4 conversion in comparison to Li/MgO, however, its C_2 selectivity was rather low.

5.2.3. Methane Activation

Davydov et al. investigated the character of the primary CH_4 activation on MgO (179). They observed that the CH_4 activation on MgO formed CH_3 groups.

The effect of CO_2 on the selectivity of OCM and ODH of C_2H_6 over Li/MgO at temperatures below 650 °C was investigated by Wang and co-workers. It was found that secondary reactions of the methyl radicals on the catalyst surface are inhibited by CO_2 (180). In this publication, it was also commented that Korf et al. did not observe an effect of CO_2 on the C_2 selectivity (28). The reason could be that the reaction temperature in Korf's experiments was 780–800 °C and the selectivity of 78%, was already high. The main source of CO_2 at this

temperature was the total oxidation of C_2H_6 and C_2H_4 in the gas phase (181). Thus, the importance of surface phenomena, like secondary reactions of the methyl radicals, decreased, however, the formation of methyl radical still took place (180).

The effect of CO_2 on the activation energy for the $CH_3\cdot$ formation and the overall CH_4 consumption in the OCM over Li/MgO was investigated by Xu et al. [182]. They found that in the gas phase, CO_2 increased the intrinsic activation energy for the $CH_3\cdot$ formation by 100% with increasing partial pressure of CO_2. The activation energy approached a limiting value of 209 kJ/mol at CO_2 partial pressures higher than 0.001 bar, a value which is definitely being achieved under typical reaction conditions for the OCM. CO_2 acted as a catalyst poison, because it adsorbed at the basic oxygen ions, which were believed to be responsible for the activation of CH_4. At lower temperatures, more active sites were poisoned than at higher temperatures.

Coulter and Goodman showed that the rate-limiting step of the OCM depended on the CO_2 coverage of the catalyst. Their results indicated that at low partial pressures of CO_2, the C-H bond cleavage is the rate determining step, while at high partial pressures of CO_2 the desorption of CO_2 is the rate determining step (183).

Cant et al. observed that the rate of conversion of CH_4 over Li/MgO is 1.5 times larger than the rate of CD_4, indicating that the C-H bond breaking is the rate determining step (184). The influence of a possible rearrangement of OH, respectively, OD sites on the catalyst were excluded via experiments with D_2O addition.

Lapszewicz and Jiang studied the relationship between activity, selectivity, and basicity and the ability of C-H and O-O bond scission of γ-Al_2O_3, MgO and monoclinic or cubic Sm_2O_3 (185). Isotopic exchange rates were measured to determine the ability of these materials to activate the reactants of the OCM. Since a correlation was not found, it was concluded that the formation of the methyl radical cannot be explained simply by a one-step mechanism.

5.3. Reaction Network

5.3.1. Reaction Intermediates

Bhumkar and Lobban observed *in situ* the surface features of Li/MgO and its interactions with adsorbates at steady state and transient conditions, applying diffuse reflectance Fourier transform infrared spectroscopy (DRIFTS) (168). Under reaction conditions, adsorbed CO_2 strongly bonded to OH groups and carbonate was found. CO_2 in the gas phase reduced the catalytic activity due to adsorption and reaction to carbonate. However, H_2O had a positive effect on the carbonate decomposition.

The presence of carbene during the OCM reaction was shown by Martin and Mirodatos (186). They introduced C_2H_4 into the reactor, which was transformed into cyclopropane. Later this was confuted by Mims and co-workers (187).

Martin et al. studied the heterogeneous and homogeneous processes involved in the OCM over Li/MgO (188). They compared the conversion, selectivities, and yields of CH_4/O_2 and C_2H_6/O_2 mixtures. The observed differences were likely to be due to the much shorter lifetime of the $C_2H_5\cdot$ radical, preventing subsequent heterogeneous deep oxidation. CH_4 mixed with other hydrocarbons led to cross coupling products, if the C-H bond strength is relatively small (for example propene and toluene in contrast to benzene). Cross-coupling of CH_4 and C_2H_4 was also observed by Lunsford et al. (159).

Nibbelke et al. investigated the heterogeneous steps of the OCM over Li/MgO and Li/Sn/MgO. As mentioned above, for a fully satisfying explanation of the obtained results, a methoxy species was postulated, which was the only carbon containing intermediate leading to the formation of CO_2 (161).

5.3.2. Product Formation

Geerts and co-workers investigated the individual reaction steps in the oxidative coupling of methane over Li/MgO, studying the oxidation of C_2H_6, C_2H_4, and CO separately (189). It was found, that the conversion of C_2H_6 to C_2H_4 was faster than the total oxidation of C_2H_6, irrespective of the catalyst. The conversion of C_2H_6 proceeded much faster than the conversion of CH_4. The combustion proceeds mainly via C_2H_4, which would be a serious constraint for the maximal achievable yield.

Campbell and Lunsford investigated the contribution of the gas phase radical coupling in the oxidative coupling of methane. They found a good agreement between the yield and the methyl radical formation. The CO_2 partial pressure was also found to be an important variable (190).

Van Kasteren et al. used low pressure experiments to discriminate between the homogeneous and the heterogeneous reactions (191). The Li/MgO in the OCM was proposed to activate CH_4 and to produce methyl radicals, which couple in the gas phase, in case a sufficient amount of third bodies are available. Furthermore, it was shown that Li/MgO was involved in the total oxidation of C_2H_6, C_2H_4, and CO.

This is in agreement with the work of Campbell et al. (192), concluding that at least 40–45% of the C_2 molecules were the product of gas phase coupling. That no significant hydrogen exchange was observed, indicates that the C-H breaking is an irreversible step.

In studies of the OCM with Li/MgO with a reactant mixture of CH_4, CD_4, and O_2 (193–195), no significant hydrogen exchange between CH_4 and CD_4 was detected. The only detected reaction products were:

1. Saturated products:
   a. C_2H_6
   b. CH_3CD_3
   c. C_2D_6
2. Unsaturated products:
   a. C_2H_4
   b. CH_2CD_2
   c. C_2D_4.

Depending on the concentration of the reactants, the relative concentration of the different products could be predicted. Based on these results, it was proposed that the formation of C_2H_6 occurred via the gas phase coupling of methyl radicals, and the oxidative dehydrogenation of C_2H_6 in the gas phase was the source of C_2H_4. However, the absence of hydrogen exchange is remarkable, because over pure MgO it has been reported to take place for C_2 hydrocarbons at 300 °C and for CH_4 at 400 °C (196), and the activation energy was determined to be 193 kJ/mol ± 14 kJ/mol (197). Even so, taking place at elevated temperatures, other researchers also reported the exchange between CH_4 and D_2 over MgO (185, 198). Balint and Aika could observe an isotopic exchange between CD_4 and the hydroxyl groups of the 1 wt% Li/MgO at room temperature (199).

Mims et al. also investigated the oxidative coupling of methane with CH_4/CD_4 mixtures (187). The results were in agreement with Nelson et al. (193–195). The OCM reaction mechanism via methylene, which was proposed by Martin and Mirodatos (186), could be excluded, because the only products formed are C_2H_6, CH_3CD_3, and C_2D_6.

A close relationship between the formation rate of C_2H_6 per unit surface area and the density of strong basic sites on the surface was observed by Choudhary et al. (16).

Hargreaves et al. observed at low O_2 conversions ($\leq$10%) high selectivities (60%) towards H_2CO and nearly no selectivity towards C_2 products. However, at an O_2 conversion of approximately 10%, a selectivity switch was observed. The selectivity towards H_2CO was negligible, while the C_2 approached 30%. The presence of H_2 was also observed, despite incomplete O_2 conversion (200).

5.3.3. Consecutive Reaction: Ethane to Ethylene

C_2H_6 is the primary C_2 product in OCM, but already below the temperature required for the C_2H_6 formation the oxidative dehydrogenation of C_2H_6 to C_2H_4 proceeds. Therefore, it is important not only to consider the coupling

of methyl radicals to C_2H_6, but also the ODH of C_2H_6, to produce the desired product C_2H_6.

Morales and Lunsford reported that 3 wt% Li/MgO was an effective catalyst for the ODH of C_2H_6 (181). They also showed that CO_x species were produced from the total oxidation of C_2H_6 as well as C_2H_4. They could further show that above temperatures of 675 °C the gas phase reactions became predominant. It was assumed that even the ODH of C_2H_6 reaction involved the generation of radicals, $C_2H_5\cdot$ radicals in case of the ODH of C_2H_6.

Chevalier and co-workers also observed that under reaction conditions of the OCM (800 °C), C_2H_6 was non-oxidatively dehydrogenated to C_2H_4 (42).

The importance of consecutive reactions was studied over the Li/MgO catalyst by van Kasteren et al. (201). The experiments were carried out at low pressures (0.0001–0.015 bar). It was found that C_2H_6 was converted 4 times faster than CH_4, mostly to C_2H_4. C_2H_4 was still oxidized 2.6 times faster than CH_4. The conclusion was that there should be an upper limit of the C_{2+} yield, which can be achieved with Li/MgO.

5.3.4. Consecutive Reaction: Total Oxidation

Reviewing the study of the single steps of the OCM reactions, Geerts et al. found that the main reaction pathway for the combustion proceeded via C_2H_4 (189). In the absence of a catalyst, the main combustion product was CO, while in the presence of a catalyst, CO_2 dominated. Similar results were observed by Mirodatos and co-workers. C_2H_6 was oxidized to CO already at 600 °C in the gas phase. At this temperature, the oxidative coupling was still very limited. This was identified as one of the biggest problems of the oxidative coupling of methane (202).

Roos and co-workers also compared the reaction pathways of C_2H_6 and C_2H_4 over Li/MgO and Ca/Sm_2O_3 (203). None of the molecules were found to be stable under reaction conditions. The total oxidation of C_2H_6 and C_2H_4 contributed significantly to the overall reaction network. Since Ca/Sm_2O_3 was the most active catalyst, its total oxidation activity for C_2H_6 and C_2H_4 was at least partially responsible for its lower selectivity compared to Li/MgO.

Nelson and co-workers and Cant and co-workers studied the kinetic isotope effect and the contribution of the oxidation of the C_2 products to the CO_2 formation with isotopic tracer experiments over Li/MgO with isotopic reactant mixtures (184, 193–195, 204, 205). They could show that above 740 °C 30–80% of the CO_2 derived from the oxidation of the C_2 hydrocarbons, while below 700 °C, were responsible for less than 10% of the CO_2 formation. Two pathways for the C_2 oxidation were possible:

1. competition of the C_2 products with CH_4 for O_2 in surface promoted reaction, and
2. competition for $CH_3\cdot$ by abstraction and combination, leading to the formation of CO_x.

Furthermore, their experiments showed that an exchangeable pool of CO_2 existed in the catalyst, indicating that Li_2CO_3 is present during the reaction. Besides, it was also found that the first step of activation was the bond breaking of a C-H bond.

In 1994, Mims and co-workers traced the secondary reactions of C_2H_4 with computer models and isotopic experiments (206). The oxidation of C_2H_4 had only little effects on the CH_4 conversion, even at comparable partial pressures. From the comparison with computer models, the surface was seen to quantitatively quench much of the oxidative gas phase radical chemistry. The C_3 and C_4 yield and the isotopic distributions agreed well with the described gas phase pathways.

The origin of CO_2 in the OCM was investigated with isotope experiments by Shi et al. (207). The results showed that the rate of CO_x formation from C_2 products was several times larger than the CO_x formation from CH_4, even for Li/MgO at temperatures below 700 °C. The rate constants for the formation of CO_x from CH_4 and from C_2H_4 depended on several factors like type of catalyst, reaction temperature, CH_4 to O_2 ratio, and type of oxidant. Under the studied reaction conditions, the ratio of CO_x formed from CH_4 and from C_2H_4, the C_2 selectivity and the C_2 yield tended to increase with increasing temperature. This suggested that the amount of CH_4 being converted to CO_x decreased.

5.3.5. Consecutive Reaction: Formation of Hydrogen, Reforming, and Water Gas Shift Reaction

Hargreaves and co-wokers studied the formation of H_2 in the OCM over MgO (208). H_2 had an unexpectedly high selectivity in the OCM reaction. The source was the water gas shift reaction but also thermal cracking of C_2H_6. However, the partial oxidation became more dominant at higher flow rates and low oxygen conversions.

Kinetic and mechanistic aspects of the ODH of C_2H_6 on Li/MgO were studied by Swaan et al. (209). The results indicated that H_2 and CO are unlikely to be the product of steam reforming, CO_2 reforming of C_2H_6, or the water gas shift reaction. H_2 and CO are most likely produced by the decomposition of ethoxy species on the surface.

Balint and Aika investigated the water gas shift reaction and the methane steam reforming over 1% Li/MgO with temperature programmed reactions and isotope labeled compounds (199). The experimental results suggested, that the contribution of water gas shift reaction to the amounts of CO_2 and H_2 formed in the oxidative coupling of methane was important, which is in contradiction to the results of Swaan et al. (209). Steam reforming of methane could not be observed. However, an isotopic exchange between CD_4 and the OH groups of the Li/MgO was observed at room temperature.

5.4. Debate About the Active Center

5.4.1. Defect Sites with Lithium and Oxygen

In their EPR experiments, Lunsford et al. found an EPR signal, which was in agreement with the signal Abraham et al. assigned to [Li^+O^-] (147). The methyl radical formation was correlated with the relative intensity of EPR signals, which were assigned to the concentration of the [Li^+O^-] centers, shown in Figure 6. Depending on this correlation it was concluded that the active center is [Li^+O^-] (10). They suggest that methyl radicals are formed via a hydrogen abstraction from CH_4 by the [Li^+O^-] centers. The mechanism proposed by Lunsford et al. is shown in Figure 7. An alternative pathway for the regeneration may also be possible, with an electron trapped in an oxygen ion vacancy (9).

However, no direct proof, e.g., by ENDOR, was given that the observed signal at $g = 2.054$ was indeed caused by [Li^+O^-]. Furthermore, the signal was never detected directly upon quenching from OCM conditions but only upon quenching after heating in air or pure O_2. It is, therefore, highly questionable whether the correlation observed in Figure 7 is indicative of the mechanism—suggested by Lunsford et al.

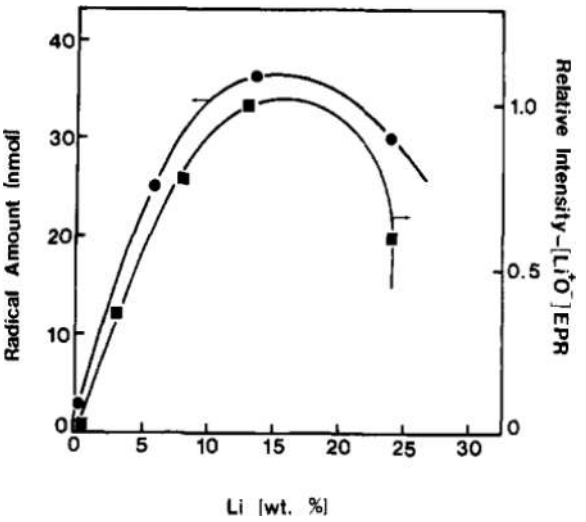

Figure 6: The amount of radicals and (Li^+O^-) centers formed as a function of lithium doping into MgO (Aldrich Gold Label). All reactions were carried out under the following conditions: T = 500 °C, collection period, 25 min (after 4 h on line), 0.50 g of catalyst, argon flow 3.8 cm^3min^{-1}, CH_4 flow 1.14 ccm^3min^{-1}, O_2 flow 0.023 cm^3min^{-1}. Preconditioned at 450 °C, 2.5 h, 300 $cm^3\,min^{-1}$ O_2. The samples were quenched in liquid nitrogen after a 2 h exposure to air at 700 °C. Figure unchanged from (10). Reprinted from Journal of the American Chemical Society, Vol. 107/1, Driscoll, D.J.; Martir, W.; Wang, J.X.; Lunsford, J.H. Formation of Gas Phase Methyl Radicals over Magnesium Oxide. *J. Am. Chem. Soc.* **1985**, *107* (1), 58–63. Copyright with permission from the American Chemical Society via the Copyright Clearance Center.

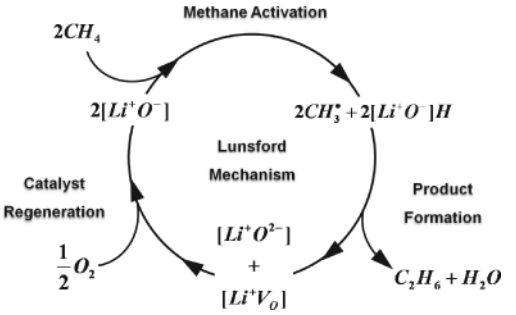

Figure 7: The mechanism of the CH_4 activation over Li/MgO and the regeneration of the active center as proposed by Lunsford and co-workers.

In 1986, the $[Li^+O^-]$ centers in Li/MgO were characterized by Wang and Lunsford (210). They found indications that these centers were formed at isolated substitutional Li^+ ions. These defects were believed to be responsible for the activation of CH_4. Later, Lunsford slightly modified his suggestion to $O^{\delta-}$ or O_3^- to take into account that the CH_4 activation is rate limiting for the OCM, whereas the activation by O^- was shown to be relatively rapid at low temperatures (85).

Peng and co-workers investigated the surface composition and the reactivity of Li/MgO with kinetic and XPS measurements (134). Under reaction conditions, they observed two Li containing phases in Li/MgO, namely $[Li^+O^-]$ and Li_2CO_3. The O(1s) XPS peaks were assigned to the surface $[Li^+O^-]$ and its concentration. Due to the correlation of the CH_4 conversion and the concentration of surface $[Li^+O^-]$, it was demonstrated that the $[Li^+O^-]$ species is the active center. Moreover, they determined that the concentration of the $[Li^+O^-]$ species seemed to be saturated at a Li loading of 0.2 wt%. They presumed that Li in excess to this, evaporated from the surface and/or diffused into the MgO. This value is in agreement with the discussion on the optimal loading of Li (78) and the experiments for the re-appraisal of the Li loading of Hutchings and co-workers (79).

However, Myrach et al. could not detect EPR signal compatible with $[Li^+O^-]$ (118).

5.4.2. F-Center

Wu et al. investigated the OCM over model catalysts of MgO and Li/MgO with combined surface science techniques under ultra high vacuum (UHV) conditions and kinetic measurements at elevated pressures. Their results indicated that the $[Li^+O^-]$ centers were not responsible for the activation of CH_4, but in fact the formation of F-type centers in the near surface region (211–214). The formation of C_2H_6 could be correlated with the F-type defects, determined by spectroscopic methods (213, 215). The effect of the pretreatment on the

active site of MgO and Li/MgO was also investigated (216). The C_2 product formation over MgO increased with increasing pretreatment temperature indicating that the active site for the CH_4 activation was most probably an F-type defect. This was in agreement with the thin film model (215). The formation of these defects was postulated as the rate determining step. However, for Li/MgO the rate determining step depended on the reactant gas mixture, namely whether O_2 was present or absent. Li is considered to be a promoter for the F-type defects, which could explain that in Li/MgO the rate determining step was different compared to MgO. It was suggested that in the presence of O_2, the decomposition of Li_2CO_3 was the rate determining step and in the absence of O_2 it was the H abstraction from CH_4 (216).

Nelson and Tench studied the chemisorption of O_2 on MgO. The experiments showed that in an O_2 atmosphere, the F-centers disappeared at 350 °C (217). However, statistical thermodynamics predict that at higher temperatures, more F-centers should be formed. If the F-centers are stable under OCM, conditions are unknown.

5.4.3. Mobile Lithium Carbonate Film

The deactivation of the Li/MgO catalysts was investigated in detail by Mirodatos and co-workers (119). It was found that a tight interface between Li_2CO_3 and MgO phases enabled an optimal catalytic performance. This was the case after a treatment, which allowed the liquefaction of the alkali salt. However, the static model of Li substitution, proposed by Ito et al. (9), Driscoll et al. (10), and Lin and co-workers (218), does not agree exactly with the model of the mobile Li_2CO_3-film coating the MgO (119). The role and the fate of the surface active site of Li/MgO was also studied (122). Uncarbonated MgO was reported to have a very poor activity for coupling and total oxidation. However, for Li/MgO, the total oxidation activity was reported to depend on the accessible surface area of Li_2CO_3, and the coupling activity was suggested to require an association of Li and Mg phases being enhanced after high temperature treatment. Under reaction conditions, the total oxidation selectivity was reported to decrease, due to the decomposition of Li_2CO_3.

5.5. Pure MgO

Aika and Lunsford investigated the dehydrogenation of alkanes by O^- on MgO, with EPR and catalytic experiments (219). The formation of alkenes was observed at 25 °C, the maximum was reached at 300 °C. For the reaction with alkanes, an alkoxide intermediate was proposed. For CH_4, a methoxide group was proposed, which decomposed at 450 °C, to form mainly H_2.

Iwamoto and Lunsford studied the oxidation of alkanes and alkenes by O_2^- on MgO, using EPR and catalytic experiments (220). Stochiometric reactions were observed with simple hydrocarbons at 175 °C, resulting in oxygenates,

hydrocarbons, and CO_2. It was proposed that the first step for the reaction of hydrocarbons with O_2^- is the abstraction of a hydrogen atom. Garrone and co-workers discussed in a note the formation of O_2^- on MgO in more detail (221).

Takita and Lunsford investigated the oxidation of alkanes by O_3^- on MgO, using EPR and catalytic experiments (222). The evidence suggested a direct reaction of the O_3^- with the hydrocarbons, rather than a dissociation of the O_3^- with subsequent reaction.

Ito et al. observed the activation of CH_4 on MgO at lower temperatures by means of TPD and ESR (electron spin resonance) experiments (223). It was found that the C-H bond was easily activated on the MgO surface, even below room temperature. Furthermore, the nature of the active site was discussed and it was shown that on MgO in low coordinated states the CH_4 adsorbs in the heterolytically dissociated state.

Hargreaves and co-workers reported the structural effects of the oxidative coupling of methane on two samples of MgO (80). MgO obtained via the thermal decomposition of carbonates was found to show higher C_2 selectivities than MgO obtained via burning Mg. The two MgO samples had different morphologies, which demonstrated that the morphology of MgO was an important factor for the OCM.

Zhen et al. characterized and studied the catalytic properties of MgO obtained from different preparation procedures (224). The used MgO materials were pure commercial MgO prepared via decomposition of $MgCO_3$ and the decomposition of $Mg(NO_3)_2$. The structural data and the catalytic performance were correlated and the important factors for the catalytic performance, namely temperature and specific surface area, were discussed.

Aika and Karasuda scrutinized MgO and its active site (225–227). It was proposed that the active site in MgO was an electron-deficient oxygen source, O^- for instance (225). Oxygen exchange experiments confirmed this (226). Later, they proposed that the adsorption of H_2O could be responsible for the generation of the active site (227). Figure 8 shows a model for the flux of oxygen atoms for different types of oxygen in MgO-based catalysts.

Hutchings and co-workers studied the oxidative coupling of methane in the presence of nitric oxides over MgO and Li/MgO (175). Since different trends for these two catalysts were observed, it was suggested that the reaction mechanism for the OCM over MgO and Li/MgO is different.

5.6. Summary

Based on the works of Abraham et al. (101), Chen et al. (103), Lacey et al. (106), Boldu et al. (107), Olson et al. (108), Chen et al. (109), and Abraham et al. (147) on Li doped MgO single crystals, $[Li^+O^-]$ defects most certainly exist, but their formation requires high temperature treatment under oxidative

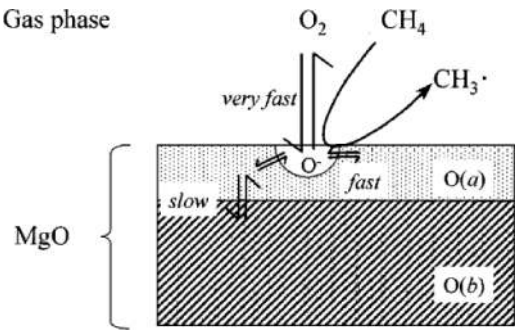

Figure 8: Model for oxygen atom flux in MgO-based catalysts, as proposed by Karasuda et al. Figure unchanged from (226). Reprinted from Journal of Catalysis, Vol. 171/2, Karasuda T.; Aika, K. Isotopic Oxygen Exchange between Dioxygen and MgO Catalysts for Oxidative Coupling of Methane. *J. Catal.* **1997**, *171* (2), 439–448. Copyright with permission from Elsevier via the Copyright Clearance Center.

conditions followed by rapid thermal quenching. The need of oxidizing conditions for the formation of these $[Li^+O^-]$ defects can be easily rationalized by writing down the formation equation in the Kröger Vink notation (see Reaction 7). Due to the monovalent nature of Li^+ compared to Mg^{2+}, excess gas phase O_2 is required for charge compensation.

$$Li_2O + 2Mg^{X}_{Mg} + {}^1/_2O_2 \rightarrow 2Li'_{Mg} + 2O^{\cdot}_{O} + 2MgO \qquad (7)$$

As a matter of fact, the EPR signal at $g = 2.054$ (9, 10, 210), that Lunsford attributed to $[Li^+O^-]$ according to the work of Abraham et al. was only observed when the Li/MgO catalysts were calcined for an extended period of time in air or O_2 followed by quenching in liquid O_2 or liquid N_2. Typical OCM conditions, on the other hand, are very reducing (CH_4/O_2 between 4 and 20, H_2 as reaction product) and indeed, a detection of the signal at $g = 2.054$ after quenching from reaction conditions was never reported. Furthermore, it was never proven, e.g., by ENDOR, that the paramagnetic center at $g = 2.054$ is really neighbored by a Li ion.

Also the apparent correlation between the amount of $CH_3\cdot$ radicals formed under OCM reaction conditions over Li/MgO materials and the concentration of $[Li^+O^-]$ centers measured after post-reaction calcination for 2 h at 700 °C in air followed by quenching in liquid N_2 (Fig. 6) does not prove that $CH_3\cdot$ radicals are being formed at these centers and released in the gas phase. At OCM temperatures, no catalyst is required for OCM at all as C_2H_6 and C_2H_4 are already formed in significant amounts in an empty reactor tube as shown, for example, by Yates and Zlotin (Table 2). Therefore, it is not surprising that $CH_3\cdot$ radicals can be detected at the end of a glowing reactor tube by a technique as sensitive as EPR. Even though there is no doubt that Li/MgO and also other materials

catalyzing OCM improve C_2 selectivity compared to pure gas phase chemistry (Table 2) the question remains how the catalyst does that. Several scenarios can be considered whether the reviewed material can prove or disprove one or the other:

1. Reactions occur in the gas phase (via radicals) and at the surface of the catalyst and both networks are coupled by the usual transport of species and heat. In this case, any solid surface (catalyst, support, reactor wall, etc.) can quench radicals from the gas phase possibly suppressing unselective oxidation pathways leading to the observed increase in C_2 selectivity as compared to undisturbed gas phase chemistry (Table 2).
2. Radicals are actively produced at the catalyst surface and released in the gas phase where they participate in gas phase radical chain reactions. In this case, the catalyst would act as sort of an initiator of gas phase radical reactions. The released radicals must not necessarily be $CH_3\cdot$, but could also be OH· or other reactive species.
3. Coupling to C_2 occurs primarily at the catalyst surface followed by deep oxidation either at the surface or in the gas phase.
4. The catalyst dehydrogenates the primary reaction product C_2H_6 regardless of whether it is formed in the gas phase or at the catalyst surface effectively to C_2H_4, which is less prone to further oxidation to CO_x.

From their non-steady state experiments, Dahl (165) and Choudhary (166) consistently reported that lattice oxygen from the catalyst contributes to the conversion of CH_4. This fact is in contradiction to the discussed F-centers and the mobile Li_2CO_3 film. However, it was not unambiguously proven that the oxygen does derive from the bulk. Furthermore, it generally remains unclear how these results can be related to other mechanistic assumptions.

Isotope labeling experiments with CH_4/CD_4 mixtures conducted by Mims et al. and others and the exclusive observation of symmetrically labeled C_2 products, point indeed to $CH_3\cdot$ radicals as precursors for C_2 formation while the carbene mechanism as suggested by Martin and Mirodatos did not find any further experimental or theoretical substantiation. The positive kinetic isotope effect reported by Cant et al. points to cleavage of the first C-H bond as rate limiting step. Again, taking into account that only symmetrically substituted C_2 products were observed by Mims et al. and others, this first C-H bond breaking step seems to be irreversible, whereas other publications report an easy H,D scrambling on MgO. The only way to combine these conflicting results is that the first C-H breaking occurs in the gas phase and not at the surface of Li/MgO. Attributing most of the OCM chemistry to reactions in the gas phase could explain also why hundreds of chemically different materials

catalyze OCM with similar performance at temperatures of 750 °C but not why Li/MgO and other materials enhance C_2 selectivity.

6. TERNARY SYSTEMS

6.1. Effect of Metal Oxides on Li/MgO

Li/MgO has been treated with different dopants; a general overview is shown in Table 3. The main idea of doping Li/MgO was to prevent the loss of Li, either by modification of the solid phase or by change the reaction conditions towards milder conditions.

In an earlier study, Bi et al. investigated the OCM reaction over a series of alkali, alkaline earth, and rare earth metal oxides, prepared by an impregnation method. SiO_2, Al_2O_3, and several different MgO materials were used as support material. MgO was found to be the most promising support and Li/Ce/MgO to be the most promising catalyst (136).

Korf et al. observed the effect of additives, various oxides of transition metal oxides and rare earth oxides, on Li/MgO in the oxidative coupling of methane (229). A number of dopants, for instance, Sn, Dy, Ti, and Tb, did

Table 3: Summary of different dopants of Li/MgO and the corresponding references.

No.	Dopant	Reference
1	Na	(209, 228)
2	Ca	(229)
3	Ti	(229)
4	V	(229)
5	Cr	(230)
6	Mn	(86, 87, 229–235)
7	Fe	(230)
8	Co	(228, 229)
9	Ni	(229, 236)
10	Zn	(86, 87, 229–231)
11	Zr	(228, 237, 238)
12	Nb	(125, 228)
13	Mo	(229)
14	Cd	(86, 87)
15	Sn	(161, 228, 229, 237, 239–242)
16	La	(136, 229)
17	Ce	(136, 243–247)
18	Pr	(136)
19	Nd	(136)
20	Sm	(136)
21	Tb	(229)
22	Dy	(229)
23	Pb	(229)
24	Bi	(229, 248, 249)

not effect the C_2 selectivity, however, the temperature required to achieve the optimal yield was lowered. An explanation could be that the formation of the active oxygen species is favored. Other additives showed minor improvements without an effect on the selectivity (La, Ni) or lowered the required temperature to reach a certain conversion (Co, Mn, Pb, Bi). A comparison of the different additives showed that Li/Sn/MgO is a very promising system.

Swaan and co-workers studied various promoted Li/MgO in the ODH of C_2H_6 (250). Li/Na/MgO showed a C_2H_4 selectivity of 86% at a C_2H_6 conversion of 38%. Thermal investigations showed that an eutectic melt of $LiNaCO_3$ is formed at 490 °C, which exists as a molten phase. This was probably the reason for the improved selectivity. Fuchs et al. found a similar effect for the cracking and the ODH of C_2H_6 and C_2H_8 over Li/Dy/MgO (251).

Choudhary et al. investigated the effect of Mn, Cd, and Zn oxides on pure MgO and Li/MgO in the oxidative coupling of methane (86). Doping led to sintering of the MgO but also led to an increase in C_2 selectivity. The involvement of lattice oxygen in the coupling reaction was shown by experiments in a pulsed micro-reactor.

Larkins and Nordin reported the effect of doping Li/MgO with different metal oxides, such as Fe, Mn, Zn, and Cr (230). The catalytic activity could be attributed to the physico-chemical properties of the catalyst, in particular to the presence of reducible sites on the surface. Especially Cr, but also Mn, seemed to favor the formation of total oxidation products, while Zn and Fe led to higher C_2 selectivities, probably due to the absence of reducible sites. The presence of these dopants was also involved in changes of the surface morphology.

Larkins and Nordin tested the performance of MgO, with and without Li_2CO_3 being present in the preparation, loaded with different amounts of ZnO and Mn oxides in the oxidative coupling of methane (231). If no Li_2CO_3 was present, the total oxidation of CH_4 dominates. At a reaction temperature of 805 °C, the Zn containing catalysts resulted in CH_4 conversion higher than 25% and a C_2 selectivity of around 60%, however, this catalyst was not better than the undoped Li_2CO_3/MgO. For low loadings of Mn, the CH_4 conversion was higher than 35% with a C_2 selectivity of around 50%. Increasing the loading of Mn resulted in a decrease of conversion and C_2 selectivity.

Studying the structural features of Li/Mn/MgO (232), the group of Mariscal found that the incorporation of Li inhibited certain reactions of the Mn-MgO phases, resulting in a higher Mn dispersion.

Later, Kanno and Kobayashi observed the different modification effects of Li on two Mn/MgO samples, one with lower and one with higher Mn content (233). They discriminated between the different lattice oxygen species of Mn/MgO involved in the OCM (234). The oxygen of MgO was found to be active for the methyl radical formation, while the oxygen of Mn-MgO was found to be active for the oxidative dehydrogenation of C_2H_6.

Zhang et al. studied the role of Li in Li/Mn/MgO with atomic absorption spectroscopy (AAS), XRD, and infrared-photoacoustic spectroscopy (235). Catalysts from which the Li had been washed off showed a lower C_2 selectivity, indicating that the presence of Li is important.

Since Li/Sn/MgO was considered to be a very promising catalytic system (229), the mechanism of the oxidative coupling of methane on this system was investigated in detail (239). The results were in agreement with a Langmuir Hinshelwood mechanism and it was concluded that the rate determining step involves the reaction of an adsorbed CH_4 with an adsorbed diatomic oxygen species.

The particular role of Sn in the Li/Sn/MgO was investigated by van Keulen et al. (240). It was shown that the addition of Sn to Li/MgO stabilized the catalytic activity; Li was retained on the support under reaction conditions and, therefore, suppressed deactivation. On adding larger amounts of Sn, $Li_2Mg_3SnO_6$ was formed as a new phase. Pure $Li_2Mg_3SnO_6$ was also active for the oxidative coupling of methane. The C_2 yield versus time was also shown, with a decline of 12% to 7% over 150 h time on stream.

Nibbelke et al. scrutinized the heterogeneous steps of the OCM over MgO, Li/MgO, and Li/Sn/MgO (161). They observed that doping with Li, even more so the addition of Sn, led to an increase of the oxygen diffusion and to an increase in the amount of exchangeable oxygen.

Mallens and co-workers did TAP experiments (temporal analysis of products) with Sn/Li/MgO (252). From these experiments, they concluded that methyl radicals were produced at the surface and combined in the gas phase. C_2H_4 was formed from C_2H_6 via the oxidative dehydrogenation in the gas phase. Both C_2 products could be converted into CO, which could further be oxidized to CO_2. C_2H_6 and CH_4 could be directly converted into CO_2 by adsorbed O_2. However, lattice oxygen could also play a role in this. For the non selective reactions of C_2H_6, gas phase and lattice oxygen seemed to play a role. The addition of Sn to Li/MgO increased the amount of reactive oxygen in the uppermost lattice (241).

The group of Nagaoka reported on the effect of Sn on Li/MgO (242). They proposed two active centers. One was O^-, a surface oxide ion with an electron deficit, being generated when small amounts of Sn (less than 1 mol%) were added to Li/MgO. Another one was the O^{2-} of a complex oxide, containing Sn, which was formed when large amounts of Sn were added. A redox cycle of Sn^{4+} and Sn^{2+} could be formulated involving O^{2-}. Furthermore, it was shown that the addition of Sn reduced the formation of Li_2CO_3, which covered the surface of the catalyst.

Hoogendam and co-workers explored the importance of mixed oxides in the catalytic behavior of Li/MgO doped with Sn or Zr (237). Doped with Sn, the phase, which was responsible for the improved properties, seemed to be

$Li_2Mg_3SnO_6$, with a cubic structure like MgO. Doping with Zr resulted in various mixed oxides with different properties.

Zr-doped Li/MgO was studied in more detail by Hoogendam et al. (238). It was found that increasing the Li loading led to a decrease in the initial activity, while the selectivity was unaffected. The life-time of Li/Zr/MgO depended on the Li loading, and increasing amounts of Li extended the life-time. The presence of Li_2MgZrO_4 increased the stability of the catalyst, while $Li_2Mg_3ZrO_6$ was an active and selective phase, but not stable under reaction conditions.

McNamara et al. investigated the effect of adding Nb and Zr to Li/MgO and Li/Na/MgO (228). For comparison, Sn and Co, which promoted Li/MgO and Li/Na/MgO, were used. The resulting catalysts were more active and selective than the unpromoted Li/MgO; furthermore, the optimum yield could be obtained at lower temperatures. A similar effect was observed for Li/Na/MgO.

Swaan et al. observed the effect of Nb on Li/MgO in the OCM and ODH of C_2H_6 (125). In the OCM, at 600 °C reaction temperature, a catalyst with 16 wt% Nb showed an activity 10 times higher than undoped Li/MgO. However, for the ODH of C_2H_6, only a slight improvement was found. Generally, Li/Nb/MgO produced more CO_2, therefore, it had a lower selectivity to the desired C_2 products. Two phases with Li and Nb were found, however, the active phase remained unclear. The loss of Li from Li/Nb/MgO was comparable to that of pure Li/MgO. The addition of Nb increased the specific surface area. Above the melting point of Li_2CO_3, the catalyst deactivated, the specific surface area decreased, and the amount of the two Li/Nb phases sharply decreased. The addition of CO_2, which had previously been reported to avoid deactivation of Li/MgO (124), did not suppress the deactivation of Li/Nb/MgO.

Bartsch et al. studied the kinetics of the oxidative coupling of methane over Ce/Li/MgO (244–246). Later, Dittmeyer and Hofmann made a kinetic analysis of these data and simulated reactor performance over this catalyst (243).

Ramasamy et al. reported the influence of important reaction parameters, such as temperature, feed gas composition, and space velocity, for the oxidative coupling of methane over Li/Ni/MgO (236). Catalyst deactivation was observed, which the authors suggested as probable reasons for a loss of Li and coke deposition.

Tiwari and co-workers studied the OCM over Li/Ce/MgO and Li/Ce/MgO-CaO (247). Li/Ce/MgO-CaO showed a drastically improved C_2 selectivity compared to Li/Ce/MgO.

6.2. Effect of Chlorine on Li/MgO

That Cl^- containing catalysts improved the selectivity in the oxidative dehydrogenation had already been shown by different researchers, among others Otsuka et al. and citations therein (253).

Burch and co-workers injected pulses of chlorinated compounds (CH_2Cl_2 and $CHCl_3$) during the reaction, using Li/MgO and other catalysts (254). The chlorinated compounds drastically increased the C_2 selectivity. This effect was explained with the suppression of the total oxidation by the chlorine containing promoters. Moreover, it was observed that these promoters enhanced the ODH of C_2H_6 reaction. It was concluded that using gaseous chlorinated compounds could be an alternative to alkali doping of metal oxides.

Later, Burch et al. found that the role of chlorine over MgO was the modification of the catalyst surface to enhance the selectivity to C_2H_4 and C_2H_6 (255). That the response of C_2H_4 and C_2H_6 on the introduction of CH_2Cl_2 was different was taken as evidence that the dehydrogenation of C_2H_6 is not due to gas phase reactions involving chlorine radicals. The surface concentration of chlorine at the catalyst surface was observed to be 3%.

Conway and Lunsford showed that the addition of Cl^- to Li/MgO significantly improved the yield in the ODH of C_2H_6 (256). Under their reaction conditions, they observed that Cl^- was slowly lost from the catalyst. The Cl^- reduces the uptake of CO_2, which was actually a poison for the Li/MgO. They also assumed that the presence of Cl^- could change the form of oxygen on the surface, which was necessary for the activation. Their results demonstrated that the activation of CH_4 forming methyl radicals was the main pathway for the formation of CO_x and not the total oxidation of C_2H_4 or C_2H_6. For Li/MgO without chlorine, Roos et al. (157) and Geerts et al. (189) obtained contrary results.

Doping Cl/Li/MgO with different metal oxides (Sn, La, Nd, and Dy) further improved the performance (256). Dy is the best dopant, since the reaction temperature could be lowered to 570–585 °C, hereby suppressing the non-selective gas phase reaction.

Hinson et al. showed that the preparation of Cl/Li/MgO, via a sol-gel synthesis, resulted in a stable and active catalyst (257).

Ruckenstein and Khan studied bi-alkali promoted Cl/MgO (248, 249). Compared to mono-alkali MgO, the CH_4 and O_2 conversion and the C_2 selectivity was improved (60 h time on stream).

Lunsford et al. examined the effect of Cl^- on Li/MgO in the OCM (258). The catalyst drastically changed its behavior at an Cl^- to Li^+ ratio of nearly 1. The C_2H_4/C_2H_6 ratio became large, due to the improved activity towards ODH of C_2H_6. Adding amounts of Cl^- reduced the strong basicity of the catalyst; it, therefore, did not react with CO_2 anymore, because the Cl^- inhibited the formation of Li_2CO_3. The activity for methyl formation was the same for Cl^--doped and pure Li/MgO only after poisoning with CO_2, otherwise Li/Cl/MgO had a lower activity. Under typical reaction conditions (650 °C), chlorine left the catalyst as HCl, small amounts of CH_3Cl were also detected. The decay of CH_4 conversion and C_2H_4 productivity was different, which indicated that these reactions were catalyzed by two different active centers.

A related study considered the role of chlorine in OCM process over MgO and Li/MgO catalysts. Lewis and Catlow (259) investigated the effects of adding chloride ions on the (001) surface of pure and Li-doped MgO. They concluded that chloride in MgO segregates to the surface and especially to low coordinate sites. This segregation induces modification in the activity of any active sites located at or near these surface sites. In the case of Li/MgO catalyst, the surface chloride competed with oxygen holes for Li and leads to the formation of a stable [Li^+Cl^-] defect cluster. The presence of this cluster influences the catalytic properties, such as selectivity for C_2H_4.

6.3. Summary

Doping of Li/MgO with metal oxides led partially to improved catalytic performance and stability. The most frequently used dopants with a positive effect are Ce, Sn, Zr, and Mn. The structural analysis indicates that together with Li and MgO new multi-metal-oxide phases are formed. For many ternary systems, different phases with variable compositions could be detected. The individual role of these phases is sometimes discussed, however, generally it remains unclear. F-centers are discussed for Li/MgO as active center (see Section 5.4), however, for doped Li/MgO they have not been discussed. For some materials, such as Li/Sn/MgO, different surface oxygen species were discussed to be the active center. Some experiments also showed that the doping of Li/MgO with certain metal oxides increased the oxygen diffusion in the catalyst material. The mechanism and the active center of these materials may very well be different from Li/MgO.

The addition of chlorine, either to the catalyst during preparation or as chlorine containing compounds in the feed, improve the yield, especially in the oxidative dehydrogenation of C_2H_6. When chlorine was added to the catalysts, it was slowly lost during the reaction, probably as HCl. Although the effect of the chlorine addition seemed not to be due to the involvement in the gas phase reactions, the actual effect remains unclear.

The doping of Li/MgO, either with metal oxides or with chlorine, leads to an improved catalyst, although the requirements for an industrial application are still not met. The main aim of reducing the loss of Li has not been achieved and the systems are too complex for a fundamental understanding of the role of the catalyst in the oxidative coupling of methane.

7. THEORETICAL STUDIES

7.1. Studies on MgO

The electronic and geometric structure of MgO bulk and (001) surface was intensively studied in the past (260). MgO became a classical model system for both experimental and theoretical studies of catalysis on oxides. It has been

clearly demonstrated that the pristine (100) surface, which is the most stable one, is chemically inert, and that the catalytic activity of the material is due to extended and point defects.

Despite the apparent simplicity of the structure of the pristine (001) surface, one can expect an appreciable number of chemically distinct types of defects. First, the Mg and O atoms can have different coordination numbers (261, 262). Ions of low coordination can be found at corners or edges. Different basic sites generated by increasing the pretreatment temperature appear to correspond to ions with different coordination numbers. However, the relation between the coordination numbers of the ions and catalytic active sites for different reaction types is still not well understood. In a recent study, Chizallet et al. investigated dehydroxylated MgO powder surfaces with a combined experimental and theoretical approach (263, 264). In this work, photoluminescence excitation spectra of pretreated MgO surfaces were assigned using time-dependent density functional theory (TD-DFT) cluster calculations. This approach elucidated the nature of the adsorption sites of different molecules, such as H_2O, on the surface irregularities of MgO (263). Figure 9 shows a schematic representation of the irregularities on the surface of MgO, and the terminology is shown in Table 4.

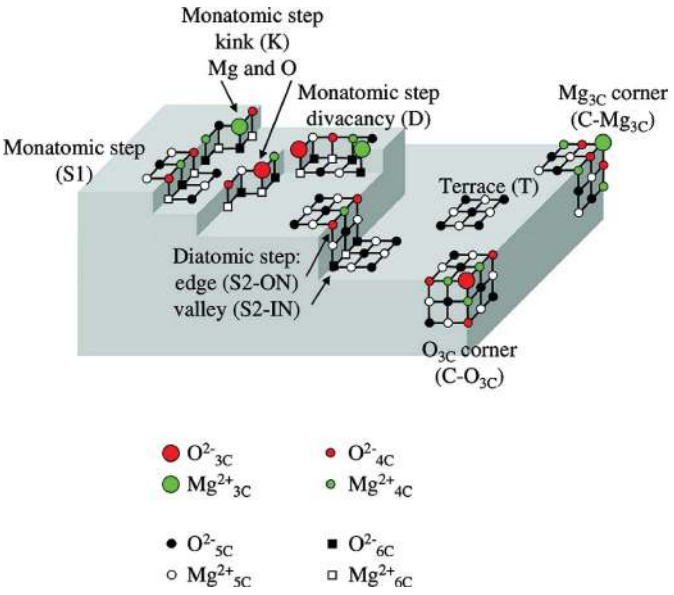

Figure 9: Schematic representation of irregularities on the MgO surface as presented by Chizallet et al., as adapted from Figure 11 of the work of Che and Tench (265). Unchanged figure from (263). The terminology is shown in Table 4. Reprinted from Chizallet, C.; Costentin, G.; Lauron-Pernot, H.; Krafft, J.M.; Che, M.; Delbecq, F.; Sautet, P. Assignment of Photoluminescence Spectra of MgO Powders: TD-DFT Cluster Calculations Combined to Experiments. Part I: Structure Effects on Dehydroxylated Surfaces. *J. Phys. Chem. C* **2008,** *112* (42), 16629–16637. Copyright with permission from the American Chemical Society via the Copyright Clearance Center (color figure available online).

Table 4: Label, nature, and formula as used in Figure 9. Adapted from (263).

Nature	Label	Formula
(100) Plane	T	$Mg_{13}O_{14}Mg_{17}$
	T′	OMg_5
Monatomic step	S1	$Mg_{20}O_{14}Mg_{10}$
Diatomic step: edge	S2-ON	$Mg_{10}O_{10}Mg_{10}$
	S2-ON′	$Mg_{10}O_{16}Mg_{22}$
Diatomic step: valley	S2-IN	$Mg_{22}O_9$
Corner: $O^{2-}{}_{3C}$-terminated	C-O_{3C}	$Mg_{13}O_{13}Mg_{12}$
Corner: $Mg^{2+}{}_{3C}$-terminated	C-Mg_{3C}	$Mg_7O_9Mg_{10}$
Divacancy	D-Mg_{3C}-O_{3C}	$Mg_9O_{10}Mg_{13}$
Kink: $O^{2-}{}_{3C}$-terminated	K-O_{3C}	$Mg_{19}O_{13}Mg_9$
Kink: $Mg^{2+}{}_{3C}$-terminated	K-Mg_{3C}	$Mg_{21}O_{14}Mg_{10}$

The second type of defects includes point defects, such as O and Mg vacancies, Mg-O pair vacancies, and interstitials. These defects can form in the subsurface and at the surface at the sites with different coordination, and can be neutral or charged. Thus, a large variety of new sites with unique chemical and spectroscopic properties can be present at the MgO surfaces. While many of these sites were characterized both experimentally and theoretically, there are still unanswered questions, in particular about the relative abundance and charge states of the defects at catalytic conditions.

The O^- centers (i.e., either an oxygen ad-atom with one additional electron, or an oxygen atom with a localized hole in the lattice) have attracted attention due to their high chemical activity. They can be formed by irradiation or doping. That the O^- centers on oxide surfaces have the ability of cleaving a C-H bond is well known. Mehandru et al. demonstrated by theoretical calculations that the high electron affinity of O^- indeed strongly promotes the CH_4 activation on MgO (266). They showed that an O^- ion in a $Mg_{21}O_{20}{}^{3+}$ cluster is able to abstract a hydrogen from a CH_4 forming a methyl radical with very low activation energy. They also found that the adsorption of methyl radicals on the MgO surface is relatively weak (∼1 eV), confirming the scenario in which methyl radicals desorb easily from the surface and react in the gas phase.

7.2. Studies on Li/MgO

In general, alkali metals were added to inorganic oxides to modify the electrical and conducting properties of the material. In fact, doping with alkali metals can lead to new chemical properties due to the creation of vacancies or changes in the valance state of other atoms resulting from charge imbalance within a material. In the specific case of Li-doped MgO, the presence of monovalent Li ions, which replaced divalent Mg ions in the crystal structure, created an unpaired electronic hole found in the oxygen 2p band.

Theoretical studies concerning Li/MgO catalyst can be classified into three categories as follows:

1. Electronic structure of Li-doped MgO;
2. Defect formation energies and *ab initio* atomistic thermodynamics of Li-doped MgO surfaces;
3. Theoretical studies of adsorption and dissociation of CH_4 on Li-doped MgO surfaces.

7.2.1. Electronic Structure of Li-Doped MgO

Following the mechanism of OCM over Li-doped MgO proposed by Ito and Lunsford (8) and Ito and co-workers (9), theoretical studies concentrated mainly on the geometry and electronic structure of the so-called $[Li^+O^-]$ centers, i.e., Li substitutional defects with a localized electronic hole, and the energetics of the hydrogen abstraction step of OCM [(267) and references therein]. Both periodic (268–273) and cluster (267, 270, 274–281) models of the active site have been used. It has been demonstrated that the electronic structure of the $[Li^+O^-]$ centers is sensitive to the level of theory employed. Specifically, comparison of generalized gradient approximation (GGA), GGA with on-site coulomb interaction correction (GGA+U), and Hartree-Fock (HF) calculations showed that atomic and electronic structure of the Li-doped MgO surface are sensitive to the amount of the exact exchange accounted for in calculations (276, 282, 283). Inexact treatment of exchange in DFT with standard exchange-correlation functionals results in the self-interaction error, giving rise to an artificial electron delocalization. Thus, standard DFT functionals used in calculations of extended systems are expected to underestimate the localization (284) of both the unpaired electron and the accompanying hole around O^- in the surface $[Li^+O^-]$ defects. EPR and ENDOR measurements (100–102, 147) indicated that the trapped hole in the bulk is mostly localized on a single oxygen atom, although not completely, and that one of the six bonds between Li and the nearest neighbor O atoms is elongated by about 0.3–0.4 Å compared to the Mg-O distance in pure MgO. These conclusions are in good agreement with periodic UHF calculations (285–287). GGA calculations of the geometric structure of MgO surface with the Li atom in the subsurface layer gave slightly smaller elongation of the Li^+-O^- distance along the normal to the surface (270, 282), as should be expected for the surface versus the bulk.

The information on the hole localization is not conclusive. It has been claimed that pseudopotential GGA calculations (270) give a spin-density distribution around the surface $[Li^+O^-]$ defects with subsurface Li similar to the HF spin-density in the bulk (285, 286), while the all-electron frozen core GGA calculations (282) give several times larger delocalization of the spin-density, with largest spin-density still being at the single oxygen anion. However, the

criteria for the spin-density localization were different and somewhat arbitrary in these studies, and were not related to any experimental observation. In the case of GGA+U calculations (272, 273, 282, 283), the degree of the hole localization depends on the choice of the parameter U, which was chosen to give a strong localization. Note that no experimental data are available on the degree of the hole localization at the surface [Li^+O^-] defects.

Most of the previous theoretical work was concentrated on studies of the [Li^+O^-] centers at the (100) surface of MgO. Indeed, this and the equivalent (010) and (001) surfaces are most stable, so that no other terminations were observed experimentally for pure MgO. The situation, however, changes when MgO is doped with Li. It was demonstrated in a recent combined experimental and theoretical study (118) that Li doping induces formation of (111) terminations, resulting in apparent rounding of initially cubic MgO nanocrystals. A preceding theoretical work of Scanlon et al. (273) investigated the electronic structure and energetics of the [Li^+O^-] centers at the (100), (110), and (111) terminations, as well as their activity towards the hydrogen abstraction from CH_4. They have concluded that the energetics associated with hydrogen adsorption are strongly surface dependent, and indicated the (111) termination as the most promising catalytically.

7.2.2. *Defect Formation Energies and Ab Initio Atomistic Thermodynamics of Li-Doped MgO Surfaces*

As has been pointed out at the beginning of this section, defects can dramatically change the chemical properties of an oxide surface. Therefore, it is important to know these chemical properties, as well as the concentration and distribution of the defects at the surface. For this, accurate knowledge of Gibbs free energies of formation for different defects is needed. Initial theoretical information on the formation energies is usually obtained from *ab initio* calculations corresponding to 0 K (i.e., about −273 °C) and fixed values of chemical potentials for species and electrons.

In this regard, an important theoretical result has been obtained by Yang et al. (271). They found that the Li substitutional defects strongly promote formation of oxygen vacancies in MgO. This is explained by the electron transfer from the neutral vacancies to the oxygen surrounding the Li substitutional defects. The Li defects create empty states near the top of the valence band, stabilizing the charged oxygen vacancies (F^+ and F^{2+}). In the recent study by Scanlon et al. (273), the formation energy of the oxygen vacancy adjacent to two Li substitutional defects was calculated also for other MgO surface terminations (110) and (111), and it was found that the energies are similar for each surface. No analysis of the dependence of the formation energies of charged defects in Li-doped MgO on the electron chemical potential were reported in the literature to date.

As the number of particles in a system increases, so does the number of states, and the statistics start to play an increasing role at finite temperatures. As a result, the structure and composition of a solid surface is a function of temperature and pressure of the gas above the surface (288–290). Thus, surface chemical properties cannot be simply predicted from calculations of one particular surface configuration at zero temperature. Moreover, a catalytic surface in contact with the gas flow of reactants and products is an open thermodynamic system (291, 292). The difference between the thermodynamic metastable states and what is called a steady state of catalysis is significant: the surface reactions under the condition of a constant supply of reactants and removal of products can alter the structure and composition of the surface in an important way (291).

Despite the above instances, the question about structure and composition of the surface of Li-doped MgO under working conditions and the steady state of OCM have not been addressed in the literature. First steps in this direction were undertaken in the combined experimental-theoretical study of Myrach et al. (118), where the *ab initio* atomistic thermodynamics approach was used to estimate the concentration and distribution of various kinds of defects at the Li-doped MgO (001) surface as a function of temperature and O_2 pressure. The theoretical results are in good agreement with the experimental observations of Li-doped MgO films supported on Mo (001) surface. As the films are annealed to temperatures above 727 °C, a pattern of one-monolayer-deep rectangular holes on the MgO surface is observed, which is explained by the promoted formation of oxygen vacancies in Li-rich islands on the MgO (001) surface. According to the calculations, the oxygen vacancies indeed become abundant defects at the surface at elevated temperatures even at high pressures. In fact, the predicted concentration of the vacancies is so high that it should result in an instability of the surface. This is consistent with recent experimental measurements showing drastic changes in the morphology of MgO nanocrystals in the presence of Li (50). The possibility of Li-induced morphological changes of MgO particles was indicated in an earlier theoretical study by Watson (293).

7.2.3. Theoretical Study on Adsorption of Methane on Li-Doped MgO Surface

As described in Section 5, it is generally accepted that in the OCM reaction catalyzed by Li-doped MgO, the C-H bond-breaking step occurs at the catalyst surface. Although there is no direct evidence for this specific role of the surface (see Section 5), many researchers suggested that the good catalytic properties of MgO and Li/MgO are due to the defective sites, such as vacancies, electronic holes, and low-coordinated ions at steps and corners (13, 84, 223).

According to the mechanism proposed by Ito and Lunsford (8) and Ito et al. (9), the CH_4 is activated by surface O^- species. It has been speculated that such species would be stabilized by the Li substitutional defects in the form

of the surface [Li^+O^-] centers. Many theoretical studies have been devoted to the calculation of the activation energy and reaction energetics for the H-abstraction from CH_4 on the surface oxygen adjacent to a Li substitutional defect. Experimental values for the activation energy range from 0.93 eV (88) to 2.43 eV (190). It was suggested that the range of the experimental numbers is due to reactive sites of different nature. There is also a range of theoretical values for the activation energy in the case when Li is in the subsurface MgO (100) layer, between 0.05 and 1.2 eV, with the lower values corresponding to higher-level methods (276, 277). Periodic Hartree-Fock calculations with an *a posteriori* correlation correction (268) gave 0.78 eV for the activation energy. Catlow et al. (267) reported the value of 0.77 eV calculated using a hybrid DFT functional and a cluster model.

It has been pointed out that along with the approximate treatment of the electron correlation, one should be careful to avoid errors associated with cluster models of the extended surfaces (267, 268). While the study by Ackermann et al. (276) showed a strong dependence of the activation energy on the level of theory employed, it was based on a rather small embedded cluster model. The study by Børve and Pettersson (277) showed the importance of non-dynamic correlation effects for the transition-state wave function, but also for a very small cluster model, and not including surface relaxation. On the other hand, in addition to the reduced self-interaction error and inclusion of electron correlation effects using a hybrid functional, the study of Catlow et al. used a fairly large cluster model (267), and gave the results very similar to the periodic calculations by Orlando et al. (268). The importance of the robust determination of the reaction path has been emphasized as well (267, 270).

The activation energy in the case when Li is in the top layer was obtained using the GGA+U method (273), and was found to be 1.21 eV. The same authors have also calculated the activation energy on Li-doped MgO surfaces with (110) and (111), and obtained the values 1.12 eV for (110), and 0.81 eV for the oxygen-terminated (111) surface and 1.21 eV for the Mg-terminated surface. In these studies, the value of U was chosen to match the geometry of the Li substitutional defects in the bulk with the experimental estimate of the geometry derived from ENDOR measurements (101), and to ensure a strong localization of the hole (282). However, the experimental estimate was based on a point-charge and dipole model calculation, and was indicated by the authors as not conclusive. As was mentioned above, the information on the hole localization is not conclusive as well.

Thus, the activation of the dehydrogenation reaction is still a matter of discussion. The same is relevant for the reaction energetics. Using a hybrid DFT functional, Catlow et al. found that the reaction is exothermic with the reaction energy −5 kcal/mol (267). Orlando et al. reported a reaction energy of ∼0 kcal/mol, obtained with the periodic Hartree-Fock method, independent on whether a correlation correction is included or not (268). The results

obtained by Børve and Pettersson suggest that the reaction is endothermic by 8.5 kcal/mol (277), but the issues with the model reliability discussed above are also applicable here.

An alternative mechanism was also proposed, in which the active surface site is not a [Li^+O^-] defect but a surface oxygen vacancy (118, 213, 214, 294). As explained above, Li substitutional defects promote the formation of O vacancies. This proposal of a new mechanism is in line with experimental data obtained by HREELS experiments (211, 213, 214). The results of these studies indicated that the C_2H_6 yield of the catalytic conversion is not dependent on the density of [Li^+O^-] defects, but instead is strongly correlated with the oxygen vacancy concentration (213, 214). In addition, the authors demonstrated that, while the oxygen vacancy is thermally stable, the [Li^+O^-] defect suffers from thermal instability. Theoretical studies of the reactivity of oxygen vacancies in different charge states on the MgO (001) surface are scarce. Orlando et al. investigated the reactivity of the neutral vacancy (F^0 center) towards dissociation of H_2 and hydrogen abstraction from CH_4, using the periodic Hartree-Fock method with *a posteriori* correlation correction (295). The results of the calculations suggested that F^0 centers are reactive species and they can adsorb atomic hydrogen, but the adsorption energy is not sufficient to promote the dehydrogenation of CH_4. The CH_4 dissociation on the F^+ center with an adjacent Li substitutional defect was also found by the same authors to be endothermic, but it was much less endothermic than in the case of the neutral oxygen vacancy. Dash and Gillan also predicted a high endothermicity of the hydrogen abstraction from CH_4 at the F^0 centers, using periodic DFT with a GGA functional (269). Pacchioni and Ferrari studied the interaction of O_2, CO, and H_2 with oxygen vacancies on the (100) surface of MgO, using the Hartree-Fock method and an embedded cluster model (296). The oxygen vacancies exhibited a high reactivity towards these gases compared to the regular sites of the MgO surface. Furthermore, it has been found that the reaction proceeds via the formation of radical anions, O_2^- and CO^-.

7.3. Summary

While some understanding of the electronic structure and chemical properties of Li-doped MgO surfaces has been achieved due to the numerous theoretical studies, it is clear that more studies are necessary. It has been demonstrated that both the electronic structure and calculated reactivity of defects on MgO surface towards the hydrogen abstraction from CH_4 require a high level of theory for a reliable analysis. In particular, the accurate description of oxygen vacancies and Li substitutional defects appears to be quite challenging. The reason for this is that, despite advances in computational tools and hardware, modeling of defects in extended systems with high level theoretical methods remains problematic due to a large supercell size required

for convergence, and at the same time computationally expensive scaling with the system size. Similar problems occur in cluster calculations. This is particularly important for charged defects, for which the relaxation and screening effects are quite long-range.

Another important aspect of the catalysis on Li/MgO surfaces is the concentration of defects at realistic temperature and pressure conditions. Our theoretical studies, in conjunction with recent experiments, have demonstrated that the concentration of defects is so high, that the surface becomes unstable at relevant temperatures. This instability results in morphological changes of the surface, creating a new catalytically active material. Therefore, experiments aiming at characterization of the new material are needed for the further development of our understanding of the catalysis on Li-doped MgO.

In the light of the results briefly summarized in this review, these experiments will benefit from theoretical analysis of relative stabilities of different Li/MgO surface terminations, namely (100), (110), and (111), as well as point defect concentrations and charge states on terraces, steps, corners, and kinks, at realistic conditions. It is also important to analyze the influence of hydrogen and carbon on the surface stability.

8. KINETIC STUDIES

Studying the kinetics of methane oxidative coupling is important to understand the mechanism of this high temperature reaction and to develop it into an industrial process. A proper kinetic model, viz. a compilation of reaction steps and corresponding rate equations links consumption and production rates of all reacting surface and gas phase species in a quantitative manner. As the focus of this review is on mechanistic aspects of methane oxidative coupling on Li/MgO, a discussion of published kinetic models for this system will be presented in the following. Taking into account that OCM is a prime example for a heterogeneous-homogeneous reaction, the discussion cannot be limited to surface kinetic schemes alone but will also include gas phase reactions. After a brief review of OCM gas phase chemistry, kinetic models combining surface reaction steps on Li/MgO or related systems with gas phase reaction steps will be reviewed in more detail. The chapter closes with a summary of what the authors consider of being the status quo in OCM kinetics and a personal view of future research targets.

8.1. OCM Gas Phase Kinetics

At temperatures above 600 °C, OCM occurs, to a certain extent, in the gas phase without any catalyst being necessary though with poor selectivity to C_2 products (C_2H_6 and C_2H_4). It has been observed experimentally and theoretically that a high CO/CO_2 ratio and high H_2 selectivity is typical for gas phase

OCM compared to the reaction with a catalyst. The main interest of gas phase kinetic studies is to evaluate the contribution of gas phase reactions to catalytic OCM, in particular if the catalytic reaction is conducted at high temperature and pressure (297).

Numerous gas phase OCM kinetic studies have been reported in the literature (140, 142, 143, 298–302). In many cases, values of Arrhenius parameters for simple gas phase reactions were selected from databases of combustion chemistry (303, 304). Comparatively few kinetic models have been specifically developed for methane-rich OCM stoichiometry, such as the model of Geerts and co-workers (298) or the model published by Zanthoff and Baerns (302). The number of gas phase reactions included in these models varies considerably. For example, Geerts et al. (298) and Zanthoff and Baerns (302) report both 164 elementary reactions whereas the model of Chen et al. (143) includes only 66 reactions.

In some works (298, 301, 302), good agreement is reached between kinetic simulations and experimental results. The model described by Geerts et al. (298) pointed out that the main reactive species in gas phase methane oxidation are the radicals H·, OH·, CH_3·, and OH_2·. The main carbon reaction path involved CH_3·, C_2H_6, C_2H_5·, and C_2H_4. All carbon species are rapidly oxidized in the gas phase to CO. After a comparison between experiments and simulation of both catalytic and homogeneous gas phase reactions, the authors claimed that Li/MgO is not only a methyl radical producer but also a radical scavenger. Chen et al. (143) observed that large amounts of methyl radicals are formed through branched chains, which degenerate to produce C_2H_6. The oxidative dehydrogenation of C_2H_6 leads then to C_2H_4. In 1990, Lunsford et al. (305) also highlighted the importance of branched-chain reactions in the gas phase with respect to the generation of methyl radicals. In agreement with Geerts et al. (298), Lunsford (305) concluded that the catalyst might generate some CH_3· radicals, which desorb into the gas phase, but that the main radical pool is formed by chain branching in the gas phase.

In the majority of cases, only partial agreement between model predictions and experiments is obtained. For example, Lane and Wolf observed that the experimental dependence of the CH_4 and O_2 conversion on space time did not agree with the model. At 1000 °C, the experimental CH_4 conversion rate was four orders of magnitude higher than calculated. On the other hand, the dependence of the coupling selectivity on conversion was successfully described (140).

In summary, all kinetic gas phase studies indicate that gas phase radical reactions play an important role in catalytic OCM, in particular, at high temperature high pressure conditions. Even though small amounts of ethane and ethylene are formed in pure gas phase OCM, the overall effect of gas phase reactions seems to be detrimental to catalytic OCM mainly because gas phase radical reactions are unselective in nature and lead to deep oxidation

of coupling products mainly to CO. What causes concern is that, despite the long history of kinetic studies on gas phase methane oxidation, experimental data are not sufficiently captured by the suggested models. Some discrepancies might be due to the fact that many reaction steps for OCM modeling were taken from combustion models that are typically optimized for methane lean stoichiometries whereas OCM operates in methane excess. However, the most important deficiency in existing gas phase kinetic models is probably that they do not account properly for radical generation or radical scavenging on solid surfaces, which is a largely unexplored topic in the literature.

8.2. Kinetic Simulation Including Both Gas Phase and Surface Reactions

Based on what was said before, it seems certain that OCM proceeds through a mechanism in which catalytic reactions interact with non-catalytic gas phase radical reactions. In 1936, Polyakov et al. were the first who reported such a mechanism for the complete combustion of CH_4 (306). In 1981, Fang and Yeh published the results of their study of CH_4 pyrolysis over ThO_2/SiO_2 and suggested a reaction mechanism based on methyl radical formation on the catalyst surface (307). C_2H_6 was produced by coupling of two $CH_3\cdot$ radicals in the gas phase.

In the case of OCM, the mechanistic framework shown in Eqs. (8)–(10) was suggested involving methyl radical formation on the catalyst surface by homolytic dissociation of CH_4 followed by desorption of a fraction of these radicals in the gas phase (302).

$$CH_4 + O_s^- \rightarrow CH_3\cdot + OH_s^- \tag{8}$$

$$2OH_s^- \rightarrow H_2O + O_s^{2-} + \square \tag{9}$$

$$1/2O_2 + O_s^{2-} + \square \rightarrow 2O_s^- \tag{10}$$

A proof that methyl radicals are formed on the catalyst surface and being released into the gas phase during OCM reaction was provided by EPR spectroscopy as already mentioned in Section 5.1. Furthermore, it should be noted that Reaction (10) is not a single elementary step. Several other reactions, for example, the dissociation of O_2, electron transfers, or ionic mobility, can occur. However, less details about these reactions are known, so the catalytic cycle is lumped into these three steps.

From a kinetic point of view, some isotope exchange studies were performed to determine the rate determining step. The kinetic isotope effect (KIE) during OCM was reported for the first time in 1988 by Cant et al. (184, 308).

In this study, CH_4 was substituted by an exactly equal pressure of CD_4 and it was determined whether the overall conversion rate was affected. The experiments were carried out at 750 °C with Li/MgO as catalyst. The authors concluded that C-H bond scission [Reaction (8)] is the rate-limiting step because of a significant reduction in methane conversion upon deuterium substitution. Other studies, including not only Li/MgO but also Sm_2O_3, $SrCO_3$ or $Na/MnO_x/SiO_2$, confirmed this conclusion (187, 204, 309, 310). Furthermore, Nelson et al. demonstrated differences in selectivity with CD_4 instead of CH_4 (204). Indeed, selectivity to hydrocarbons was lower with CD_4 and did not change with decreasing flow rate. This decrease of selectivity implies that either CO_x and C_2 products are formed by different slow steps or, if a common step with $CH_3\cdot$ radical is involved, then CO_x formation occurs on the catalyst. However, Shi et al. questioned the idea that C-H bond cleavage is the only rate-limiting step (177). In his study, the origin of the kinetic isotope effect during OCM over a Li/MgO catalyst at 700 °C was investigated using several different experimental methods and by a kinetic model that includes both heterogeneous and homogeneous reactions. The authors showed that a variation in the H/D KIE, based on CH_4 and CD_4 conversion, was observed when a constant partial pressure of CH_4 was maintained while the partial pressure of O_2 was changed. The variation in KIE with respect to the oxygen partial pressure indicates that the rate of C-H bond scission [Reaction (8)] at the catalyst surface is comparable to the rate of incorporation of oxygen into the lattice [Reaction (10)]. Therefore, Shi et al. concluded that no unique rate determining step exists. They suggested that the relative rates of the CH_4 activation step and the oxygen incorporation step may be influenced by several operating parameters, such as the total pressure of the reactants or the temperature. Shi and co-workers highlighted in the same publication the influence of N_2O as oxidant. Indeed, the oxygen incorporation into the lattice was found to be rate-limiting under a pressure of CH_4 equal to 190 Torr, even in large excess of N_2O. At lower CH_4 pressures, i.e., 0.4 Torr, the rate-determining step in large excess of N_2O was the formation of $CH_3\cdot$ radicals.

In a complementary study, without KIE experiments, Zanthoff and Baerns suggested that the primary coupling reaction to C_2H_6 is second order with respect to the methyl radical concentration (302). The authors proposed further that the non-selective reactions are first order with respect to the concentration of methyl radicals and the different compounds containing oxygen. Based on these suggestions, Zanthoff and Baerns derived some suggestions for an optimum catalyst design. First of all, a high concentration of methyl radicals is required to obtain high C_2 selectivities because the coupling step is of second order. This should be most easily achieved close to the catalytic surface if CH_4 adsorption and dissociation is fast. Moreover, adsorption capacity for methyl radicals on the catalytic surface is required. The rate constant for the coupling step, if it occurs at the surface, should be enhanced by the catalyst.

Simultaneously the gas phase radicals containing reactive oxygen ($HO_2\cdot$, $OH\cdot$, $O\cdot$) should be consumed by interaction with the hydrogen dissociated from the adsorbed CH_4 molecule.

Further kinetic studies on Li/MgO were published at the beginning of the 90's (158, 311–314). Roos et al. derived rate equations for CH_4 consumption and regressed these on experimental data obtained in a gradientless reactor (158). In this study, the authors concluded that the rate determining step involves reactions of CH_4 adsorbed on the catalyst surface with a diatomic oxygen species. The adsorption of O_2 is assumed to be relatively weak. They also found that the poisoning effect of CO_2 has to be taken into account in kinetic evaluation. Consequently, a Langmuir-Hinshelwood type mechanism, with competitive adsorption of CH_4, O_2, and CO_2, is required in this case. CH_4 may be adsorbed on the same site or on an adjacent surface site than CO_2. In the kinetic model described by Tung and Lobban, the rate equations for the production of C_2 products and CO_2 were derived from a four-step reaction mechanism (314). The evaluation of the kinetic parameters was carried out by non-linear regression using the Levenberg-Marquardt method using experimental data measured at low conversion. The authors observed C_2H_6 selectivities greater then 90%. Under their operating conditions no CO or C_2H_4 was produced, indicating that these are secondary reaction products. It is noteworthy that the last two kinetic models consist only of catalytic surface reactions.

The first OCM study combining catalytic and non-catalytic gas phase reactions was presented by Aparicio et al. (311). Physico-chemical relations and thermodynamic constraints were used to evaluate kinetic parameters. The model involved 12 irreversible reactions. The simulation results were then compared to the experimental data published by Lunsford et al. Satisfactory agreement between the model and the experiment was found. Furthermore, the authors proposed new conclusions. The most important idea was that the active sites for the OCM reaction are obtained via two elementary steps. In the first step, surface peroxide species are formed by adsorption of gaseous O_2. In the second step, methane-activating sites are produced as the surface peroxide species undergo O-O bond cleavage. Another mechanistic kinetic model was developed by Tjatjopoulos and Vasalos (313). The proposed model consisted of 38 surface reactions for the heterogeneous network and 164 gas phase reactions. The gas phase reaction scheme was adopted from the studies of Geerts and co-workers (298). Surface kinetic parameters were estimated on the basis of scaling arguments and published experimental data. The CH_4 conversion and coupling product selectivities obtained using the kinetic model agreed satisfactorily with the experimental data over the investigated range of CH_4/O_2 ratios of 2–10. Using an Eley-Rideal type mechanism, the authors demonstrated that the CH_4 consumption rate exhibits a saturation-type dependence on CH_4 partial pressure. According to their results, the selectivity maximum

observed in experiments near 700 °C is caused by the temperature variation of the surface concentration of active centers that exhibit a maximum there. In the same year, Shi et al. published a different model (312). The homogeneous network was extracted from the model of Zanthoff and Baerns and included 156 gas phase reactions (302, 315). This model was combined with a heterogeneous network describing the kinetic effects with respect to CH_4 and O_2 partial pressure correctly. In this publication, Lunsford et al. confirmed one more time that surface reactions are responsible for most of the CH_4 conversion and that coupling of methyl radicals occurs in the gas phase. Based on the same heterogeneous network, Lunsford et al. proposed a study of the catalytic conversion of CH_4 and C_2H_4 to C_3H_6 using a (LiCl + NaCl)/MgO catalyst (159). An extended homogeneous network including 188 gas phase reactions and C_3 and C_4 species was used in this study to describe gas phase chemistry.

The most recent micro-kinetic model of the OCM reaction over Li/MgO and Sn/Li/MgO catalysts was reported by Sun and Co-workers in 2008 (316). This model is based on extensive studies published by Marin's research group (161, 241, 300, 317–319). In a first version, the model comprises 10 catalytic reactions coupled to 39 gas phase chain reactions and accounts for irreducible mass-transport limitations for reactive intermediates (317, 318). This model adequately described the experimental observations over a broad range of operating conditions. In the 2008 publication (316), a second extended version was presented consisting now of 14 surface reactions combined with 39 gas phase reactions. Furthermore, 13 so called catalyst descriptors, such as chemisorption enthalpies, sticking coefficients, or the density of active sites, were implemented in the model and regressed to the experimental data starting from physically reasonable values. Only one active site is considered in this model without that the chemical nature of this site is specified. The kinetic model is embedded in a one-dimensional heterogeneous reactor model. Sun and co-workers summarized the kinetic model in a general scheme for the OCM reactions involving reactants and products as reproduced in Figure 10.

The development of the gas phase reaction network used by Sun et al. (316) started from the model reported by Chen et al. (143) including 66 reactions. By a sensitivity analysis, Sun and co-workers identified some reactions that were kinetically not relevant (316). Reactions involving C_3 hydrocarbons were added to the model in order to be able to simulate the experiments in which C_2H_6 was added to the feed. After these modifications, the final network consisted of 39 reactions among 13 stable molecules and 10 radicals.

Because the model of Sun and co-workers seems to be the most sophisticated it was of interest to the authors to check whether it is predictive not only for the experimental data published by Sun et al. themselves but also for data published by other groups. To perform this study, experimental data from the authors and from the literature measured for OCM on Li/MgO catalyst (9, 64, 85, 161, 320) were used as the benchmark. The kinetic simulations

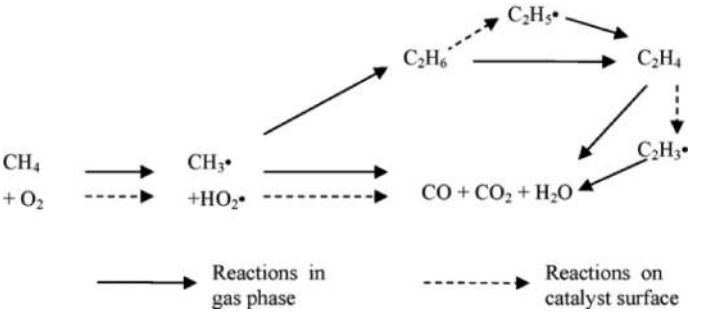

Figure 10: General Scheme of the reaction network in the oxidative coupling of methane proposed by Sun and co-workers. Figure unchanged from (316). Reprinted from Catalysis Today, Vol. 137/1, Sun, J.J.; Thybaut, J.W.; Marin, G.B. Microkinetics of Methane Oxidative Coupling. *Catal. Today* **2008**, *137* (1), 90–102, Copyright with permission from Elsevier via the Copyright Clearance Center.

were carried out with the same model and the same software used by Sun and co-workers (316). The gas phase and surface reactions with their Arrhenius parameters were introduced in the CHEMKIN software. Thermodynamic data distributed with the CHEMKIN software were used. Some operating conditions such as the pressure, temperature, CH_4/O_2 ratio, and the total flow rate had to be incorporated into the software. Moreover, the values of the BET specific surface area of the catalyst and the density of active sites had to be defined. BET surface areas were available in all selected references, while the active site density was taken from Sun et al. (316) for all simulations. Figures 11 and 12 show parity plots comparing the experimental and simulated methane conversion and C_2 selectivity results, respectively.

As can be expected, the simulation and the experimental results are reasonably close for the data for which the model was optimized. For independent data, CH_4 conversion is predicted reasonably well (Fig. 11) up to about 15% conversion. Above this value, experimental and simulated CH_4 conversion values differ substantially. C_2 selectivity is generally overpredicted by the model (Fig. 12) with deviations up to 33%.

It can, therefore, be concluded that even the most recent micro-kinetic model published by Marin and co-workers shows major deficiencies in particular for predicting C_2 selectivity data of independent experimental studies. It seems that a general OCM model is hard to implement because of the wide range of possible operation conditions. The use of any published micro-kinetic model for industrial reactor design is therefore not advisable. In fact, simplified kinetic models have been successfully used to describe experimental results as demonstrated by Dittmeyer and Hoffmann. concerning OCM on a Ce/Li/MgO catalyst (243). The model proposed in this study consisted of a total of 33 reactions, 23 of which occured in the gas phase. Most of the kinetic parameters were obtained by means of multi-response regression based on several concentration and temperature profiles.

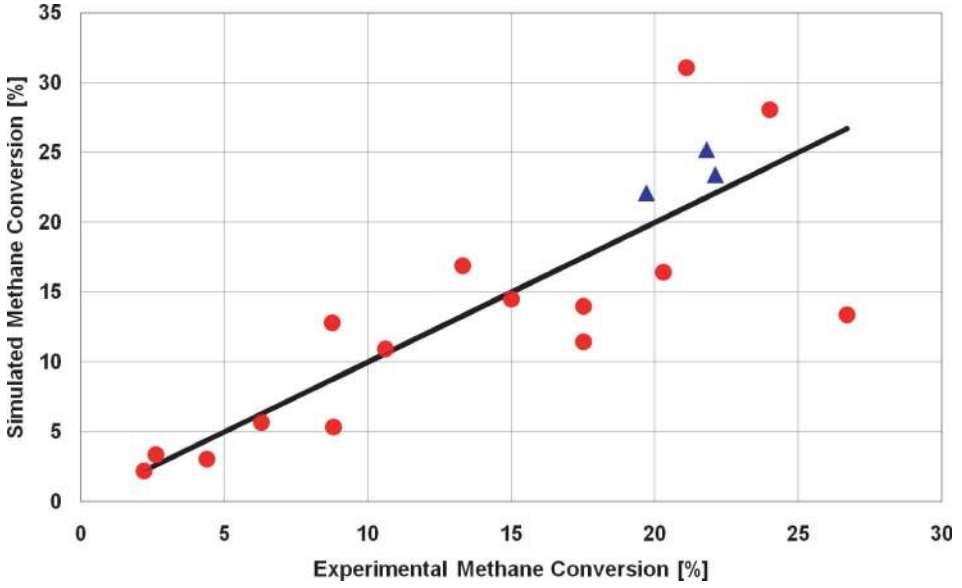

Figure 11: Parity plot for experimental and simulated CH_4 conversion. The • represents published results and the ▲ represents the predictions by the micro-kinetic model of Sun and co-workers (316) (color figure available online).

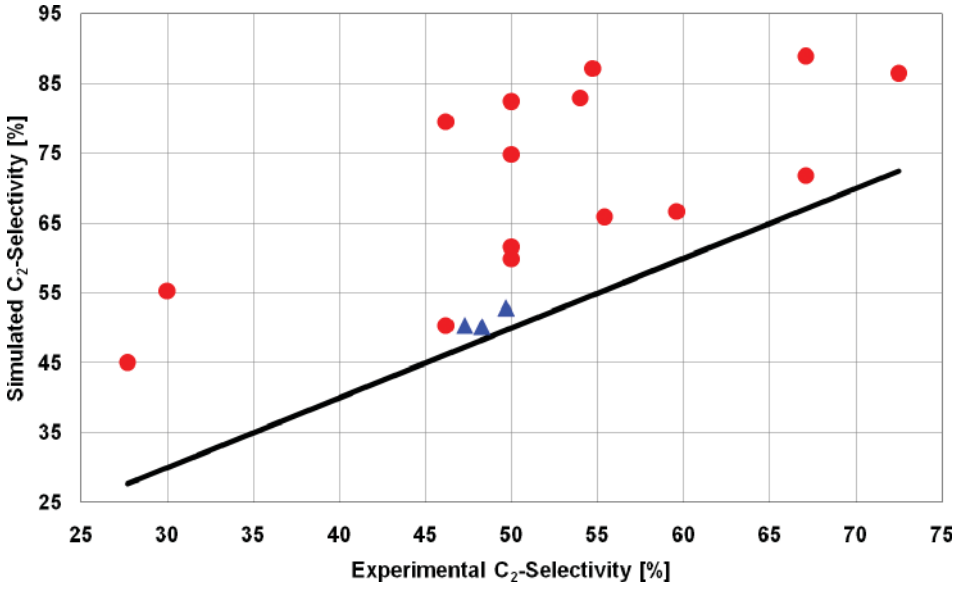

Figure 12: Parity plot for experimental and simulated C_2H_4 conversion. The • represents published results and the ▲ represents the predictions by the micro-kinetic model of Sun and co-workers (316) (color figure available online).

8.3. OCM Kinetics: Status Quo and Research Perspective

In summary it can be said that the current kinetic understanding of methane oxidative coupling is still insufficient despite 30 years of research. This is first and foremost due to the fact that OCM is a prime example for a heterogeneous-homogeneous reaction, viz. for a reaction network comprising catalytic reactions at the catalyst surface, pure gas phase reactions mediated by free radicals and radical liberation as well as radical scavenging between the gas phase and the catalyst. As a consequence of this complex surface-gas phase, coupling any classical kinetic approach, such as casting the rate equations into power laws, Langmuir Hinshelwood or Mars van Krevelen type rate expressions will inevitably fail because the kinetic parameters in these equations are not only catalyst specific but depend intricately on the packing density of the catalyst bed, the porosity of the catalyst granules, pre- and post-catalytic chemistry, reactor pressure, feed composition, in fact on all variables that influence gas phase chemistry in one way or another. It is, therefore, very unlikely that any formal kinetic model deduced from a particular set of experimental data will be predictive for conditions other than those used in setting up the model. In light of the strong nonlinear behavior of coupled surface gas reactions even minor deviations in the catalyst packing or other variables will cause strong changes in the results even though the very same catalyst is used.

In an excellent recent review, Sinev et al. (321) elaborate on the different approaches in describing OCM kinetics and the interested reader is referred to this review for further details. One important aspect as highlighted by Sinev is the complex reciprocal influence of methane, ethane, and ethylene oxidation kinetics, which is not captured by actual kinetic models. In nearly all cases, the data on which the kinetic models were developed have been measured at low conversion and on separate feed streams containing only one hydrocarbon at a time. What is missing are kinetic data derived from mixtures of the different hydrocarbons. The reciprocal influence of CH_4 and C_2H_6 during their simultaneous oxidation has been described in several publications dealing with kinetic simulation (322, 323) without that the results have found widespread appreciation. For example, it was shown that oxidation of the primary C_2 coupling product C_2H_6, which is more reactive than methane, can stimulate CH_4 oxidation by formation of a radical pool at a higher concentration level consisting in particular of alkyl or peroxy radicals (324, 325).

In light of this complexity it becomes clear that the only way to put OCM kinetics on solid foundations is to use micro-kinetic models describing the reaction network on an elementary step basis as it is standard in other disciplines, such as combustion research. It goes without saying that such a model has to include surface and gas phase reaction steps interlinked by appropriate coupling steps that describe the release of reactive intermediates such as radicals from the catalyst surface but also scavenging of gas phase radicals by the solid.

The model of Sun and co-workers (316) is a good example in this regard even though it does not capture all experimental details yet and certainly needs improvement. However, it outlines the methodology how a microkinetic surface and gas phase model can be developed for OCM and how, by means of catalyst descriptors, the model can be transferred from one catalyst to another.

In light of the state of knowledge that is currently available on OCM, it is clear that the development of a predictive microkinetic OCM model will require a great deal of further research. Taking as example the density of active sites as an important model parameter. As long as it is uncertain what the active site on an OCM catalyst is, it will be impossible to assign numeric value to the active site density. It should actually be considered that several active sites might exist on an OCM catalyst given the high reaction temperatures that level out differences in activation barriers to some extent making reactions on several sites comparable in rate. Another largely unexplored problem is how gas phase radicals interact with solid surfaces as presented by the catalyst, support material, or even the reactor walls. Much fundamental research will be necessary to assign rate parameters to this important class of steps linking surface and gas phase chemistry. Therefore, OCM marks a touchstone for kinetic research in the 21st century and researchers from the various disciplines should be encouraged to contribute building the OCM model.

9. SUMMARY AND CONCLUSION

At first glance, the mechanism of methane oxidative coupling on Li/MgO as depicted in Figure 7 seems scientifically sound and widely accepted in the reviewed literature. This mechanism is mainly based on a series of papers from the Lunsford group (8, 9, 11, 148, 210). However, a close look at these publications and at results published by other groups raises doubts about methyl radical generation on $[Li^+O^-]$ centers followed by their desorption and recombination in the gas phase as potential OCM mechanism.

In the research and the characterization of $[Li^+O^-]$, suitable preparative routes for the generation of these $[Li^+O^-]$ centers have been neglected in favor of the rather simple synthetic route of wet impregnation. The addition of Li to MgO, however, results in a variety of modifications of the MgO with different physical and spectroscopic characteristics. Different active centers have been proposed, but the real nature remains unclear.

The evidence for the presence of $[Li^+O^-]$ was only provided by Abraham and co-workers, using EPR and ENDOR experiments. All other researchers only relied on the EPR signal at $g = 2.054$. But this signal is not unique. Moreover, the contribution of the gas phase reaction without a catalyst can be large. Experiments with isotopic labeled reactants showed no mixed reaction products, but an H/D exchange was observed at temperatures below reaction

conditions. Together, these facts put a question mark on the exact role of the catalyst in the oxidative coupling of methane.

In fact, Li/MgO seems to be only one of dozens if not hundreds of chemically totally different materials that catalyze OCM at high temperatures (approximately 750 °C) making it very unlikely that a specific center such as $[Li^+O^-]$ is required to activate CH_4. Other catalysts, La_2O_3 for instance, which do not contain Li^+, Na^+, or K^+, were also found to be active OCM catalysts.

The facts on Li/MgO, that we consider as being proven are:

1. Loss of surface area up Li-addition.
2. Loss of Li during time on stream.
3. Strong influence of gas phase reactions. The latter are a function of temperature, residence time, gas phase composition, free gas phase volume to surface area ratio, and possibly the nature of the surface.
4. Pure MgO, Li/MgO, and Li_2CO_3 are active OCM catalysts with comparable performance.
5. Positive isotope exchange effect.
6. Carbene mechanism is unlikely.
7. Irreversible C-H activation (no isotope scrambling), as H,D scrambling is observed on MgO. It could be that C_2 formation is a pure gas phase process.
8. Li/MgO active for ODH of C_2H_6 to C_2H_4.
9. Gas phase oxidation product is CO, surface oxidation product is CO_2.
10. Gas phase O_2 necessary for C_2 formation.

Doping of Li/MgO with additional metal oxides, especially transition metal oxides, partially led to improved catalysts, however, without meeting the practical needs. New multi-metal-oxide phases form, with various compositions and the loss of Li can be reduced. However, the structure of such materials is even more complex, therefore, a sound structure activity relationship has not been established yet.

The contribution of the gas phase might be high and underestimated in the literature. A strong gas phase contribution may also explain the vast differences of the catalytic test results, as the applied testing conditions seem to have a stronger influence than the composition or the morphology of the catalyst.

In summary, there is no doubt that OCM on Li/MgO and other materials proceeds via a combination of surface and gas phase reactions steps with the involvement of radicals as key intermediates. However, the stoichiometric coupling of $CH_3\cdot$ radicals in the gas phase released from $[Li^+O^-]$ sites at the

Li/MgO surface lacks any solid experimental or theoretical foundation even though this mechanism, probably because of seductive simplicity, found its way into many textbooks and reviews on this subject matter. Because Li/MgO, regardless of the initial preparation route, deactivates due to continuous loss of Li over many hours time on stream, it is furthermore questionable whether Li/MgO is really a good catalyst for studying the principles of OCM as any kinetic or characterization data taken on this material are only a snapshot at some point on the deactivation trajectory, which was in hardly any publication followed until a true study state was achieved explaining the vastly scattering results published in the literature. The transient nature of Li/MgO coupled to parallel occurring gas phase reactions, which in turn are sensitive to temperature, pressure, surface to gas phase volume, dilution with inert gases etc. make mechanistic OCM studies extremely challenging. Therefore, accepting Figure 7 as "the" OCM mechanism on Li/MgO seems too early. Many more fundamental studies under well defined conditions will be necessary to unravel this complex reaction network.

ACKNOWLEDGMENTS

We would like to thank the Deutsche Forschungsgemeinschaft for funding the Excellence Cluster "Unicat" (Unifying Concepts in Catalysis) and the International Max Planck Research School of the Fritz Haber Institute of the Max Planck Society for financial support. Dr. Sergey Levchenko acknowledges support from the Alexander von Humboldt Foundation, and Dr. Raimund Horn thanks the Deutsche Forschungsgemeinschaft for an Emmy Noether grant. Mr. Sebastian Arndt is in debt to Mr. Torsten Otremba, without his automatization of the experimental set-up, there would not have been sufficient time for the preparation of this manuscript. Moreover, Mr. Arndt would like to thank his trainees, Anna Paliszewska and Domenic Jelinski, for their support with the ongoing research during the work on this review and Pauline Mazurkiewiez for her help with the literature search. We also thank Dr. Thomas Risse, Dr. Yilmaz Aksu, and Prof. Dr. Helmut Schubert and his research group for their help with the evaluation of certain analytical methods and procedures.

ABBREVIATIONS

AAS	Atomic Absorption Spectroscopy
BET	Brunauer Emmett Teller
CVD	Chemical Vapor Deposition
DC	Direct Current
DFT	Density Functional Theory
DRIFTS	Diffuse Reflectance Fourier Transform Infrared Spectroscopy

ENDOR	Electron Nuclear Double Resonance Spectroscopy
EPR	Electron Paramagnetic Resonance
ESR	Electron Spin Resonance
eV	Electron Volt
FT-IR	Fourier Transform Infrared Spectroscopy
GGA	Generalized Gradient Approximation
GGA+U	Generalized Gradient Approximation with on-site Coulomb Interaction Correction
HF	Hartree-Fock
HREELS	High Resolution Electron Energy Loss Spectroscopy
HR-TEM	High Resolution Transmission Electron Microscopy
IR	Infrared
KIE	Kinetic Isotope Effect
LC	Low Coordination
MAS	Magic Angle Spinning
MBOH	2-methyl-3-butyn-2-ol
NMR	Nuclear Magnetic Resonance Spectroscopy
OCM	Oxidative Coupling of Methane
ODH	Oxidative Dehydrogenation
SEM	Scanning Electron Microscopy
SFC	Self Consistent Field
SSITKA	Steady State Isotopic Transient Kinetic Analysis
STY	Space Time Yield
TAP	Temporal Analysis of Products
TD	Time Dependent
TD-DFT	Time Dependent Density Functional Theory
TEM	Transmission Electron Microscopy
TPD	Temperature Programmed Desorption
TPR	Temperature Programmed Reaction
UHF	Unrestricted Hartree-Fock
UHV	Ultra High Vacuum
XANES	X-ray Absorption Near Edge Structure
XPS	X-Ray Photoelectron Spectroscopy
XRD	X-Ray Diffraction

REFERENCES

[1] Keller, G.E.; Bhasin, M.M. Synthesis of Ethylene via Oxidative Coupling of Methane: I. Determination of Active Catalysts. *J. Catal.* **1982**, *73*, 9–19.

[2] Hinsen, W.; Baerns, M. Oxidative Kopplung von Methan zu C_2-Kohlenwasserstoffen in Gegenwart unterschiedlicher Katalysatoren. *Chem. Ztg* **1983**, *107*, 223–226.

[3] Wolf, E.E., Ed. *Methane Conversion by Oxidative Processes—Fundamental and Engineering Aspects*. Van Nostrand Reinhold: New York, 1992.

[4] Maitra, A.M. Critical Performance Evaluation of Catalysts and Mechanistic Implications for Oxidative Coupling of Methane. *Appl. Catal., A* **1993**, *104*, 11–59.

[5] Zhang, Z.L.; Verykios, X.E.; Baers, M. Effect of Electronic Properties of Catalysts for the Oxidative Coupling of Methane on Their Selectivity and Activity. *Catal. Rev. Sci. Eng.* **1994**, *36*, 507–556.

[6] Bhasin, M.M; Slocum, D.W., Eds. *Methane and Alkane Conversion Chemistry*. Plenum Press: New York, 1995.

[7] Thybaut, J.W.; Sun, J.J.; Olivier, L.; van Veen, A.C.; Mirodatos, C.; Marin, G.B. Catalyst Design Based on Microkinetic Models: Oxidative Coupling of Methane. *Catal. Today* **2011**, *159*, 29–36.

[8] Ito, T.; Lunsford, J.H. Synthesis of Ethylene and Ethane by Partial Oxidation of Methane over Lithium-Doped Magnesium Oxide. *Nature* **1985**, *314*, 721–722.

[9] Ito, T.; Wang, J.X.; Lin, C.H.; Lunsford, J.H. Oxidative Dimerization of Methane over a Lithium-Promoted Magnesium-Oxide Catalyst. *J. Am. Chem. Soc.* **1985**, *107*, 5062–5068.

[10] Driscoll, D.J.; Martir, W.; Wang, J.X.; Lunsford, J.H. Formation of Gas-Phase Methyl Radicals over MgO. *J. Am. Chem. Soc.* **1985**, *107*, 58–63.

[11] Lin, C.H.; Ito, T.; Wang, J.X.; Lunsford, J.H. Oxidative Dimerization of Methane over Magnesium and Calcium Oxide Catalysts Promoted with Group IA Ions: The Role of $[M^+O^-]$ Centers. *J. Am. Chem. Soc.* **1987**, *109*, 4808–4810.

[12] Iwamatsu, E.; Moriyama, T.; Takasaki, N.; Aika; K. Oxidative Coupling of Methane over Promoted Magnesium Oxide Catalysts: Relation Between Activity and Specific Surface Area. *Stud. Surf. Sci. Catal.* **1988**, *36*, 373–382.

[13] Iwamatsu, E.; Moriyama, T.; Takasaki, N.; Aika; K. Oxidative Coupling of Methane over Na^+- and Rb^+-Doped MgO Catalysts. *J. Catal.* **1988**, *113*, 25–35.

[14] Iwamatsu, E.; Aika, K.I. Kinetic Analysis of the Oxidative Coupling of Methane over Na^+-Doped MgO. *J. Catal.* **1989**, *117*, 416–431.

[15] Choudhary, V.R.; Pataskar, S.G.; Pandit, M.Y.; Gunjikar, V.G. Thermal Analysis of Basic Magnesium Carbonate Containing Different Alkali Metal Carbonates. *Thermochim. Acta* **1991**, *180*, 69–80.

[16] Choudhary, V.R.; Rane, V.H.; Pandit, M.Y. Comparison of Alkali Metal Promoted MgO Catalysts for Their Surface Acidity/Basicity and Catalytic Activity/Selectivity in the Oxidative Coupling of Methane. *J. Chem. Technol. Biotechnol.* **1997**, *68*, 177–186.

[17] Haag, S.; van Veen, A.C.; Mirodatos, C. Influence of Oxygen Supply Rates on Performances of Catalytic Membrane Reactors: Application to the Oxidative Coupling of Methane. *Catal. Today* **2007**, *127*, 157–164.

[18] Olivier, L.; Haag, S.; Mirodatos, C.; van Veen, A.C. Oxidative Coupling of Methane Using Catalyst Modified Dense Perovskite Membrane Reactors. *Catal. Today* **2009**, *142*, 34–41.

[19] Chen, Q.; Couwenberg, P.M.; Marin, G.B. The Oxidative Coupling of Methane with Cofeeding of Ethane. *Catal. Today* **1994**, *21*, 309–319.

[20] Edwards, J.H.; Tyler, R.J.; White, S.D. Oxidative Coupling of Methane over Lithium-Promoted Magnesium Oxide Catalysts in Fixed-Bed and Fluidized-Bed Reactors. *Energy Fuels* **1990**, *4*, 85–93.

[21] Phillips, M.D.; Eastman, A.D. Effect of Li/MgO Methane Coupling Catalyst on Alonized Steel Reactors. *Catal. Lett.* **1992**, *13*, 157–174.

[22] Slagtern, Å.; Dahl, I.M.; Jens, K.J.; Hansen, E.; Seiersten, M. Reactor Materials for Use with the Li/MgO Methane Coupling Catalyst. *Appl. Catal., A* **1992**, *91*, 13–25.

[23] Santos, A.; Menéndez, M.; Santamaría, J. Oxidative Coupling of Methane over Li/Sn/MgO Catalysts. Use of a Fluidized Bed Reactor at Low Gas Velocities. *Stud. Surf. Sci. Catal.* **1997**, *107*, 373–378.

[24] Miguel, M.P.; Coronas, J.; Meméndez, M.; Santamaría, J. Methane Oxidative Coupling over Different Alkali-Doped Catalysts: A Comparison of Ceramic Membrane Reactors and Conventional Fixed Bed Reactors. *React. Kinet. Catal. Lett.* **1996**, *59*, 277–284.

[25] Taniewski, M.; Lachowicz, A.; Skutil, K.; Czechowicz, D. The Effect of Dilution of the Catalyst Bed on Its Heat-Transfer Characteristics in Oxidative Coupling of Methane. *Chem. Eng. Sci.* **1996**, *51*, 4271–4278.

[26] Taniewski, M.; Lachowicz, A.; Skutil, K. Effective Utilisation of the Catalyst Bed Deactivating in the Course of Oxidative Coupling of Methane. *Chem. Eng. Sci.* **1997**, *52*, 935–939.

[27] Amin, N.A.S.; Pheng, S.E. Influence of Process Variables and Optimization of Ethylene Yield in Oxidative Coupling of Methane over Li/MgO Catalyst. *Chem. Eng. J.* **2006**, *116*, 187–195.

[28] Korf, S.J.; Roos, J.A.; de Bruijn, N.A.; van Ommen, J.G.; Ross, J.R.H. Oxidative Coupling of Methane over Lithium Doped Magnesium Oxide Catalysts. *Catal. Today* **1988**, *2*, 535–545.

[29] Matsuura, I.; Utsumi, Y.; Doi, T. Oxidative Coupling of Methane over Lithium-Doped Ultrafine Crystalline Magnesium Oxide. *Appl. Catal.* **1989**, *47*, 299–306.

[30] Choudhary, V.R.; Chaudhari, S.T.; Pandit, M.Y. Highly Stable Li-Doped Magnesium Oxide Catalyst for Oxidative Conversion of Methane to Higher Hydrocarbons. *J. Chem. Soc., Chem. Commun.* **1991**, 1158–1159.

[31] Camino, J.I.; Holgado, M.J.; Rives, V. Li/MgO Catalysts, I. Effect of Precursor Salts on Their Structural and Surface Properties. *React. Kinet. Catal. Lett.* **1991**, *44*, 469–473.

[32] Camino, J.I.; Holgado, M.J.; Rives, V. Li/MgO Catalysts: II. A DTA and TG Study of Precursors. *React. Kinet. Catal. Lett.* **1991**, *45*, 35–39.

[33] Holgado, M.J.; Rives, V.; San Roman, S. Li/MgO Catalysts. III. Effect of Precursor Salts on the Catalytic Activity in Methane Oxidative Coupling. *React. Kinet. Catal. Lett.* **1992**, *48*, 455–460.

[34] Choudhary, V.R.; Mulla, S.A.R.; Pandit, M.Y.; Chaudhari, S.T.; Rane, V.H. Influence of Precursors of Li_2O and MgO on Surface and Catalytic Properties of Li-Promoted MgO in Oxidative Coupling of Methane. *J. Chem. Technol. Biotechnol.* **2000**, *75*, 828–834.

[35] Kuo, Y.F.; Behrend, F.; Lerch, M. Effect of the Specific Surface Area of Li/MgO Catalysts in the Oxidative Coupling of Methane. *Z. Phys. Chem.* **2007**, *221*, 1017–1037.

[36] López, T.; Garcia-Cruz, I.; Gomez, R. Synthesis of Magnesium Oxide by the Sol-Gel Method: Effect of the pH on the Surface Hydroxylation. *J. Catal.* **1991**, *127*, 75–85.

[37] López, T.; Gómez, R.; Ramírez-Solís, A.; Poulain, E.; Novaro, O. Li/MgO Sol-Gel Catalysts. *J. Mol. Catal.* **1994**, *88*, 71–84.

[38] Gomez, R.; Lopez, T.; Herrera, L.; Castro, A.A.; Scelza, O.; Baronetti, G.; Lazzari, E.; Cuan, A.; Campos, M.; Poulain, E.; Ramirez-Solis, A.; Novaro, O. Oxidative Coupling of Methane over Sol-Gel Magnesium Oxide Catalysts: Effect on Selectivity to Olefin Formation. *Stud. Surf. Sci. Catal.* **1993**, *75*, 2213–2216.

[39] Trionfetti, C.; Babich, I.V.; Seshan, K.; Lefferts, L. Formation of High Surface Area Li/MgO—Efficient Catalyst for the Oxidative Dehydrogenation/Cracking of Propane. *Appl. Catal., A* **2006**, *310*, 105–113.

[40] Trionfetti, C.; Babich, I.V.; Seshan, K.; Lefferts, L. Efficient Catalysts for Olefins from Alkanes: Sol-Gel Synthesis of High Surface Area Nano Scale Mixed Oxide Clusters. *Top. Catal.* **2006**, *39*, 191–198.

[41] Roussy, G.; Marchal, E.; Thiebaut, J.M.; Kiennemann, A.; Maire, G. C_2^+ Selectivity Enhancement in Oxidative Coupling of Methane over Microwave-Irradiated Catalysts. *Fuel Process. Technol.* **1997**, *50*, 261–274.

[42] Chevalier, C.H.; Ramirez de la Piscina, P.; Ceruso, M.; Choplin, A.; Basset, J.M. Oxidative Dimerization of Methane: A Surface Organometallic Approach to Lithium Doped Magnesia or Silica Catalysts. *Catal. Today* **1989**, *4*, 433–439.

[43] Heitz, S.; Aksu, Y.; Merschjann, C.; Driess, M. Methylmagesium Alkoxide Clusters with Mg_4O_4 Cubane- and Mg_7O_8 Biscubane-Like Cores: Organometallic Precursors for Low-Temperature Formation of MgO Nanoparticles with Variable Surface Defects. *Chem. Mater.* **2010**, *22*, 1376–1385.

[44] Heitz, S.; Epping, J.D.; Aksu, Y.; Driess, M. Molecular Heterobimetallic Approach to Li-Containing MgO Nanoparticles with Variable Li-Concentrations Using Lithium-Methylmagnesium Alkoxide Clusters. *Chem. Mater.* **2010**, *22*, 4563–4571.

[45] Berger, T.; Schuh, J.; Sterrer, M.; Diwald, O.; Knözinger, E. Lithium Ion Induced Surface Reactivity Changes on MgO Nanoparticles. *J. Catal.* **2007**, *247*, 61–67.

[46] Martin, G.A.; Turlier, P.; Ducarme, V.; Mirodatos, C.; Pinabiau, M. Beneficial Effect of Silica Addition to Li/MgO Catalysts Used for the Oxidative Coupling of Methane. *Catal. Today* **1990**, *6*, 373–380.

[47] Sarkas, H.W.; Arnold, S.T.; Hendricks, J.H.; Kidder, L.H.; Jones, C.A.; Bowen, K.H. An Investigation of Catalytic Activity in Mixed Metal Oxide Nanophase Materials. *Z. Phys. D: At. Mol. Clusters* **1993**, *26*, 46–50.

[48] Choudhary, V.R.; Mulla, S.A.R.; Uphade, B.S. Influence of Support on Surface Basicity and Catalytic Activity in Oxidative Coupling of Methane of Li-MgO Deposited on Different Commercial Catalyst Carriers. *J. Chem. Technol. Biotechnol.* **1998**, *72*, 99–104.

[49] Zavyalova, U.; Girgsdies, F.; Korup, O.; Horn, R.; Schlögl, R. Microwave-Assisted Self-Propagating Combustion Synthesis for Uniform Deposition of Metal Nanoparticles on Ceramic Monoliths. *J. Phys. Chem. C* **2009**, *113*, 17493–17501.

[50] Zavyalova, U.; Geske, M.; Horn, R.; Weinberg, G.; Frandsen, W.; Schuster, M.; Schlögl, R. Morphology and Microstructure of Li/MgO Catalysts for the Oxidative Coupling of Methane. *ChemCatChem* **2010**, *3*, 949–959.

[51] Baerns, M. *Methane Conversion by Oxidative Processes*. Van Nostrand Reinhold: New York, 1992, pp. 382–402.

[52] Käßner, P.; Baerns, M. Comparative Characterization of Basicity and Acidity of Metal Oxide Catalysts for the Oxidative Coupling of Methane by Different Methods. *Appl. Catal., A* **1996**, *139*, 107–129.

[53] Davydov, A.A.; Shepotko, M.L.; Budneva, A.A. Basic Sites on the Oxide Surfaces: Their Effect on the Catalytic Methane Coupling. *Catal. Today* **1995**, *24*, 225–230.

[54] Davydov, A.A. Basic Sites on the Surface of Oxide Catalysts Responsible for Oxidative Methane Coupling. *Chem. Eng. Technol.* **1995**, *18*, 7–11.

[55] Kuś, S.; Otremba, M.; Tórz, A.; Taniewski, M. The Effect of Gas Atmosphere Used in the Calcination of MgO on Its Basicity and Catalytic Performance in Oxidative Coupling of Methane. *Appl. Catal., A* **2002**, *230*, 263–270.

[56] Kuś, S.; Taniewski, M. The Effect of Some Impurities on the Basicity of MgO Tested by the Transformation of 2-Butanol and on Its Catalytic Performance in Oxidative Coupling of Methane. *Fuel Process. Technol.* **2002**, *76*, 41–49.

[57] Bailly, M.L.; Chizallet, C.; Costentin, G.; Krafft, J.M.; Lauron-Pernot, H.; Che, M. A Spectroscopy and Catalysis Study of the Nature of Active Sites of MgO Catalysts: Thermodynamic Brønsted Basicity Versus Reactivity of Basic Sites. *J. Catal.* **2005**, *235*, 413–422.

[58] Chizallet, C.; Costentin, G.; Lauron-Pernot, H.; Che, M.; Bonhomme, C.; Maquet, J.; Delbecq, F.; Sautet, P. Study of the Structure of OH Groups on MgO by 1D and 2D ^{1}H MAS NMR Combined with DFT Cluster Calculations. *J. Phys. Chem. C* **2007**, *111*, 18279–18287.

[59] Chizallet, C.; Petitjean, H.; Costentin, C.; Lauron-Pernot, H.; Maquet, J.; Bonhomme, C.; Che, M. Identification of the OH groups responsible for kinetic basicity on MgO surfaces by ^{1}H MAS NMR. *J. Catal.* **2009**, *268*, 175–179.

[60] Choudhary, V.R.; Rane, V.H.; Chaudhari, S.T. Influence of Various Promoters on the Basicity and Catalytic Activity of MgO Catalysts in Oxidative Coupling of Methane. *Catal. Lett.* **1990**, *6*, 95–98.

[61] Díez, V.K.; Apesteguía, C.R.; Di Cosimo, J.I. Acid-Base Properties and Active Site Requirements for Elimination Reactions on Alkali-Promoted MgO Catalysts. *Catal. Today* **2000**, *63*, 53–62.

[62] Martin, G.A.; Mirodatos, C. *Methane Conversion by Oxidative Processes*. Van Nostrand Reinhold, 1992, pp. 351–381.

[63] Spoto, G.; Gribov, E.N.; Ricchiardi, G.; Damin, A.; Scarano, D.; Bordiga, S.; Lamberti, C.; Zecchina, A. Carbon Monoxide MgO from Dispersed Solids to Single Crystals: A Review and New Advances. *Prog. Surf. Sci*. **2004**, *76*, 71–146.

[64] Choudhary, V.R.; Rane, V.H.; Gadre, R.V. Influence of Precursors Used in Preparation of MgO on Its Surface Properties and Catalytic Activity in Oxidative Coupling of Methane. *J. Catal*. **1994**, *145*, 300–311.

[65] Choudhary, V.R.; Pataskar, S.G.; Gunjikar, V.G.; Zope, G.B. Influence of Preparation Conditions of Basic Magnesium Carbonate on its Thermal Analysis. *Thermochim. Acta* **1994**, *232*, 95–110.

[66] Choudhary, V.R.; Pataskar, S.G.; Zope, G.B.; Chaudhari, P.N. Surface Properties of Magnesium Oxide Obtained from Basic Magnesium Carbonate: Influence of Preparation Conditions of Magnesium Carbonate. *J. Chem. Technol. Biotechnol*. **1995**, *64*, 407–413.

[67] Choudhary, V.R.; Pandit, M.Y. Surface Properties of Magnesium Oxide Obtained from Magnesium Hydroxide: Influence on Preparation and Calcination Conditions of Magnesium Hydroxide. *Appl. Catal*. **1991**, *71*, 265–274.

[68] Ardizzone, S.; Bianchi, C.L.; Fadoni, M.; Vercelli, B. Magnesium Salts and Oxide: An XPS Overview. *Appl. Surf. Sci*. **1997**, *119*, 253–259.

[69] Ardizzone, S.; Bianchi, C.L.; Vercelli, B. MgO Powders: Interplay between Adsorbed Species and Localisation of Basic Sites. *Appl. Surf. Sci*. **1998**, *126*, 169–175.

[70] Mellor, I.M.; Burrows, A.; Coluccia, S.; Hargreaves, J.S.J.; Joyner, R.W.; Kiely, C.J.; Martra, G.; Stockenhuber, M.; Tang, W.M. Probing Possible Structure Sensitivity in the Exchange of Isotopic Oxygen with the Surface of MgO. *J. Catal*. **2005**, *234*, 14–23.

[71] Kimble, J.B.; Kolts, J.H. Playing Matchmaker with Methane. *Chem. Tech*. **1987**, *17*, 501–505.

[72] Lee, J.S.; Oyama, S.T. Oxidative Coupling of Methane to Higher Hydrocarbons. *Catal. Rev. Sci. Eng*. **1988**, *30*, 249–280.

[73] Kimble, J.B.; Kolts, J.H. Oxidative Coupling of Methane to Higher Hydrocarbons. *Energy Progr*. **1986**, *6*, 226–229.

[74] Korf, S.J.; Roos, J.A.; de Bruijn, N.A.; van Ommen, J.G.; Ross, J.R.H. Lithium Chemistry of Lithium Doped Magnesium Oxide Catalysts Used in the Oxidative Coupling of Methane. *Appl. Catal*. **1990**, *58*, 131–146.

[75] Galuszka, J. Carbon Dioxide Chemistry During Oxidative Coupling of Methane on a Li/MgO Catalyst. *Catal. Today* **1994**, *21*, 321–331.

[76] Turek, A.M.; Wachs, I.E.; DeCanio, E. Acidic Properties of Alumina-Supported Metal Oxide Catalysts: An Infrared Spectroscopy Study. *J. Phys. Chem*. **1992**, *96*, 5000–5007.

[77] Busca, G.; Lorenzelli, V. Infrared Spectroscopic Identification of Species Arising from Reactive Adsorption of Carbon Oxides on Metal Oxide Surfaces. *Mater. Chem*. **1982**, *7*, 89–126.

[78] Spencer, M.S.; Lunsford, J.H.; Roberts, M.W.; Cunningham, J.; Burch, R.; Krylov, O.V.; Moffat, J.B.; Hutchings, G.J.; Joyner, R.W.; Ichikawa, M.; Datye, A.K.; Haber, J.; Serwicka, E.M.; Thomas, J.M. General Discussion. *Faraday Discuss. Chem. Soc*. **1989**, *87*, 47–64.

[79] Hutchings, G.J.; Scurrell, M.S.; Woodhouse, J. Oxidative Coupling of Methane Using Li/MgO Catalyst: Re-Appraisal of the Optimum Loading of Li. *Catal. Lett*. **1990**, *5*, 301–308.

[80] Hargreaves, J.S.J.; Hutchings, G.J.; Joyner, R.W. Structural Aspects of the Oxidative Coupling of Methane. *Catal. Today* **1990**, *6*, 481–488.

[81] Hargreaves, J.S.J.; Hutchings, G.J.; Joyner, R.W.; Kiely, C.J. Structural Aspects of Magnesium Oxide Catalysts for the Oxidative Coupling of Methane. *Catal. Today* **1991**, *10*, 259–266.

[82] Hargreaves, J.S.J.; Hutchings, G.J.; Joyner, R.W.; Kiely, C.J. The Relationship between Catalyst Morphology and Performance in the Oxidative Coupling of Methane. *J. Catal*. **1992**, *135*, 576–595.

[83] Hargreaves, J.S.J.; Hutchings, G.J.; Joyner, R.W.; Kiely, C.J. Relationship between Morphology and Catalytic Performance of Lithium and Gold Doped Magnesium Oxide Catalysts for the Oxidative Coupling of Methane. *Catal. Today* **1992**, *13*, 401–407.

[84] Lewis, D.W.; Grimes, R.W.; Catlow, C.R.A. Defect Processes at Low Coordinate Surface Sites of MgO and Their Role in the Partial Oxidation of Hydrocarbons. *J. Mol. Catal. A: Chem*. **1995**, *100*, 103–114.

[85] Lunsford, J.H.; Cisneros, M.D.; Hinson, P.G.; Tong, Y.D.; Zhang, H.S. Oxidative Dimerization of Methane over Well Defined Lithium-Promoted Magnesium Oxide Catalysts. *Faraday Discuss. Chem. Soc*. **1989**, *87*, 13–21.

[86] Choudhary, V.R.; Rajput, A.M.; Akolekar, D.B.; Seleznev, V.A. Oxidative Conversion of Methane to C_2-Hydrocarbons over Lithium, Manganese, Cadmium and Zinc Promoted MgO Catalysts I. Catalyst Performance in Presence of Free Oxygen. *Appl. Catal*. **1990**, *62*, 171–187.

[87] Choudhary, V.R.; Sansare, S.D.; Rajput, A.M.; Akolekar, D.B. Oxidative Conversion of Methane to C_2 Hydrocarbons over Li, Mn, Cd and Zn Promoted MgO Catalysts II: Performance of Fresh and Reoxidised Catalysts in the Absence of Free Oxygen. *Appl. Catal*. **1991**, *69*, 187–200.

[88] Sinev, M.Y.; Bychkov, V.Y.; Korchak, V.N.; Krylov, O.V. Oxidative Coupling of Methane with Participation of Oxide Catalyst Lattice Oxygen. *Catal. Today* **1990**, *6*, 543–549.

[89] Taniewski, M.; Lachowicz, A.; Lachowicz, R.; Czechowicz, D.; Skutil, K. Evidence for a High Oxygen Mobility in Li/MgO. *Catal. Lett*. **1994**, *26*, 355–363.

[90] Anderson, A.G.; Norby, T. Liquid Phases in Li:MgO as Studied by Thermoanalytical Methods, Electron Microscopy, and Electrical Conductivity Measurements. *Catal. Today* **1990**, *6*, 575–586.

[91] Mitoff, S.P. Bulk Versus Surface Conductivity of MgO Crystals. *J. Chem. Phys*. **1964**, *41*, 2561–2562.

[92] Haggin, J. Oxidative Coupling Technology May Offer New Route To Olefins. *Chem. Eng. News* **1990**, *68*, 26–28.

[93] Norby, T.; Anderson, A.G. Electrical Conductivity and Defect Structure of Lithium-Doped Magnesium Oxide. *Appl. Catal*. **1991**, *71*, 89–102.

[94] Balint, I.; Aika, K.I. Defect Chemistry of Lithium-Doped Magnesium Oxide. *J. Chem. Soc., Faraday Trans*. **1997**, *93*, 1797–1801.

[95] Balint, I.; Aika, K.I. Specific Defect Sites Creation by Doping MgO with Lithium and Titanium. *Appl. Surf. Sci*. **2001**, *173*, 296–306.

[96] Tardío, M.M.; Ramírez, R.; González, R.; Chen, Y. p-Type Semiconducting Properties in Lithium-Doped MgO Single Crystals. *Phys. Rev. B* **2002**, *66*, 134202.

[97] Balint, I.; Aika, K.I. Study on Surface DC Conductivity of Various MgO Catalysts: Nature of Defect and the Role in Methane Activation. *Stud. Surf. Sci. Catal*. **1994**, *81*, 177–186.

[98] Balint, I.; Aika, K.I. Interaction of Water with 1% Li/MgO: DC Conductivity of Li/MgO Catalyst for Methane Selective Activation. *J. Chem. Soc., Faraday Trans*. **1995**, *91*, 1805–1811.

[99] Abraham, M.M.; Butler, C.T.; Chen, Y. Growth of High-Purity and Doped Alkaline Earth Oxides: I. MgO and CaO. *J. Chem. Phys*. **1971**, *55*, 3752–3756.

[100] Schirmer, O.F. Trapped-Hole Centers Containing Lithium in MgO, CaO and SrO. *J. Phys. Chem. Solids* **1971**, *32*, 499–509.

[101] Abraham, M.M.; Unruh, W.P.; Chen, Y. Electron-Nuclear-Double-Resonance Investigations of $[Li]^0$ and $[Na]^0$ Centers in MgO, CaO, and SrO. *Phys. Rev. B* **1974**, *10*, 3540–3545.

[102] Rius, G.; Herve, A. Endor Spectrum of the V_{Li} Center in MgO at 4.2 K. *Solid State Commun*. **1974**, *15*, 399–402.

[103] Chen, Y.; Tohver, H.T.; Narayan, J.; Abraham, M.M. High-Temperature and Ionization-Induced Effects in Lithium-Doped MgO Single Crystals. *Phys. Rev. B* **1977**, *16*, 5535–5542.

[104] Chen, Y.; Montesa, E.; Boldú, J.L.; Abraham, M.M. Neutron Irradiations in Oxidized Lithium-Doped MgO Crystals. *Phys. Rev. B* **1981**, *24*, 5–10.

[105] Narayan, J.; Abraham, M.M.; Chen, Y.; Tohver, H.T. Transmission Electron Microscope Studies on Li-Doped MgO. *Philos. Mag. A* **1978**, *38*, 247–257.

[106] Lacey, J.B.; Abraham, M.M.; Boldú, J.L.; Chen, Y.; Narayan, J.; Tohver, H.T. Oxidation and Reduction of Lithium-Containing MgO at High Temperatures. *Phys. Rev. B* **1978**, *18*, 4136–4142.

[107] Boldu, J.L.; Abraham, M.M.; Chen, Y. Valence Compensation of Thermally Generated $[Li]^0$ Defects in MgO. *Phys. Rev. B* **1979**, *19*, 4421–4426.

[108] Olson, D.N.; Orera, V.M.; Chen, Y.; Abraham, M.M. Thermally generated $[Li]^0$ Centers in CaO. *Phys. Rev. B* **1980**, *21*, 1258–1263.

[109] Chen, Y.; Abraham, M.M.; Boldu, J.L.; Orera, V.M. Current-Voltage Characteristics of Li-Doped MgO Oxidized at Elevated Temperatures. *J. Phys. Colloques* **1980**, *41*, C6–398–C6–400.

[110] Chen, Y.; Abraham, M.M. Trapped-Hole Centers in Alkaline-Earth Oxides. *J. Phys. Chem. Solids* **1990**, *51*, 747–764.

[111] Gonzalez, R.; Chen, Y.; Tsang, K.L. Diffusion of Deuterium and Hydrogen in Doped and Undoped MgO Crystals. *Phys. Rev. B* **1982**, *26*, 4637–4645.

[112] González, R.; Chen, Y. Deuteron Diffusion and Photoluminescence in Lithium-Doped MgO Crystals. *Phys. Rev. B* **1987**, *35*, 8202–8206.

[113] Anpo, M.; Sunamoto, M.; Doi, T.; Matsuura, I. Oxidative Coupling of Methane over Ultrafine Crystalline MgO Doped with Li. Role of Lower Coordinative Surface Sites Produced by Li-Doping. *Chem. Lett.* **1988**, *17*, 701–704.

[114] Padró, C.L.; Grosso, W.E.; Baronetti, G.T.; Castro, A.A.; Scelza, O.A. Surface Characterization and Catalytic Behavior of Li/MgO in Oxidative Coupling of Methane. *Stud. Surf. Sci. Catal.* **1994**, *82*, 411–418.

[115] Aritani, H.; Yamada, H.; Nishio, T.; Imamura, S.; Hasegawa, S.; Tanaka, T.; Yoshida, S. Formation of Defects in Near-Surface Region over Li or Mn-Doped MgO Studied by Mg K-Edge XANES. *Chem. Lett.* **1999**, *28*, 359–360.

[116] Aritani, H.; Yamada, H.; Nishio, T.; Shiono, T.; Imamura, S.; Kudo, M.; Hasegawa, S.; Tanaka, T.; Yoshida, S. Characterisation of Li-Doped MgO Catalysts for Oxidative Coupling of Methane by Means of Mg K-Edge XANES. *J. Phys. Chem. B* **2000**, *104*, 10133–10143.

[117] Trionfetti, C.; Babich, I.V.; Seshan, K.; Lefferts, L. Presence of Lithium Ions in MgO Lattice: Surface Characterization by Infrared Spectroscopy and Reactivity towards Oxidative Conversion of Propane. *Langmuir* **2008**, *24*, 8220–8228.

[118] Myrach, P.; Nilius, N.; Levchenko, S.V.; Gonchar, A.; Risse, T.; Dinse, K.P.; Boatner, L.A.; Frandsen, W.; Horn, R.; Freund, H.J.; Schlögl, R.; Scheffler, M. Temperature-Dependent Morphology, Magnetic and Optical Properties of Li-Doped MgO. *ChemCatChem* **2010**, *2*, 854–862.

[119] Mirodatos, C.; Perrichon, V.; Durupty, M.C.; Moral, P. Deactivation of Alkali Promoted Magnesia in Oxidative Coupling of Methane. *Stud. Surf. Sci. Catal.* **1987**, *34*, 183–195.

[120] Iwamatsu, E.; Moriyama, T.; Takasaki, N.; Aika; K.I. Importance of the Specific Surface Area of the Catalyst in the Oxidative Dimerization of Methane over Promoted Magnesium Oxide. *J. Chem. Soc., Chem. Commun.* **1987**, 19–20.

[121] Perrichon, V.; Durupty, M.C. Thermal Stability of Alkali Metals Deposited on Oxide Supports and Their Influence on the Surface Area of the Support. *Appl. Catal.* **1988**, *42*, 217–227.

[122] Mirodatos, C.; Martin, G.A.; Bertolini, J.C.; Saint-Just, J. The Nature, Role and Fate of Surface Active Sites in Li/MgO Oxidative Coupling Catalysts. *Catal. Today* **1989**, *4*, 301–310.

[123] van Kasteren, J.M.N.; Geerts, J.W.M.H.; van der Wiele, K. Working Principle of Li Doped MgO Applied for the Oxidative Coupling of Methane. *Stud. Surf. Sci. Catal.* **1990**, *55*, 343–349.

[124] Korf, S.J.; Roos, J.A.; de Bruijn, N.A.; van Ommen, J.G.; Ross, J.R.H. Influence of CO_2 on the Oxidative Coupling of Methane over a Lithium Promoted Magnesium Oxide Catalyst. *J. Chem. Soc., Chem. Commun.* **1987**, 1433–1434.

[125] Swaan, H.M.; Li, Y.; Seshan, K.; van Ommen, J.G.; Ross, J.R.H. The Oxidative Coupling of Methane and the Oxidative Dehydrogenation of Ethane over a Niobium Promoted Lithium Doped Magnesium Oxide Catalyst. *Catal. Today* **1993**, *16*, 537–546.

[126] Aigler, J.M.; Lunsford, J.H. Oxidative Dimerization of Methane over MgO and Li^+/MgO Monoliths. *Appl. Catal.* **1991**, *70*, 29–42.

[127] Roos, J.A.; Bakker, A.G.; Bosch, H.; van Ommen, J.G.; Ross, J.R.H. Selective Oxidation of Methane to Ethane and Ethylene over Various Oxide Catalysts. *Catal. Today* **1987**, *1*, 133–145.

[128] Hutchings, G.J.; Scurrell, M.S.; Woodhouse, J.R. Effect of O_3 versus O_2 as Oxidants for Methane. *Stud. Surf. Sci. Catal.* **1988**, *36*, 415–419.

[129] Al-Zahrani, S.M.S.; Song, Q.; Lobban, L.L. Effects of CO_2 during Oxidative Coupling of Methane over Li/MgO: Mechanisms and Models. *Ind. Eng. Chem. Res.* **1994**, *33*, 251–258.

[130] Al-Zahrani, S.M.S.; Lobban, L.L. Effects of Steam and Liquid Water Treatment on the Oxidative Coupling of Methane over a Li/MgO Catalyst. *Ind. Eng. Chem. Res.* **1995**, *34*, 1060–1073.

[131] Al-Zahrani, S.M.S.; Lobban, L.L. The Effects of Gas Composition and Process Conditions on the Oxidative Coupling of Methane over Li/MgO Catalyst. *Stud. Surf. Sci. Catal.* **1996**, *100*, 383–396.

[132] Baerns, M.; Ross, J.R.H. *Perspectives in Catalysis*. IUPAC International Union of Pure and Applied Chemistry: Oxford, 1992, pp. 315–335.

[133] Roos, J.A.; Korf, S.J.; Bakker, A.G.; de Bruijn, N.A.; van Ommen, J.G.; J.R.H.Ross. The Oxidative Coupling of Methane: Catalyst Requirements and Process Conditions. *Stud. Surf. Sci. Catal.* **1988**, *36*, 427–432.

[134] Peng, X.D.; Richards, D.A.; Stair, P.C. Surface Composition and Reactivity of Lithium-Doped Magnesium Oxide Catalysts for Oxidative Coupling of Methane. *J. Catal.* **1990**, *121*, 99–109.

[135] Hutchings, G.J.; Scurrell, M.S.; Woodhouse, J.R. The Role of Surface O^- in the Selective Oxidation of Methane. *J. Chem. Soc., Chem. Commun.* **1987**, 1388–1389.

[136] Bi, Y.L.; Zhen, K.J.; Jiang, Y.T.; Teng, C.W.; Yang, X.G. Catalytic Oxidative Coupling of Methane over Alkali, Alkaline Earth and Rare Earth Metal Oxides. *Appl. Catal.* **1988**, *39*, 185–190.

[137] Machocki, A. Oxidative Coupling of Methane at Moderate (600–650 °C) Temperatures. *Catal. Lett.* **1994**, *26*, 85–93.

[138] Asami, K.; Omata, K.; Fujimoto, K.; Tominaga, H. Oxidative Coupling of Methane in the Homogeneous Gas Phase under Pressure. *J. Chem. Soc., Chem. Commun.* **1987**, 1287–1288.

[139] Ekstrom, A.; Regtop, R.; Bhargava, S. Effect of Pressure on the Oxidative Coupling of Methane. *Appl. Catal.* **1990**, *62*, 253–269.

[140] Lane, G.S.; Wolf, E.E. Methane Utilization by Oxidative Coupling: I. A Study of Reactions in the Gas Phase during the Cofeeding of Methane and Oxygen. *J. Catal.* **1988**, *113*, 144–163.

[141] Pinabiau-Carlier, M.; Ben Hadid, A.; Cameron, C.J. The Effect of Total Pressure on the Oxidative Coupling of Methane Reaction under Cofeed Conditions. *Stud. Surf. Sci. Catal.* **1991**, *61*, 183–190.

[142] Chen, Q.; Couwenberg, P.M.; Marin, G.B. Effect of Pressure on the Oxidative Coupling of Methane in the Absence of Catalyst. *AlChE J.* **1994**, *40*, 521–535.

[143] Chen, Q.; Hoebink, J.H.B.J.; Marin, G.B. Kinetics of the Oxidative Coupling of Methane at Atmospheric Pressure in the Absence of Catalyst. *Ind. Eng. Chem. Res.* **1991**, *30*, 2088–2097.

[144] Parida, K.M.; Rao, S.B. Importance of Specific Surface Area and Basic Sites of the Catalyst in Oxidative Coupling of CH_4 over Li/MgO Catalysts Prepared by Precipitation Methods. *React. Kinet. Catal. Lett.* **1991**, *44*, 95–101.

[145] Aika, K.; Fujimoto, N.; Kobayashi, M.; Iwamatsu, E. Oxidative Coupling of Methane over Various Metal Oxides Supported on Strontium Carbonate Catalysts. *J. Catal.* **1991**, *127*, 1–8.

[146] Rynkowski, J.; Kaźmierczak, A.; Praźmowska-Wilanowski, A.; Paryjczak, T. Influence of Calcination and Lithium Promotion on the Surface Properties of Oxide Supports. *React. Kinet. Catal. Lett.* **1996**, *58*, 169–175.

[147] Abraham, M.M.; Chen, Y.; Boatner, L.A.; Reynolds, R.W. Stable $[Li]^0$ Defects in MgO Single Crystals. *Phys. Rev. Lett.* **1976**, *37*, 849–852.

[148] Driscoll, D.J.; Martir, W.; Wang, J.X.; Lunsford, J.H. The Production of Gas Phase Methyl Radicals over Lithium-Promoted MgO. *Stud. Surf. Sci. Catal.* **1985**, *21*, 403–408.

[149] Yates, D.J.C.; Zlotin, N.E. Blank Reactor Corrections in Studies of the Oxidative Dehydrogenation of Methane. *J. Catal.* **1988**, *111*, 317–324.

[150] Liu, H.F.; Liu, R.S.; Liew, K.Y.; Johnson, R.E.; Lunsford, J.H. Partial Oxidation of Methane by Nitrous Oxide over Molybdenum on Silica. *J. Am. Chem. Soc.* **1984**, *106*, 4117–4121.

[151] Hatano, M.; Hinson, P.G.; Vines, K.S.; Lunsford, J.H. Comments on "Blank Reactor Corrections in Studies of the Oxidative Dehydrogenation of Methane" by D. J. C. Yates and N. E. Zlotin. *J. Catal.* **1990**, *124*, 557–561.

[152] Yates, D.J.C.; Zlotin, N.E. Reply to Hatano, Hinson, Vines, and Lunsford's comments on "Blank Reactor Corrections in Studies of Oxidative Dehydrogenation of Methane". *J. Catal.* **1990**, *124*, 562–565.

[153] Yates, D.J.C.; Zlotin, N.E.; McHenry, J.A. Supported Lithium Tetraborate as a Catalyst for the Continuous Oxidative Dehydrogenation of Methane. *J. Catal.* **1989**, *117*, 290–294.

[154] Kalenik, Z.; Wolf, E.E. *Methane Conversion by Oxidative Processes*. Van Nostrand Reinhold: New York, 1992, pp. 30–77.

[155] Hutchings, G.J.; Scurrell, M.S.; Woodhouse, J.R. The Role of Gas Phase Reaction in the Selective Oxidation of Methane. *J. Chem. Soc., Chem. Commun.* **1988**, 253–255.

[156] Hutchings, G.J.; Scurrell, M.S.; Woodhouse, J.R. Comparison of Ethene and Ethane Primary Selectivities with Li/MgO and MgO Catalysts for Oxidative Coupling of Methane: Comments on the Role of Lithium. *J. Chem. Soc., Chem. Commun.* **1987**, 1862–1863.

[157] Roos, J.A.; Korf, S.J.; Veehof, R.H.J.; van Ommen, J.G.; Ross, J.R.H. Reaction Path of the Oxidative Coupling of Methane over a Lithium-Doped Magnesium Oxide Catalyst. *Appl. Catal.* **1989**, *52*, 147–156.

[158] Roos, J.A.; Korf, S.J.; Veehof, R.H.J.; van Ommen, J.G.; Ross, J.R.H. Kinetic and Mechanistic Aspects of the Oxidative Coupling of Methane over a Li/MgO Catalyst. *Appl. Catal.* **1989**, *52*, 131–145.

[159] Lunsford, J.H.; Qiu, P.; Rosynek, M.P.; Yu, Z.Q. Catalytic Conversion of Methane and Ethylene to Propylene. *J. Phys. Chem. B* **1998**, *102*, 167–173.

[160] Schuurman, Y.; Mirodatos, C. Uses of Transient Kinetics for Methane Activation Studies. *Appl. Catal., A* **1997**, *151*, 305–331.

[161] Nibbelke, R.H.; Scheerová, J.; de Croon, M.H.J.M.; Marin, G.B. The Oxidative Coupling of Methane over MgO-Based Catalysts: A Steady-State Isotope Transient Kinetic Analysis. *J. Catal.* **1995**, *156*, 106–119.

[162] Peil, K.P.; Goodwin, Jr., J.G.; Marcelin, G. An Examination of the Oxygen Pathway during Methane Oxidation over a Lithium/Magnesia Catalyst. *J. Phys. Chem.* **1989**, *93*, 5977–5979.

[163] Peil, K.P.; Goodwin, Jr., J.G.; Marcelin, G. Influence of Product CO_2 on the Overall Reaction Network in the Oxidative Coupling of Methane. *Stud. Surf. Sci. Catal.* **1991**, *61*, 73–79.

[164] Peil, K.P.; Goodwin, Jr., J.G.; Marcelin, G. Surface Phenomena during the Oxidative Coupling of Methane over Li/MgO. *J. Catal.* **1991**, *131*, 143–155.

[165] Dahl, I.M.; Jens, K.J.; Kvisle, S.; Slagtern, Å. Pulse Reactor Characterization Studies of a Li/MgO Catalyst for the Oxidative Coupling of Methane. *Stud. Surf. Sci. Catal.* **1991**, *61*, 81–87.

[166] Choudhary, V.R.; Rane, V.H.; Chaudhari, S.T. Pulse Reactions of Methane, Ethane and Ethylene over Li-, La- and Sm-Promoted MgO Catalysts in the Presence and Absence of Free Oxygen. *React. Kinet. Catal. Lett.* **1998**, *63*, 371–377.

[167] Keulks, G.W.; Liao, N.; An, W.; Li, D. Temperature-Programmed Studies of Surface Oxygen Species in the Oxidative Coupling of Methane. *Stud. Surf. Sci. Catal.* **1993**, *75*, 2253–2256.

[168] Bhumkar, S.C.; Lobban, L.L. Diffuse Reflectance Infrared and Transient Studies of Oxidative Coupling of Methane over Lithium/Magnesia Catalyst. *Ind. Eng. Chem. Res.* **1992**, *31*, 1856–1864.

[169] Nakamura, M.; Yanagibashi, H.; Mitsuhashi, H.; Takezawa, N. Adsorbed Oxygen Species Formed by the Decomposition of N_2O on Li/MgO Catalysts. *Bull. Chem. Soc. Jpn.* **1993**, *66*, 2467–2472.

[170] Hutchings, G.J.; Scurrell, M.S.; Woodhouse, J.R. Oxidative Coupling of Methane Using Oxide Catalysts. *Chem. Soc. Rev.* **1989**, *18*, 251–283.

[171] Hutchings, G.J.; Scurrell, M.S. *Methane Conversion by Oxidative Processes*. Van Nostrand Reinhold: New York, 1992, pp. 200–258.

[172] Hutchings, G.J.; Woodhouse, J.R.; Scurrell, M.S. Partial Oxidation of Methane over Oxide Catalysts. Comments on the Reaction Mechanism. *J. Chem. Soc., Faraday Trans. 1* **1989**, *85*, 2507–2523.

[173] Cunningham, J.; McNamara, D. Activation of Methane, Oxygen and Nitrous Oxide over Surface-Doped MgO Materials: I. Conversions in N_2O, ($N_2O + CH_4$) and ($O_2 + CH_4$) reactants. *Catal. Today* **1990**, *6*, 551–558.

[174] Hutchings, G.J.; Scurrell, M.S.; Woodhouse, J.R. Selective Oxidation of Methane in the Presence of NO: New Evidence on the Reaction Mechanism. *J. Chem. Soc., Chem. Commun.* **1989**, 765–766.

[175] Hutchings, G.J.; Scurrell, M.S.; Woodhouse, J.R. Selective Oxidation of Methane in the Presence of Nitric Oxide: Comments on the Reaction Mechanism. *Catal. Today* **1990**, *6*, 399–407.

[176] Hutchings, G.J.; Scurrell, M.S.; Woodhouse, J.R. Direct Partial Oxidation of Methane: Effect of the Oxidant on the Reaction. *Appl. Catal.* **1988**, *38*, 156–165.

[177] Shi, C.L.; Xu, M.T.; Rosynek, M.P.; Lunsford, J.H. Origin of Kinetic Isotope Effects during the Oxidative Coupling of Methane over a Li^+/MgO Catalyst. *J. Phys. Chem.* **1993**, *97*, 216–222.

[178] Yamamoto, H.; Chu, H.Y.; Xu, M.T.; Shi, C.L.; Lunsford, J.H. Oxidative Coupling of Methane over a Li^+/MgO Catalyst Using N_2O as an Oxidant. *J. Catal.* **1993**, *142*, 325–336.

[179] Davydov, A.A.; Budneva, A.A.; Aliev, S.M.; Sokolovskii, V.D. IR Spectra of Methane Adsorbed on MgO. *React. Kinet. Catal. Lett.* **1988**, *36*, 491–495.

[180] Wang, D.J.; Xu, M.T.; Shi, C.L.; Lunsford, J.H. Effect of Carbon Dioxide on the Selectivities Obtained during the Partial Oxidation of Methane and Ethane over Li^+/MgO Catalysts. *Catal. Lett.* **1993**, *18*, 323–328.

[181] Morales, E.; Lunsford, J.H. Oxidative Dehydrogenation of Ethane over a Lithium-Promoted Magnesium Oxide Catalyst. *J. Catal.* **1989**, *118*, 255–265.

[182] Xu, M.T.; Shi, C.L.; Yang, X.M.; Rosynek, M.P.; Lunsford, J.H. Effect of Carbon Dioxide on the Activation Energy for Methyl Radical Generation over Lithium/Magnesia Catalysts. *J. Phys. Chem.* **1992**, *96*, 6395–6398.

[183] Coulter, K.; Goodman, D.W. The Role of Carbon-Dioxide in the Oxidative Dimerization of Methane over Li/MgO. *Catal. Lett.* **1993**, *20*, 169–178.

[184] Cant, N.W.; Lukey, C.A.; Nelson, P.F.; Tyler, R.J. The Rate Controlling Step in the Oxidative Coupling of Methane over a Lithium-Promoted Magnesium Oxide Catalyst. *J. Chem. Soc., Chem. Commun.* **1988**, 766–768.

[185] Lapszewicz, J.A.; Jiang, X.Z. Investigation of Reactivity and Selectivity of Methane Coupling Catalysts Using Isotope Exchange Techniques. *Catal. Lett.* **1992**, *13*, 103–116.

[186] Martin, G.A.; Mirodatos, C. Evidence of Carbene Formation in Oxidative Coupling of Methane over Lithium-promoted Magnesium Oxide. *J. Chem. Soc., Chem. Commun.* **1987**, 1393–1394.

[187] Mims, C.A.; Hall, R.B.; Rose, K.D.; Myers, G.R. Oxidative Dimerization of CH_4/CD_4 Mixtures: Evidence for Methyl Intermediate. *Catal. Lett.* **1989**, *2*, 361–368.

[188] Martin, G.A.; Bernal, S.; Perrichon, V.; Mirodatos, C. Hetero-homogeneous Processes Involved in Oxidative Conversion of Methane, Ethane and Hydrocarbon Mixtures over Basic Oxides. *Catal. Today* **1992**, *13*, 487–494.

[189] Geerts, J.W.M.H.; van Kasteren, J.M.N.; van der Wiele, K. The Investigation of Individual Reaction Steps in the Oxidative Coupling of Methane over Lithium Doped Magnesium Oxide. *Catal. Today* **1989**, *4*, 453–461.

[190] Campbell, K.D.; Lunsford, J.H. Contribution of Gas-Phase Radical Coupling in the Catalytic Oxidation of Methane. *J. Phys. Chem.* **1988**, *92*, 5792–5796.

[191] van Kasteren, J.M.N.; Geerts, J.W.M.H.; van der Wiele, K. The Role of Heterogeneous Reactions during the Oxidative Coupling of Methane over Li/MgO Catalysts. *Catal. Today* **1990**, *6*, 497–502.

[192] Campbell, K.D.; Morales, E.; Lunsford, J.H. Gas-Phase Coupling of Methyl Radicals during the Catalytic Partial Oxidation of Methane. *J. Am. Chem. Soc.* **1987**, *109*, 7900–7901.

[193] Nelson, P.F.; Lukey, C.A.; Cant, N.W. Isotopic Evidence for Direct Methyl Coupling and Ethane to Ethylene Conversion during Partial Oxidation of Methane over Lithium/Magnesium Oxide. *J. Phys. Chem.* **1988**, *92*, 6176–6179.

[194] Nelson, P.F.; Cant, N.W. Oxidation of C_2 Hydrocarbon Products during the Oxidative Coupling of Methane over a Li/MgO Catalyst. *J. Phys. Chem.* **1990**, *94*, 3756–3761.

[195] Nelson, P.F.; Kennedy, E.M.; Cant, N.W. Isotopic Labelling Studies of the Mechanism of the Catalytic Oxidative Coupling of Methane. *Stud. Surf. Sci. Catal.* **1991**, *61*, 89–95.

[196] Utiyama, M.; Hattari, H.; Tanabe, K. Exchange Reaction of Methane with Deuterium over Solid Base Catalysts. *J. Catal.* **1978**, *53*, 237–242.

[197] Hargreaves, J.S.J.; Hutchings, G.J.; Joyner, R.W.; Taylor, S.H. A Study of the Methane Deuterium Exchange Reaction over a Range of Metal Oxides. *Appl. Catal., A* **2002**, *227*, 191–200.

[198] Buyevskaya, O.V.; Rothaemel, M.; Zanthoff, H.W.; Baerns, M. Transient Studies on Reaction Steps in the Oxidative Coupling of Methane over Catalytic Surfaces of MgO and Sm_2O_3. *J. Catal.* **1994**, *146*, 346–357.

[199] Balint, I.; Aika, K.I. Temperature-Programmed Desorption Study of Water-Gas Shift and Methane Steam-Reforming Reactions over Li/MgO Catalyst. *Appl. Catal., A* **2000**, *196*, 209–215.

[200] Hargreaves, J.S.J.; Hutchings, G.J.; Joyner, R.W. Control of Product Selectivity in the Partial Oxidation of Methane. *Nature* **1990**, *348*, 428–429.

[201] van Kasteren, J.M.N.; Geerts, J.W.M.H.; van der Wiele, K. Methane Oxidative Coupling Using Li/MgO Catalysts: The Importance of Consecutive Reactions. *Stud. Surf. Sci. Catal.* **1991**, *61*, 139–146.

[202] Martin, G.A.; Bates, A.; Ducarme, V.; Mirodatos, C. Oxidative Conversion of Methane and C_2 Hydrocarbons on Oxides: Homogeneous versus Heterogeneous Processes. *Appl. Catal.* **1989**, *47*, 287–297.

[203] Roos, J.A.; Korf, S.J.; Veehof, R.H.J.; van Ommen, J.G.; Ross, J.R.H. An Investigation of the Comparative Reactivities of Ethane and Ethylene in the

Presence of Oxygen over Li/MgO and Ca/Sm_2O_3 Catalysts in Relation to the Oxidative Coupling of Methane. *Catal. Today* **1989**, *4*, 441–452.

[204] Nelson, P.F.; Lukey, C.A.; Cant, N.W. Measurements of Kinetic Isotope Effects and Hydrogen/Deuterium Distributions over Methane Oxidative Coupling Catalysts. *J. Catal.* **1989**, *120*, 216–230.

[205] Cant, N.W.; Lukey, C.A.; Nelson, P.F. Oxygen Isotope Transfer Rates during the Oxidative Coupling of Methane over a Li/MgO Catalyst. *J. Catal.* **1990**, *124*, 336–348.

[206] Mims, C.A.; Mauti, R.; Dean, A.M.; Rose, K.D. Radical Chemistry in Methane Oxidative Coupling: Tracing of Ethylene Secondary Reactions with Computer Models and Isotopes. *J. Phys. Chem.* **1994**, *98*, 13357–13372.

[207] Shi, C.L.; Rosynek, M.P.; Lunsford, J.H. Origin of Carbon Oxides during the Oxidative Coupling of Methane. *J. Phys. Chem.* **1994**, *98*, 8371–8376.

[208] Hargreaves, J.S.J.; Hutchings, G.J.; Joyner, R.W. Hydrogen Production in Methane Coupling Over Magnesium Oxide. *Stud. Surf. Sci. Catal.* **1991**, *61*, 155–159.

[209] Swaan, H.M.; Toebes, A.; Seshan, K.; van Ommen, J.G.; Ross, J.R.H. The Kinetic and Mechanistic Aspects of the Oxidative Dehydrogenation of Ethane over Li/Na/MgO Catalysts. *Catal. Today* **1992**, *13*, 201–208.

[210] Wang, J.X.; Lunsford, J.H. Characterization of [Li^+O^-] Centers in Lithium-Doped Magnesium Oxide Catalysts. *J. Phys. Chem.* **1986**, *90*, 5883–5887.

[211] Wu, M.C.; Truong, C.M.; Goodman, D.W. Electron-Energy-Loss-Spectroscopy Studies of Thermally Generated Defects in Pure and Lithium-Doped MgO(100) Films on Mo(100). *Phys. Rev. B* **1992**, *46*, 12688–12694.

[212] Wu, M.C.; Truong, C.M.; Coulter, K.; Goodman, D.W. Role of F Centers in the Oxidative Coupling of Methane to Ethane over Lithium-Promoted Magnesium Oxide Catalysts. *J. Am. Chem. Soc.* **1992**, *114*, 7565–7567.

[213] Wu, M.C.; Truong, C.M.; Coulter, K.; Goodman, D.W. Investigations of Active Sites for Methane Activation in the Oxidative Coupling Reaction over Pure and Li-Promoted MgO Catalysts. *J. Catal.* **1993**, *140*, 344–352.

[214] Wu, M.C.; Truong, C.M.; Coulter, K.; Goodman, D.W. Nature of Active Sites in the Oxidative Coupling of Methane to Ethane over Li/MgO Catalysts. *J. Vac. Sci. Technol., A* **1993**, *11*, 2174–2178.

[215] Coulter, K.; Goodman, D.W. Kinetic Studies of the Oxidative Dimerization of Methane on Thin-Film MgO and Li/MgO. *Catal. Lett.* **1992**, *16*, 191–196.

[216] Coulter, K.; Szanyi, J.; Goodman, D.W. Pretreatment Effects on the Active Site for Methane Activation in the Oxidative Coupling of Methane over MgO and Li/MgO. *Catal. Lett.* **1995**, *35*, 23–32.

[217] Nelson, R.L.; Tench, A.J. Chemisorption and Surface Defects in Irradiated Magnesium Oxide. *J. Chem. Phys.* **1964**, *40*, 2736–2737.

[218] Lin, C.H.; Campbell, K.D.; Wang, J.X.; Lunsford, J.H. Oxidative Dimerization of Methane over Lanthanum Oxide. *J. Phys. Chem.* **1986**, *90*, 534–537.

[219] Aika, K.I.; Lunsford, J.H. Surface Reactions of Oxygen Ions. I. Dehydrogenation of Alkanes by O^- Ions on MgO. *J. Phys. Chem.* **1977**, *81*, 1393–1398.

[220] Iwamoto, M.; Lunsford, J.H. Surface Reactions of Oxygen Ions. 5. Oxidation of Alkanes and Alkenes by O_2^- on Magnesium Oxide. *J. Phys. Chem.* **1980**, *84*, 3079–3084.

[221] Garrone, E.; Zecchina, A.; Stone, F.S. Anionic Intermediates in Surface Processes Leading to O_2^- Formation on Magnesium Oxide. *J. Catal.* **1980**, *62*, 396–400.

[222] Takita, Y.; Lunsford, J.H. Surface Reactions of Oxygen Ions. 3. Oxidation of Alkanes by O_3^- Ion on Magnesium Oxide. *J. Phys. Chem.* **1979**, *83*, 683–688.

[223] Ito, T.; Tashiro, T.; Watanabe, T.; Toi, K.; Ikemoto, I. Activation of Methane on the MgO Surface at Low Temperatures. *Chem. Lett.* **1987**, *16*, 1723–1726.

[224] Zhen, K.J.; Li, S.Z.; Bi, Y.L.; Yang, X.G.; Wei, Q. Characterization and Catalytic Properties of MgO Prepared by Different Approaches. *Stud. Surf. Sci. Catal.* **1995**, *91*, 691–698.

[225] Aika, K.I.; Karasuda, T. Study on the Active Site Structure of MgO Catalysts for Oxidative Coupling of Methane. *Stud. Surf. Sci. Catal.* **1996**, *100*, 397–406.

[226] Karasuda, T.; Aika, K.I. Isotopic Oxygen Exchange between Dioxygen and MgO Catalysts for Oxidative Coupling of Methane. *J. Catal.* **1997**, *171*, 439–448.

[227] Karasuda, T.; Nagaoka, K.; Aika, K.I. Active Site Generation by Water for the Activation of Methane over Non-Reducible Oxide Catalysts: A Study of MgO System. *Stud. Surf. Sci. Catal.* **1998**, *119*, 283–288.

[228] McNamara, D.J.; Korf, S.J.; Seshan, K.; van Ommen, J.G.; Ross, J.R.H. The Effect of Nb_2O_5 and ZrO_2 Additions on the Behavior of Li/MgO and Li/Na/MgO Catalysts for the Oxidative Coupling of Methane. *Can. J. Chem. Eng.* **1991**, *69*, 883–890.

[229] Korf, S.J.; Roos, J.A.; Veltman, L.J.; van Ommen, J.G.; Ross, J.R.H. Effect of Additives on Lithium Doped Magnesium Oxide Catalysts Used in the Oxidative Coupling of Methane. *Appl. Catal.* **1989**, *56*, 119–135.

[230] Larkins, F.P.; Nordin, M.R. Physico-Chemical and Catalytic Properties of Doped MgO Catalysts. *Stud. Surf. Sci. Catal.* **1994**, *81*, 249–251.

[231] Larkins, F.P.; Nordin, M.R. The Effects of Transition Metal Oxides on the Methane Oxidative Coupling Activity of Doped MgO Catalysts I. Zinc and Manganese. *J. Catal.* **1991**, *130*, 147–160.

[232] Mariscal, R.; Soria, J.; Peña, M.A.; Fierro, J.L.G. Features of Li-Mn-MgO Catalysts and Their Relevance in the Oxidative Coupling of Methane. *J. Catal.* **1994**, *147*, 535–543.

[233] Kanno, T.; Kobayashi, M. The Difference in the Modification Effects of Li on Two MgO Samples of Higher and Lower Mn Contents. *J. Mater. Sci. Lett.* **1997**, *16*, 126–127.

[234] Kanno, T.; Horiuchi, J.I.; Kobayashi, M. Discrimination of Lattice Oxygen Species Involved in the Oxidative Coupling of Methane on a Mn Mixed-Mg Oxide. *React. Kinet. Catal. Lett.* **2000**, *70*, 73–80.

[235] Zhang, J.J.; Yang, X.G.; Bi, Y.L.; Zhen, K.J. Role of Li Ion in Li-Mn-MgO Catalyst for Oxidative Coupling of Methane. *Catal. Today* **1992**, *13*, 555–558.

[236] Ramasamy, S.; Mohamed, A.R.; Bhatia, S. Oxidative Coupling of Methane for the Production of Ethylene over Li-Ni/MgO Catalys. *React. Kinet. Catal. Lett.* **2002**, *75*, 353–358.

[237] Hoogendam, G.C.; van Keulen, A.N.J.; Seshan, K.; van Ommen, J.G.; Ross, J.R.H. The Importance of Mixed Oxides in the Catalytic Behavior of Sn or Zr Doped Li/MgO-Catalysts. *Stud. Surf. Sci. Catal.* **1993**, *81*, 187–192.

[238] Hoogendam, G.C.; Seshan, K.; van Ommen, J.G.; Ross, J.R.H. Oxidative Coupling of Methane over Doped Li/MgO Catalysts. *Catal. Today* **1994**, *21*, 333–340.

[239] Korf, S.J.; Roos, J.A.; Vreeman, J.A.; Derksen, J.W.H.C.; van Ommen, J.G.; Ross, J.R.H. A Study of the Kinetics of the Oxidative Coupling of Methane over a Li/Sn/MgO Catalyst. *Catal. Today* **1990**, *6*, 417–426.

[240] van Keulen, A.N.J.; Hoogendam, G.C.; Seshan, K.; van Ommen, J.G.; Ross, J.R.H. The Role of Tin in Li/Sn/MgO Catalysts for the Oxidative Coupling of Methane. *J. Chem. Soc., Chem. Commun.* **1992**, *18*, 1546–1547.

[241] Mallens, E.P.J.; Hoebink, J.H.B.J.; Marin, G.B. An Investigation of the Oxygen Pathways in the Oxidative Coupling of Methane over MgO-Based Catalysts. *J. Catal.* **1996**, *160*, 222–234.

[242] Nagaoka, K.; Karasuda, T.; Aika, K.I. The Effect of SnO_2 Addition to Li/MgO Catalysts for the Oxidative Coupling of Methane. *J. Catal.* **1999**, *181*, 160–164.

[243] Dittmeyer, R.; Hofmann, H. Oxidative Coupling of Methane over a Ce/Li/MgO-Catalyst. Kinetic Analysis and Reactor Simulation. *Stud. Surf. Sci. Catal.* **1994**, *81*, 241–247.

[244] Bartsch, S.; Falkowski, J.; Hoffmann, H. Catalyst Development for Oxidative Methane Coupling. *Catal. Today* **1989**, *4*, 421–431.

[245] Bartsch, S.; Hoffmann, H. Investigations on a Ce/Li/MgO-Catalyst for the Oxidative Coupling of Methane. *Catal. Today* **1990**, *6*, 527–534.

[246] Bartsch, S.; Pirkl, H.G.; Baumann, W.; Hoffmann, H. Kinetic Studies of the Oxidative Coupling of Methane over a Ce/Li/MgO Catalyst. *Stud. Surf. Sci. Catal.* **1991**, *61*, 147–154.

[247] Tiwari, K.K.; Roy, T.N.; Banerjee, S.; Ganguly, S.; Bhattacharyya, D.P. Oxidative Coupling of Methane to C_2-Hydrocarbons over Lithium-Cerium-Promoted MgO and MgO-CaO Catalysts. *J. Chem. Technol. Biotechnol.* **1995**, *63*, 190–194.

[248] Ruckenstein, E.; Khan, A.Z. Synergistic Effect of Bialkali Metal Chlorides Promoted Magnesia on Oxidative Coupling of Methane. *Catal. Lett.* **1993**, *18*, 27–35.

[249] Ruckenstein, E.; Khan, A.Z. Effects of Superbasic Catalysts Prepared by Promoting MgO with Bialkali Metal Compounds on the Oxidative Coupling of Methane. *J. Catal.* **1993**, *141*, 628–647.

[250] Swaan, H.M.; Toebes, A.; Seshan, K.; van Ommen, J.G.; Ross, J.R.H. The Effect of Addition of a Third Component on the Behaviour of the Lithium Doped Magnesium Catalysts for the Oxidative Dehydrogenation of Ethane. *Catal. Today* **1992**, *13*, 629–634.

[251] Fuchs, S.; Leveles, L.; Seshan, K.; Lefferts, L.; Lemonidou, A.; Lercher, J.A. Oxidative Dehydrogenation and Cracking of Ethane and Propane over LiDyMg Mixed Oxides. *Top. Catal.* **2001**, *15*, 169–174.

[252] Mallens, E.P.J.; Hoebink, J.H.B.J.; Marin, G.B. The Oxidative Coupling of Methane over Tin Promoted Lithium Magnesium Oxide: A TAP Investigation. *Stud. Surf. Sci. Catal.* **1994**, *81*, 205–210.

[253] Otsuka, K.; Liu, Q.; Hatano, M.; Morikawa, A. Synthesis of Ethylene by Partial Oxidation of Methane over the Oxides of Transition Elements with LiCl. *Chem. Lett.* **1986**, *15*, 903–906.

[254] Burch, R.; Squire, G.D.; Tsang, S.C. Role of Chlorine in Improving Selectivity in the Oxidative Coupling of Methane to Ethylene. *Appl. Catal.* **1989**, *46*, 69–87.

[255] Burch, R.; Chalker, S.; Hibble, S.J. The Role of Chlorine in the Partial Oxidation of Methane to Ethene on MgO Catalysts. *Appl. Catal., A* **1993**, *96*, 289–303.

[256] Conway, S.J.; Lunsford, J.H. The Oxidative Dehydrogenation of Ethane over Chlorine-Promoted Lithium-Magnesium Oxide Catalysts. *J. Catal.* **1991**, *131*, 513–522.

[257] Hinson, P.G.; Clearfield, A.; Lunsford, J.H. The Oxidative Coupling of Methane on Chlorinated Lithium-Doped Magnesium Oxide. *J. Chem. Soc., Chem. Commun.* **1991**, 1430–1432.

[258] Lunsford, J.H.; Hinson, P.G.; Rosynek, M.P.; Shi, C.L.; Xu, M.T.; Yang, X.M. The Effect of Chloride Ions on a Li^+-MgO Catalyst for the Oxidative Coupling of Methane. *J. Catal.* **1994**, *147*, 301–310.

[259] Lewis, D.W.; Catlow, C.R.A. A Computational Study of the Role of Chlorine in the Partial Oxidation of Methane by MgO and Li/MgO. *Top. Catal.* **1994**, *1*, 111–121.

[260] Hattori, H. Heterogeneous Basic Catalysis. *Chem. Rev.* **1995**, *95*, 537–558.

[261] Coluccia, S.; Marchese, L.; Lavagnino, S.; Anpo, M. Hydroxyls on the Surface of MgO Powders. *Spectrochim. Acta, Part A* **1987**, *43*, 1573–1576.

[262] Praliaud, H.; Coluccia, S.; Deane, A.M.; Tench, A.J. Oxidising Properties of MgO Formed by Thermal Decomposition of $Mg(OH)_2$. *Chem. Phys. Lett.* **1979**, *66*, 44–47.

[263] Chizallet, C.; Costentin, G.; Lauron-Pernot, H.; Krafft, J.M.; Che, M.; J.; Delbecq, F.; Sautet, P. Assignment of Photoluminescence Spectra of MgO Powders: TD-DFT Cluster Calculations Combined to Experiments. Part I: Structure Effects on Dehydroxylated Surfaces. *J. Phys. Chem. C* **2008**, *112*, 16629–16637.

[264] Chizallet, C.; Costentin, G.; Lauron-Pernot, H.; Krafft, J.M.; Che, M.; Delbecq, F.; Sautet, P. Assignment of Photoluminescence Spectra of MgO Powders: TD-DFT Cluster Calculations Combined to Experiments. Part II. Hydroxylation Effects. *J. Phys. Chem. C* **2008**, *112*, 19710–19717.

[265] Che, M.; Tench, A.J. Characterization and Reactivity of Mononuclear Oxygen Species on Oxide Surfaces. Vol 31. *Advances in Catalysis*, Academic Press: New York, 1982, pp. 77–133.

[266] Mehandru, S.P.; Anderson, A.B.; Brazdil, J.F. Methyl Radical Formation over Lithium-Doped Magnesium Oxide. Molecular Orbital Theory. *J. Am. Chem. Soc.* **1988**, *110*, 1715–1719.

[267] Catlow, C.R.A.; French, S.A.; Sokol, A.A.; Thomas, J.M. Computational Approaches to the Determination of Active Site Structures and Reaction Mechanisms in Heterogeneous Catalysts. *Phil. Trans. R. Soc. A* **2005**, *363*, 913–936.

[268] Orlando, R.; Corà, F.; Millini, R.; Perego, G.; Dovesi, R. Hydrogen Abstraction from Methane by Li Doped MgO: A Periodic Quantum Mechanical Study. *J. Chem. Phys.* **1996**, *105*, 8937–8943.

[269] Dash, L.K.; Gillan, M.J. Assessment of Competing Mechanisms of the Abstraction of Hydrogen from CH_4 on Li/MgO(001). *Surf. Sci.* **2004**, *549*, 217–226.

[270] Zobel, N.; Behrendt, F. Activation Energy for Hydrogen Abstraction from Methane over Li-Doped MgO: A Density Functional Theory Study. *J. Chem. Phys.* **2006**, *125*, 074715.

[271] Yang, Z.X.; Liu, G.; Wu, R.Q. Effects of Li impurities on MgO(001). *Phys. Rev. B* **2002**, *65*, 235432.

[272] Morgan, B.J.; Scanlon, D.O.; Watson, G.W. The Use of the "+*U*" Correction in Describing Defect States at Metal Oxide Surfaces: Oxygen Vacancies on CeO_2 and TiO_2, and Li-doping of MgO. *e-J. Surf. Sci. Nanotechnol.* **2009**, *7*, 389–394.

[273] Scanlon, D.O.; Walsh, A.; Morgan, B.J.; Watson, G.W. Competing Defect Mechanisms and Hydrogen Adsorption on Li-Doped MgO Low Index Surfaces: A DFT+*U* Study. *e-J. Surf. Sci. Nanotechnol.* **2009**, *7*, 395–404.

[274] Lintuluoto, M.; Nakamura, Y. Theoretical Study on the Adsorption of Methane on MgO and Li-Doped MgO Surfaces. *J. Mol. Struct. Theochem* **2004**, *674*, 207–212.

[275] Zuo, J.; Pandey, R.; Kunz, A.B. Embedded-Cluster Study of the Lithium Trapped-Hole Center in Magnesium Oxide. *Phys. Rev. B* **1991**, *44*, 7187–7191.

[276] Ackermann, L.; Gale, J.D.; Catlow, C.R.A. Interaction of Methane with a $[Li]^0$ Center on MgO(100): HF, Post-HF, and DFT Cluster Model Studies. *J. Phys. Chem. B* **1997**, *101*, 10028–10034.

[277] Børve, K.J.; Pettersson, L.G.M. Hydrogen Abstraction from Methane on a Magnesia (001) Surface. *J. Phys. Chem.* **1991**, *95*, 7401–7405.

[278] Børve, K.J. Methane Dissociation on a Nonplanar MgO(001) Surface. Theoretical Modeling of Surface Defects. *J. Chem. Phys.* **1991**, *95*, 4626–4631.

[279] Zhanpeisov, N.U.; Baerns, M. Cluster Quantum-Chemical Study of the Chemisorption of Methane on a Lithium-Promoted Magnesium Oxide Doped by Zinc Oxide. *J. Mol. Catal. A: Chem* **1995**, *99*, 139–142.

[280] Zhanpeisov, N.U.; Staemmler, V.; Baerns, M. A Quantum-Chemical MINDO/3 Study of Methane and Oxygen Interactions with a Pure and a Modified Calcium Oxide Surface. *J. Mol. Catal. A: Chem* **1995**, *101*, 51–60.

[281] Birkenheuer, U.; Corà, F.; Pisani, C.; Scorza, E.; Perego, G. Embedded-Cluster Study of Core-Level Binding Energies of Magnesium and Alkali Impurities at the Surface of MgO. *Surf. Sci.* **1997**, *373*, 393–408.

[282] Nolan, M.; Watson, G.W. The Electronic Structure of Alkali Doped Alkaline Earth Metal Oxides: Li Doping of MgO Studied with DFT-GGA and GGA + *U*. *Surf. Sci.* **2005**, *586*, 25–37.

[283] Scanlon, D.O.; Walsh, A.; Morgan, B.J.; Nolan, M.; Fearon, J.; Watson, G.W. Surface Sensitivity in Lithium-Doping of MgO: A Density Functional Theory Study with Correction for On-Site Coulomb Interactions. *J. Phys. Chem. C* **2007**, *111*, 7971–7979.

[284] Mori-Sánchez, P.; Cohen, A.J.; Yang, W.T. Localization and Delocalization Errors in Density Functional Theory and Implications for Band-Gap Prediction. *Phys. Rev. Lett.* **2008**, *100*, 146401.

[285] Lichanot, A.; Larrieu, C.; Orlando, R.; Dovesi, R. Lithium Trapped-Hole Centre in Magnesium Oxide. An *Ab Initio* Supercell Study. *J. Phys. Chem. Solids* **1998**, *59*, 7–12.

[286] Lichanot, A.; Larrieu, C.; Zicovich-Wilson, C.; Roetti, C.; Orlando, R.; Dovesi, R. Trapped-Hole Centres Containing Lithium and Sodium in MgO, CaO and SrO. An *Ab Initio* Supercell Study. *J. Phys. Chem. Solids* **1998**, *59*, 1119–1124.

[287] Dovesi, R.; Orlando, R.; Roetti, R.; Pisani, C.; Saunders, V.R. The Periodic Hartree-Fock Method and Its Implementation in the Crystal Code. *Phys. Status Solidi B* **2000**, *217*, 63–88.

[288] Reuter, K.; Scheffler, M. Composition, Structure, and Stability of $RuO_2(110)$ as a Function of Oxygen Pressure. *Phys. Rev. B* **2001**, *65*, 035406.

[289] Weinert, C.M.; Scheffler, M. Chalcogen and Vacancy Pairs in Silicon: Electronic Structure and Stabilities. In *Defects in Semiconductors*, Vol. 10–12, Bardeleben, H.J., Ed.; Trans Tech Publications: Aedermannsdorf, 1986, pp. 25–30.

[290] Scheffler, M.; Dabrowski, J. Parameter-Free Calculations of Total Energies, Interatomic Forces and Vibrational Entropies of Defects in Semiconductors. *Philos. Mag. A* **1988**, *58*, 107–121.

[291] Reuter, K.; Stampfl, C.; Scheffler, M. *Ab Initio* Atomistic Thermodynamics and Statistical Mechanics of Surface Properties and Functions. In Vol. 1, *Handbook of Materials Modeling*; Springer: Berlin Heidelberg, 2005, pp. 149–194.

[292] Scheffler, M.; Reuter, K. First-Principles Kinetic Monte Carlo Simulations for Heterogeneous Catalysis: Application to the CO Oxidation at RuO2(110). *Phys. Rev. B* **2006**, *73*, 045433.

[293] Watson, G. Atomistic and Electronic Structure Calculation of Defects at the Surfaces of Oxides. *Radiat. Eff. Defects Solids* **2002**, *157*, 773–781.

[294] Zhidomirov, G.M.; Zhanpeisov, N.U. Active Centres of Magnesium Oxide Surface and Calculations of Dissociative Chemisorption of Methane on Modified MgO. *Catal. Today* **1992**, *13*, 517–522.

[295] Orlando, R.; Millini, R.; Perego, G.; Dovesi, R. Catalytic Properties of F-Centres at the Magnesium Oxide Surface: Hydrogen Abstraction from Methane. *J. Mol. Catal. A: Chem* **1997**, *119*, 253–262.

[296] Pacchioni, G.; Ferrari, A.M. Surface Reactivity of MgO Oxygen Vacancies. *Catal. Today* **1999**, *50*, 533–540.

[297] Ahari, J.S.; Ahmadi, R.; Mikami, H.; Inazu, K.; Zarrinpashne, S.; Suzuki, S.; Aika, K.I. Application of a Simple Kinetic Model for the Oxidative Coupling of Methane to the Design of Effective Catalysts. *Catal. Today*, **2009**, *145*, 45–54.

[298] Geerts, J.W.M.H.; Chen, Q.; van Kasteren, J.M.N.; van der Wiele, K. Thermodynamics and Kinetic Modeling of the Homogeneous Gas Phase Reactions of the Oxidative Coupling of Methane. *Catal. Today* **1990**, *6*, 519–526.

[299] Labinger, J.A.; Ott, K.C. Mechanistic Studies on the Oxidative Coupling of Methane. *J. Phys. Chem.* **1987**, *91*, 2682–2684.

[300] Mackie, J.C. Partial Oxidation of Methane: The Role of the Gas Phase Reactions. *Catal. Rev. Sci. Eng*. **1991**, *33*, 169–240.

[301] Slagle, I.R.; Gutman, D. Kinetics of Polyatomic Free Radicals Produced by Laser Photolysis. 5. Study of the Equilibrium $CH_3 + O_2 \rightleftharpoons CH_3O_2$ between 421 and 538 °C. *J. Am. Chem. Soc*. **1985**, *107*, 5342–5347.

[302] Zanthoff, H.; Baerns, M. Oxidative Coupling of Methane in the Gas Phase. Kinetic Simulation and Experimental Verification. *Ind. Eng. Chem. Res*. **1990**, *29*, 2–10.

[303] Tsang, W. Chemical Kinetic Data Base for Combustion Chemistry. Part 3. Propane. *J. Phys. Chem. Ref. Data* **1988**, *17*, 887–951.

[304] Tsang, W.; Hampson, R.F. Chemical Kinetic Data Base for Combustion Chemistry. Part 1. Methane and Related Compounds. *J. Phys. Chem. Ref. Data* **1986**, *15*, 1087–1279.

[305] Lunsford, J.H. The Catalytic Conversion of Methane to Higher Hydrocarbons. *Catal. Today* **1990**, *6*, 235–259.

[306] Polyakov, M.V.; Stadnik, P.M.; Neimark, I.E. Hetrogeneous-Homogeneous Catalysis of $CH_4 + O_2$ Mixtures. *Zh. Fiz. Khim*. **1936**, *8*, 584–586.

[307] Fang, T.; Yeh, C.T. Interactions of Methane with ThO_2/SiO_2 Surface at 1073 K. *J. Catal*. **1981**, *69*, 227–229.

[308] Cant, N.W.; Kennedy, E.M.; Nelson, P.F. Magnitude and Origin of the Deuterium Kinetic Isotope Effect during Methane Coupling and Related Reactions over Lithium/Magnesium Oxide Catalysts. *J. Phys. Chem*. **1993**, *97*, 1445–1450.

[309] Burch, R.; Tsang, S.C.; Mirodatos, C.; Sanchez M., J.G. Kinetic Isotope Effects in Methane Coupling on a Reducible Oxide Catalyst. *Catal. Lett*. **1990**, *7*, 423–430.

[310] Otsuka, K.; Inaida, M.; Wada, Y.; Komatsu, T.; Morikawa, A. Isotopic Studies on Oxidative Methane Coupling over Samarium Oxide. *Chem. Lett*. **1989**, *18*, 1531–1534.

[311] Aparicio, L.M.; Rossini, S.A.; Sanfilippo, D.G.; Rekoske, J.E.; Treviño, A.A.; Dumesic, J.A. Microkinetic Analysis of Methane Dimerization Reaction. *Ind. Eng. Chem. Res*. **1991**, *39*, 2114–2123.

[312] Shi, C.; Hatano, M.; Lunsford, J.H. A Kinetic Model for the Oxidative Coupling of Methane over Li^+/MgO Catalysts. *Catal. Today* **1992**, *13*, 191–199.

[313] Tjatjopoulos, G.J.; Vasalos, I.A. A Mechanistic Kinetic Model for Oxidative Coupling of Methane over Li/MgO Catalysts. *Catal. Today* **1992**, *13*, 361–370.

[314] Tung, W.Y.; Lobban, L.L. Oxidative Coupling of Methane over Lithium/Magnesia: Kinetics and Mechanisms. *Ind. Eng. Chem. Res*. **1992**, *31*, 1621–1625.

[315] Zanthoff, H.; Zhang, Z.; Gryzbek, T.; Lehmann, L.; Baerns, M. Catalysis and Kinetics of the Oxidative Methane Coupling. *Catal. Today* **1992**, *13*, 469–480.

[316] Sun, J.J.; Thybaut, J.W.; Marin, G.B. Microkinetics of Methane Oxidative Coupling. *Catal. Today* **2008**, *137*, 90–102.

[317] Couwenberg, P.M.; Chen, Q.; Marin, G.B. Kinetics of a Gas-Phase Chain Reaction Catalyzed by a Solid: The Oxidative Coupling of Methane over Li/MgO-Based Catalysts. *Ind. Eng. Chem. Res*. **1996**, *35*, 3999–4011.

[318] Couwenberg, P.M.; Chen, Q.; Marin, G.B. Irreducible Mass-Transport Limitations during a Heterogeneously Catalyzed Gas-Phase Chain Reaction: Oxidative Coupling of Methane. *Ind. Eng. Chem. Res*. **1996**, *35*, 415–421.

[319] Hoebink, J.H.B.J.; Couwenberg, P.M.; Marin, G.B. Fixed Bed Reactor Design for Gas Phase Chain Reactions Catalysed by Solids: The Oxidative Coupling of Methane. *Chem. Eng. Sci*. **1994**, *49*, 5453–5463.

[320] DeBoy, J.M.; Hicks, R.F. The Oxidative Coupling of Methane over Alkali, Alkaline Earth, and Rare Earth Oxides. *Ind. Eng. Chem. Res*. **1988**, *27*, 1577–1582.

[321] Sinev, M.Y.; Fattakhova, Z.T.; Lomonosov, V.I.; Gordienko, Y.A. Kinetics of Oxidative Coupling of Methane: Bridging the Gap between Comprehension and Description. *J. Nat. Gas Chem*. **2009**, *18*, 273–287.

[322] Arutyunov, V.S.; Rudakov, V.M.; Savchenko, V.I.; Sheverdenkin, E.V. Relative Conversion of Lower Alkanes in Their Simultaneous Partial Gas-Phase Oxidation. *Theor. Found. Chem. Eng*. **2005**, *39*, 487–492.

[323] Sinev, M.; Arutyunov, V.; Romanets A. Kinetic Models of C_1-C_4 Alkane Oxidation as Applied to Processing of Hydrocarbon Gases: Principles, Approaches and Developments. In *Advances in Chemical Engineering*, Vol. 32, Academic Press, 2007, pp. 167–258.

[324] Miller, J.A.; Klippenstein, S.J. The Reaction between Ethyl and Molecular Oxygen II: Further Analysis. *Int. J. Chem. Kinet*. **2001**, *33*, 654–668.

[325] Slagle, I.R.; Ratajczak, E.; Gutman, D. Study of the Thermochemistry of the $CH_3 + O_2 \Leftrightarrow C_2H_5O_2$ and t-$C_4H_9 + O_2 \Leftrightarrow t$-$C_4H_9O_2$ Reactions and of the Trend in the Alkylperoxy Bond Strengths. *J. Phys. Chem*. **1986**, *90*, 402–407.